IDENTIFYING AND ANALYZING AMORPHIZATION IN BORON-RICH BORON CARBIDES

By

MARK CHRISTOPHER SCHAEFER

A dissertation submitted to the

School of Graduate Studies

Rutgers, The State University of New Jersey

In partial fulfillment of the requirements

For the degree of

Doctor of Philosophy

Graduate Program in Materials Science and Engineering

Written under the direction of

Dr. Richard A. Haber

And approved by

_____

_____

_____

_____

New Brunswick, New Jersey

October 2020

ABSTRACT OF THE DISSERTATION

Title

by MARK CHRISTOPHER SCHAEFER

Dissertation Director:

Richard A. Haber

Boron carbide is a ceramic material known for its high hardness and low density. These properties make it an ideal material to be used in armor materials. However, when subjected to shock-loading experiments, boron carbide does not perform as expected. Rather than undergo a work-hardening mechanism past a critical shock-loading point, as is the case in similar ceramic materials like silicon carbide, boron carbide suddenly fails. This abrupt failure under dynamic loading has been attributed to "amorphization," the appearance of nanometer-sized amorphous bands that limit the boron carbides ballistic performance.

Much work has been done to understand amorphization and elucidate its atomistic mechanism. These attempts to identify the peak point in boron carbide lead to several suggestions to fix boron carbides amorphous behavior as a means to improve its ballistic performance. One such alternative theorized doping the boron carbide structure with boron and silicon. Much work has been done already in understanding silicon-doped boron carbide mitigating amorphization, but little has been done in understanding boron-rich boron carbides effect on amorphous behavior. While several studies have been carried out to process boron-rich boron carbides and study their mechanical properties, no work has been experimentally carried out in understanding amorphization in these materials.

In this dissertation, boron-rich boron carbides are studied with respect to amorphization, something previously overlooked in the literature. This work is done with the

intention of supporting and validating models that suggest boron-rich boron carbides can mitigate amorphization. Methods will be developed to accurately assess and quantify the degree of amorphization in boron carbides that span the materials homogeneity range. Indentation was used as a means to activate stress-induced amorphization in samples. Raman spectroscopy will be heavily utilized in this work as a means to quickly probe samples for amorphization in a non-destructive manner.

Additionally, the use of Raman spectroscopy allows for various in situ measurements to be carried out at elevated temperatures and large pressures. These factors are critical in simulating ballistic impact parameters in the laboratory and studying these in situ can help determine the evolution of the amorphous phase as these parameters are varied.

Amorphization mitigation in boron-rich boron carbides was determined through Raman spectroscopy quantification methods developed in this thesis and were also validated through TEM imaging. Further, in situ experiments were carried out at large pressures that determined critical onset pressure conditions to induce amorphization in doped samples. This allowed for comparison between amorphization mechanisms between samples of differing compositions.

ACKNOWLEDGEMENTS

First, I want to thank my mentor and advisor, Rich. His continuous knowledge, guidance, encouragement, and mostly importantly, patience has made the last 4 years a successful journey. He has taught me valuable lessons that will carry me through life, many of which go well beyond materials, science, and engineering. Coming to grad school, I had no background in ceramics, but Rich gave me the chance, and for that I am forever grateful. I could not imagine the last 4 years any other way: it certainly wouldn't have been as fun without the Haber and his Group. You created a group that became a family, and made my time at work feel less like work.

Next up, a huge thank you to Michelle Sole. In many regards, she was also my advisor, being the Yin to Rich's Yang. Her office served as the gathering place for our morning coffee break: We came for the coffee, we stayed because of her, for being a delight and making every day a little bit better. Without her, a piece of the puzzle would have been missing.

The entire Haber group made the journey interesting and fun. A huge shout out goes to Laura, who always made me laugh when she dropped by. Next is Dr. Vlad Domnich, for being the boron carbide and Raman spectroscopy encyclopedia from which I could become an expert myself. Your help throughout my first two years was critical. To the other Haber group postdocs: Chawon, Atta, Sukanya, Berra, and Jun. They were all great to talk to and always kept me thinking. To the Haber students, deep in the trenches with me: Vince, Joe, Metin, Zeynep, Ian, Bruce, Azmi, Mustafa, Sweta, Kent, and Eoin.

Extra big shout outs go to…

Office Squad: Ian, Mustafa, and Sweta

Armor Squad: Azmi, Bruce, and Kent

Gym Squad: Ian, Sweta, Bruce, and Azmi

Marvel Movie Squad: Mustafa, Ian, and Sweta

All of the aforementioned “squads” kept the work flowing and fun constant. They all helped make this an unforgettable time, both inside and outside of work. I will forever remember and cherish the friendships made along the way.

My committee also provided great insight along the way. Dr. Michael Normandia was integral to my success. Our many conversations allowed me to understand my work and the field in a much greater detail that only could’ve come from his industry expertise. I would also like to thank my Rutgers committee members, Prof. Lehman, Prof. Birnie, and Prof. Mann. All of your input on my work was appreciated, as was your patience with me in each of your classes.

Next up is the Materials in Extreme and Dynamic Environments (MEDE) Program for funding my PhD and giving me many opportunities to present myself and my work. My research was sponsored by the Army Research Laboratory and was accomplished under Cooperative Agreement Number W911NF-12-2-0022. Additional support was received from the National Science Foundation I/UCRC Award No.1540027. The views and conclusions contained in this document are those of the authors and should not be interpreted as representing the official policies, either expressed or implied, of the Army Research Laboratory, the National Science Foundation or the U.S. Government. The U.S. Government is authorized to reproduce and distribute reprints for Government purposes notwithstanding any copyright notation herein.

Within the MEDE Program, my gratitude goes out to Professor Kevin Hemker and Dr. Ankur Chauhan from Johns Hopkins University. Their TEM expertise led to a great collaboration that bolstered my dissertation and knowledge of microscopy.

To Emma, Sharadh, and Kevin: my best friends for so long now. Thank you for your help along the way, for the fun and endless memories, and for staying in touch. I wish you all the best as you complete your PhD's.

Next up is my family. For 26 years, I have been given unlimited love and support from my parents and sister, Alexa. They always encouraged me and pushed with my schoolwork, spending so many hours reading to me as a kid, and way too much time on a seemingly never-ending list of book reports. None of this would have been possible without them: I love you all more than you will ever know.

To my newly acquired parents, Rick and Elisa. Thank you for bringing me into your family and showing me so much love and support over the last decade.

Saving the most important for last, my beautiful wife Ana. We have been together for over 9 years. We made the decision to take on this new chapter of life in New Jersey 4 years ago. Ana was the key to this entire journey for me. She is kind and intelligent, and no matter what, she has always kept me moving forward in life, no matter how difficult that sometimes was. The support and love given by her to help me finish this dissertation was truly incalculable. In so many ways, this dissertation is more hers than mine: at this point, not only does she know the work as well as I do, but she had the added challenge of dealing with me the entire time. So, kudos to you for holding things together and helping me do this. I love you so much Ana, and this dissertation is dedicated to you. I hope to share so many more happy years with you.

Figure 0: The Haber Group at the wedding of Mark and Ana Schaefer. November 2, 2019, Saratoga Springs, NY.

Table of Contents

List of Tables

List of Figures

1. Introduction

Boron carbide is a ceramic material that has a wide variety of applications. Due to the materials hardness-to-weight ratio, this material is particularly desirable in defense applications, serving as armor plating on personnel, as well as land- and air-based vehicles. Boron carbide is harder and lighter than alumina and silicon carbide, materials previously used in these applications. However, boron carbide does present one shortcoming in its performance against high-velocity threats. Impacts that exceed a critical pressure result in boron carbides anomalous brittle failure, thus limiting its effectiveness and widespread usage as an armor material candidate.[1]

This failure has been attributed to a finding dubbed “amorphization,” where nano-meter sized bands of amorphous material have been discovered in post-impacted specimens.[2, 3] The amorphization of boron carbide under high rate impacts and stresses has since been given much attention by the scientific research community. Amorphization has been identified and well established at this point, confirming its unique Raman spectra and various groups identifying amorphous bands with high-resolution imaging techniques.

In order to understand amorphization from an atomistic approach, the structure of boron carbide needs to be well established. The rhombohedral structure of boron carbide, similar to other borides, is complex, allowing many structural variations to occur in an experimental material.[4]

Models have established various weak points in the boron carbide structure and suggestions of modified amorphization-resistant boron carbides.[5-10] This led to experimental work to create these materials, one such example being a boron-rich boron carbide, where additional boron atoms substitute carbon atoms in the lattice. This boron addition further

complicates the understanding of the exact structure of the modified material. Various work was conducted producing boron-rich boron carbides, but those studies stopped short of looking into the effect the dopants had on amorphization.[11-14]

The goal of this thesis is to gain an understanding of amorphization in doped boron carbide materials. It is important to validate models predicting amorphization mitigation, and to develop accurate and repeatable methods to detect and quantify this. Experimental tests that have been previously explored in boron carbide will be used to observe amorphization in boron-rich boron carbides. This can help determine if amorphization in boron-rich boron carbides occurs by a different mechanism in situ, or if a higher stress threshold is required to induce it.

2. Background

This section will give background on the structure of boron carbide, including the properties that make this material desirable for armor and defense applications. Boron carbide is a favorable material due to it high hardness of ~30 GPa and low density of 2.52 g/cm^3.[4] Most current armor materials comprise silicon and boron carbides, as well as aluminum oxides. Hardness is a crucial factor in determining a materials ability to exhibit good performance against ballistic threats, and boron carbides exceptional hardness can explain the importance of researching and understanding the material.[15] The exact atomic configuration for boron carbide is very complex, and many explanations and possibilities are presented in the literature, which will all be stated in the following section. In addition, boron carbides limited performance in ballistic impacts will be discussed, as will amorphization, thought to be the main reason behind the materials limited ballistic performance. Amorphization will be looked at with both a theoretical and experimental approach, and the experimental approach will also identify diamond anvil cells (DAC) as being critical devices to study boron carbide and amorphization in situ under large pressures. Next, modeling to improve boron carbides performance will be reviewed. Going further, the impact these models had on proceeding experimental work creating boron-rich boron carbides will also be looked at, where doped boron carbide materials were synthesized in an effort to fix the amorphization problem. Lastly, the materials that will be directly studied and tested throughout this dissertation, to further understand amorphization in boron carbide and doped boron carbides, is also discussed.

2.1. Structure and Properties of Boron Carbide

This subsection of the literature review is dedicated to gaining a full understanding of the boron carbide structure, including its many complexities, from the most basic assumed structure to all of its possible variations that are both predicted and known to exist. Since

Raman spectroscopy will be a key instrument in collecting data and allowing in situ experiments to be carried out for this dissertation, a subsection detailing the understanding of boron carbides Raman spectra will also be discussed.

As a note, the phrase “boron carbide” in this section (2a), as well as throughout this dissertation, will refer to the material in its most commonly used form: as B_4C, containing approximately 80 at. % boron and 20 at. % carbon.

2.1a. Basic Structure of Boron Carbide

Boron carbide is a solid solution of boron and carbon atoms, comprising a 15-atom rhombohedral unit cell. This consists of a 12-atom icosahedra linked by a 3-atom chain. Within the icosahedra, there are 12 sites, 6 of which are defined as a polar site, while the other 6 are denoted as equatorial sites. The polar sites on the icosahedra correspond to atoms that bond the icosahedra together, and equatorial sites bond to the three-atom chains. Both sites bond to neighboring icosahedra. The 15-atom unit cell typically contains 12 boron atoms and 3 carbon atoms, reducing its empirical formula to B_4C. Stated differently, boron carbide is most commonly approximately 80 atomic percent boron and 20 atomic percent carbon.[4, 16] A visual of boron carbides unique structure is provided below in Figure 1.

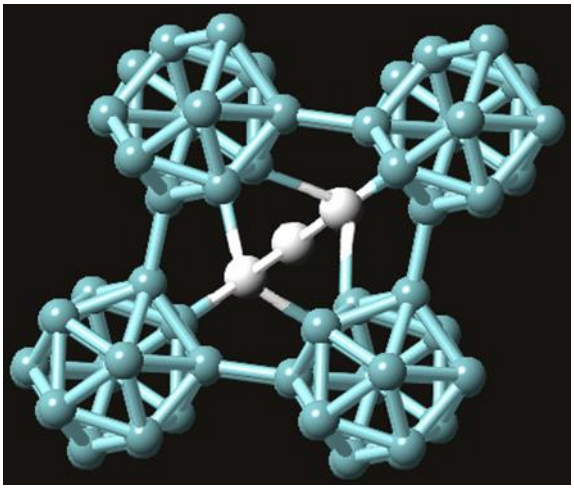

Figure 1: Atomic structure of boron carbide.

Boron carbide is of the R3m space group, with corresponding rhombohedral lattice parameters of a = 5.16 A with α = 65.7°, with the chain residing in the (111) direction. Defining boron carbide using hexagonal lattice notation, the parameters of boron carbide become a_0 = 5.60 A, c_0 = 12.07 A, thus giving a c_0/a_0 ratio of 2.155. The hexagonal unit cell also has the c-parameter parallel to the direction of the atomic chain. The two notations can be related through the (111) direction in rhombohedral notation, which corresponds to the (0001) axis in the hexagonal lattice. Hexagonal notation makes visualization much easier and will be used for the duration of this dissertation when necessary. The hexagonal unit cell is shown in blue, while rhombohedral is shown in red in Figure 2.[4]

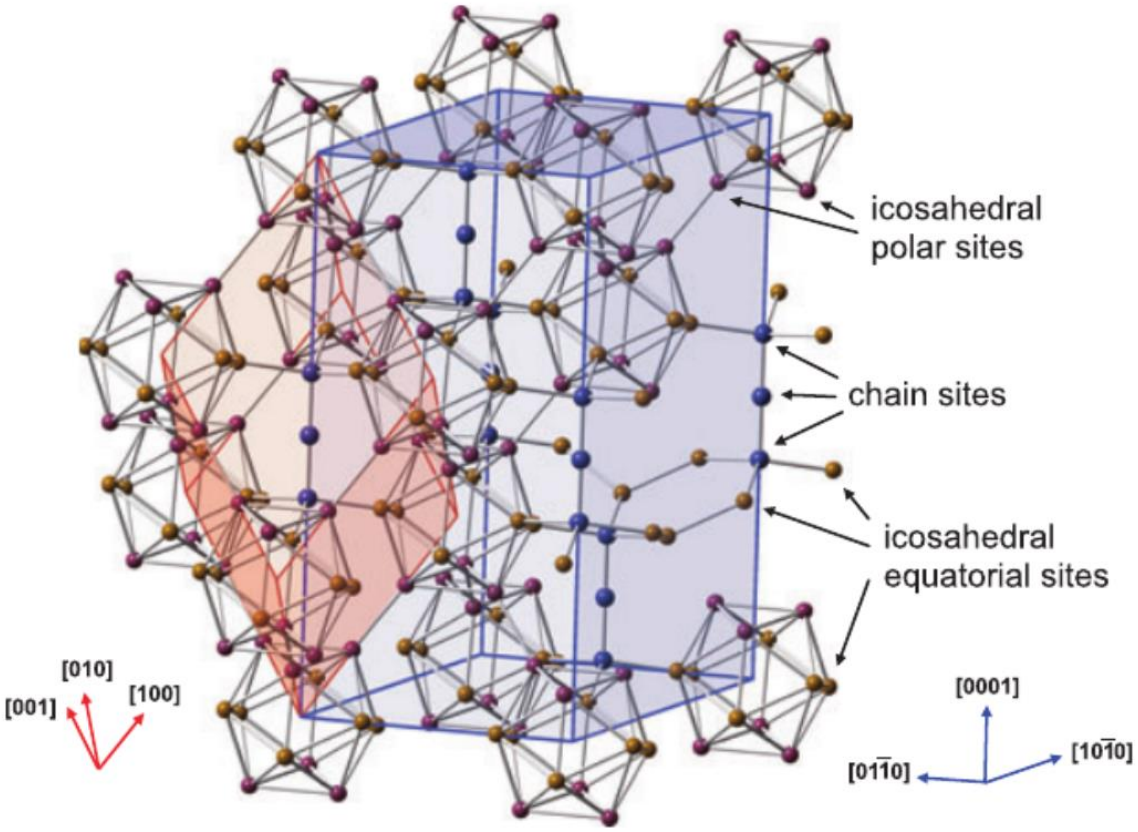

Figure 2: The boron carbide lattice defined by a rhombohedral (red) and hexagonal (blue) unit cell. Icosahedral sites, polar and equatorial, and chain site are noted by arrows.[4]

Standard notation for the boron carbide structure is as follows, and will be referred to as such for the rest of this dissertation: (12-atom icosahedra)three-atom chain.

In boron-rich icosahedral materials, boron atoms bond within the icosahedra in such a way that they become electron deficient. An atom contributes one of its three valence electrons to external bonding, so each boron atom then contributes its remaining 2 atoms to internal bonding of the icosahedra. At the same time, boron atoms bond to other constituents, such as chains or other icosahedron through covalent bonding.[17]

It was initially thought that the icosahedra was comprised solely of boron atoms, while all carbon atoms occupied chain sites, and, per previously defined notation, boron carbide is noted as $(B_{12})CCC$. However, current modeling shows that the preferred energetic state for standard B_4C is $B_{11}C_p$ icosahedra, with the carbon atom residing at a polar site in the icosahedra, with a C-B-C chain, and thus is noted as $(B_{11}C_p)CBC$.[4, 16, 18]

It is accepted that two carbon atoms cannot reside within the icosahedra due to bonding constraints. Additionally, carbon atoms, having four valence electrons, prefer to sit on the ends of the three-atom chain so they can bond to the chain and neighboring icosahedra via 4 sp^3 bonds. Since the boron atom in the middle of the chain has two bonds, but three valence electrons, it donates its extra electron to the electron-deficient icosahedra to preserve charge neutrality in the material, and also strengthen bonding in the cage structure.[4]

However, because boron and carbon are similar in atomic size and weight, they can substitute one another out in the structure, leading to many possible stable structures for boron carbide. This issue is further complicated by the fact that instruments are not able to discern individual atoms in a sample, and thus cannot fully distinguish between boron and carbon

atoms.[4] Alternative structures of boron carbide, as well as varying compositions of boron carbide, will be discussed in detail in later sections.

2.1b. The B-C Phase Diagram

Boron carbide is much more than simply B_4C (20 at. % C). To best understand boron carbide, it is wise to consult the B-C phase diagram, to better understand the conditions under which these two elements exist as a homogeneous material. There have been several noteworthy attempts to investigate the boron-carbon system, and, while a wide variety of possibilities exist, it is clear that, taken all together, there is a clear overlap where there seems to be a good understanding of the material.

Due to the higher purity of their starting constituents, Elliott's [19] phase diagram is generally believed to be one of the more accurate and reliable phase diagrams, and will be the main phase diagram referred to in this dissertation. It is also supported by Khan et. al., who recently reviewed amorphization in boron carbide and offered suggestions to improve the material through various elemental doping.[20] Elliott states that boron and carbon exist as boron carbide as a homogeneous mix from 9-20 atomic percentage carbon.[19] This diagram can be seen in Figure 3. Within that range, boron carbide exists as a solid solution of boron and carbon atoms, while still adhering to the general 15-atom unit cell consisting of 12-atom icosahedron connected by 3-atom chains.

Technically speaking, the material can only exist as a 15-atom unit cell at either 20 at. % C ($B_{12}C_3$; B_4C) or at 13.3 at. % C ($B_{13}C_2$), and any other specific composition between 9-20 at. % C is a mix of differing unit cells, some of which would have to include vacancies to accommodate other amounts of carbon. Additionally, past these homogeneity range limits, boron carbide exists with either excess boron or carbon in the matrix, respectively.

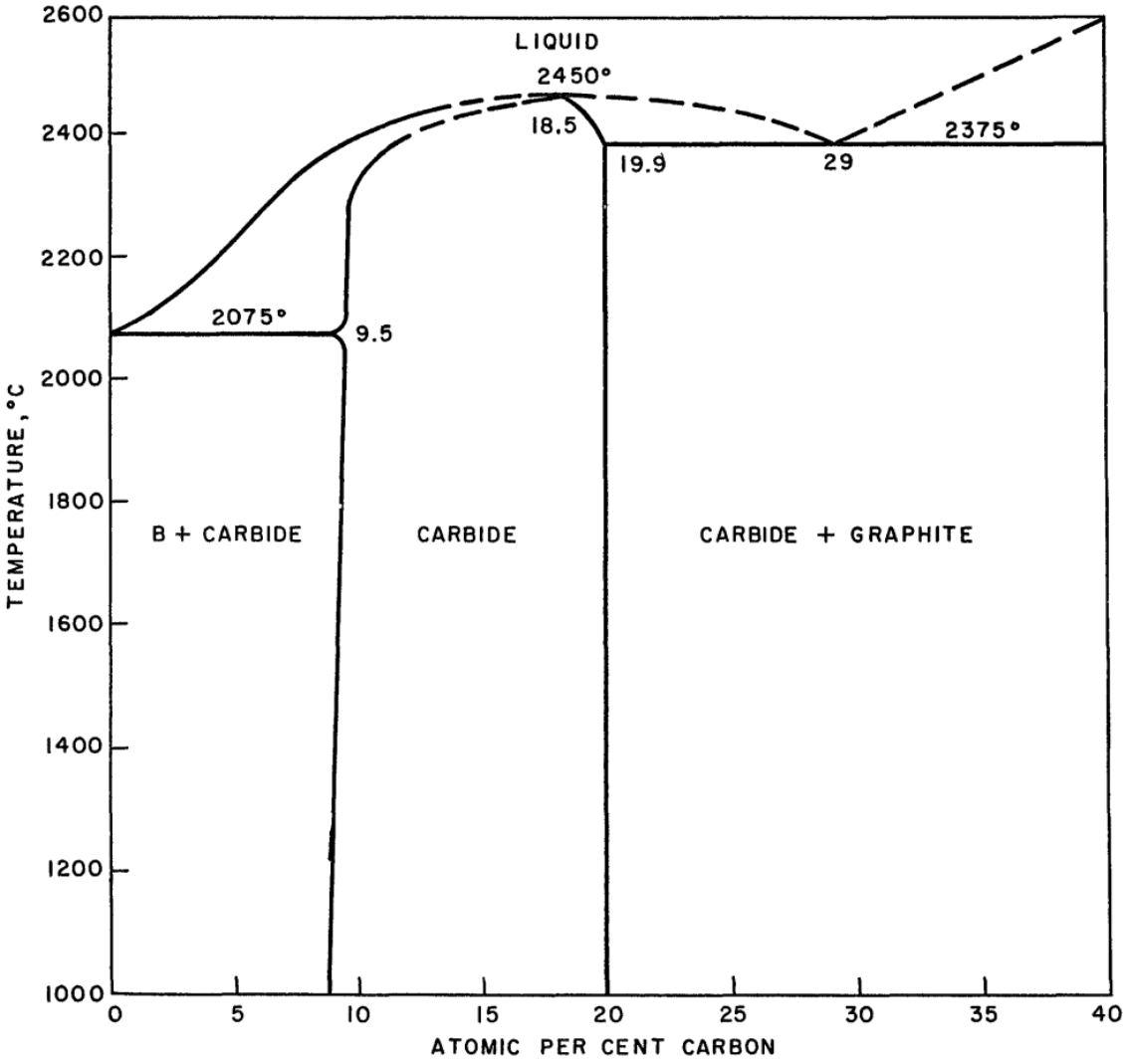

Figure 3: The boron-carbon phase diagram.[19]

Other reports agree well with the existence of boron carbide between the limits of 9-20 at. % C; their works instead have slightly differing ideas about the boron- and carbon-rich limits of the homogeneity range.[21-27] Some debate that the boron-rich limit exists slightly below 9 at. % C [22], and others say the carbon limit can exceed 20 at. % [24], and can even vary slightly based on processing conditions [24], while others say the limit is below 20 at. % C [26], corresponding to a maximum B/C ratio of 4.3.

The phase diagram in Figure 3 shows that boron carbide can exist with a larger B/C ratio of 4. Assuming a boron carbide with approximately 9-10 at. % C, the corresponding B/C ratio would be approximately 9. This allows for more boron-rich boron carbides to exist, which will be discussed in detail in later sections of this literature review.

2.1c. Structural Variations and Polytypism in Boron Carbide

Boron carbide is a complex material. The structure is complex, and this is further compounded by the atoms that comprise it, which are similar in size and bonding nature. This allows for boron and carbon atoms to have the ability to substitute one another in the structure at random, raising questions as to the "true" structure of boron carbide (B_4C). Furthermore, no physical structure is perfect, and will always have defects of various origins, especially vacancies. Defects can play a large role in determining boron carbides structure and properties, and it is also possible that not every unit cell is comprised of 15 atoms. This problem becomes even more complicated still when Elliott's [19] is considered, and the material is more boron-rich, giving the material a wide range of B/C ratios, ranging between 4 and 9. This section discusses structural disorder present in boron carbide and demonstrates how difficult it can be to fully understand any given material that is looked at. This problem has so many aspects to address, some researchers presume that each boron carbide material made must be considered on its own. This is because any variation introduced at any time during processing can result in an effectively different sample, and that differing samples can behave and exhibit properties as if it is a different material altogether.[28]

Looking at stoichiometric B_4C, which is be expanded out as $B_{12}C_3$, there are several ways boron carbide can assume this empirical designation. These differing structures with the sample reduced formula are called polytypes. Tallant suggests that $(B_{11}C)CBC$ and $(B_{12})CCC$ can both exist as stable polytypes of boron carbide.[18] Others have since confirmed this.[6-8] Taking

these possibilities further, the ($B_{11}C$) icosahedra can assume a carbon atom in either a polar or equatorial site, giving further designations to the cage structure as ($B_{11}C_p$) or ($B_{11}C_e$), respectively. For chain variations, CBC and CCC structures are possible, depending on whether or not a carbon atom resides in the icosahedra. The most stable and abundant polytype of boron carbide is ($B_{11}C_p$)CBC.[6, 8] All of this assumes that boron carbide is a perfect 15-atom unit cell without vacancies, with no chemical variation, and keeping its assumed 12 boron atoms and 3 carbon atoms. In a given material, all of the above B_4C polytypes are all possibilities within the same sample, in addition to any defect or non-stoichiometric variation of boron carbide also being present to some extent, as there is much variation from unit cell to unit cell.

Going to more boron-rich stoichiometries in the B-C system, the possibilities of unit cell variations increases further still. In addition to all the previous possibilities for B_4C, the $B_{13}C_2$ configuration presents its own set of stable polytypes. Typically, a (B_{12}) cage is to be expected, and a possible chain structure for that can be CBC. If a cage is ($B_{11}C$), a CBB chain can be present. As before, in the range from 10-20 at. % carbon, boron carbide is a homogenous solid solution of boron and carbon atoms, so carbon contents other than exactly 20 at. % (B_4C) or 13.3 at. % ($B_{13}C_2$) can be realized by more unit cells having vacancies in them. 10% of unit cells are expected to be chainless in standard boron carbide to begin with, which gives a B-V-B chain, where V is defined as a vacancy.[29] So any B/C ratio between 4 and approximately 9 can be achieved with a blend of different unit cells, all having different configurations, stoichiometries, and defects to end with the resultant characterized ratio.

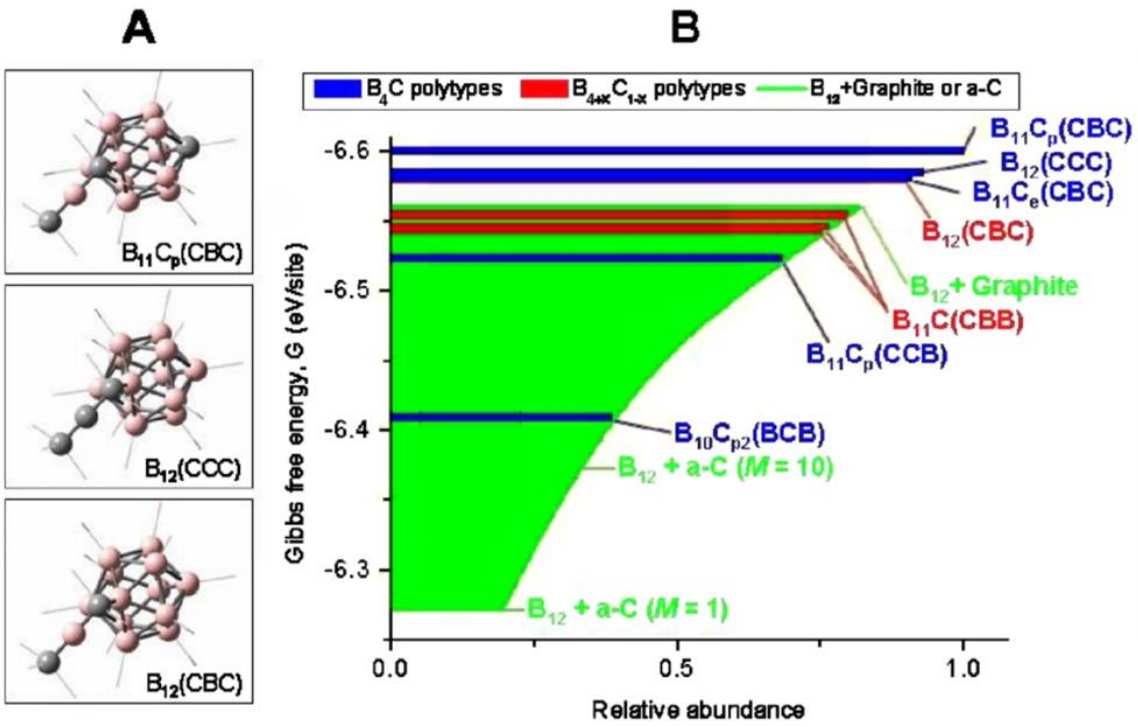

Figure 4: Three variations of boron carbide (left) and relative abundancies of various B_4C and $B_{13}C_2$ polytypes (right).[6]

Figure 4 shows Fanchini's work illuminating several possible variations on boron carbide, for both stoichiometric B_4C and boron-rich boron carbide polytypes.[6] It is important to keep in mind that with any given sample of boron carbide, any and all of the above-mentioned possibilities can exist in the same sample. It is surmised that hundreds of stable polytypes exist for boron carbide, and even processing conditions have an effect on the resulting material, in relation to which polytypes are more prevalent.[4, 30, 31]

2.1d. Raman Spectra of Boron Carbide

Raman spectroscopy is a technique used to identify vibrational modes within crystalline materials. The surface of a material is probed with a monochromatic energy source, and that light interacts with electrons in the sample. This excites the electrons to a virtual, higher energy state, and when they drop back down to their initial state, a new photon is released. Excitations result in vibrations and rotations of molecules. This inelastically scattered energy is collected

and the difference between this and the initial energy of the laser is measured as the Raman shift. Inelastically scattered light is collected, usually as the energy lost by exciting the electron, and this is called the Stokes shift. If the outcoming photon has a higher energy than the initial laser source, this is called the anti-Stokes shift, although this occurrence is much less common, and stronger more intense signals are gathered from the Stokes shift, where one is measuring the energy lost from the initial source. The energy shift is measured in units called inverse centimeters (cm^{-1}) and probes a region ranging from 100-5000 cm^{-1}.

For ceramic materials, Raman spectra can show varying intensity of features, depending on grain formation aligning as a result of sintering pressure directionality.[32]

Raman spectroscopy was crucial to completing the work in this dissertation, because of its quick, non-destructive method of quickly probing a material, where, coupled with the literature, quick conclusions can be drawn as to the relative structures of varying boron carbide samples. Raman spectroscopy also allowed for various in situ experiments to be carried out, where phase changes can be measured as they are responding to changing parameters such temperature and pressure.

Since Raman spectroscopy is so important to this dissertations work, a detailed analysis of the Raman-active modes of experimentally produced boron carbide will be discussed here.

Boron carbide, like all other Raman-active materials, exhibits a unique Raman spectra that gives information about bonding within the material. For boron carbide specifically, a unique spectral fingerprint is seen between 200-1200 cm^{-1}. The penetration depth of the Raman laser is thought to be approximately 5 um for polycrystalline boron carbide.[33] These peaks give information on the icosahedra ad chain structure in the material, so that, when experiments are carried out in situ, I am able to discern how the material is being effected as external parameters are varied, and which structures within boron carbide are more susceptible

to change or deform. What will be discussed here is the most basic experimental spectrum seen for boron carbide (B_4C). This spectrum is also very representative of the material, regardless of any structural variation or polytypism that will be present in an experimentally made material, as was mentioned in the previous section of this dissertation. As this dissertation delves more into changing and tailoring the boron carbide structure, and identifying failure-related phases in the material, sub-sections discussing their resulting Raman signatures will be addressed there, and this section will remain focused on the Raman data representing standard B_4C.

Since Raman spectroscopy consists of broad and narrow peaks, it is good to note that broader peaks represent modes and features that are slightly more amorphous or disordered, compared to more crystalline structures yielding sharper peaks. So, broader peaks seen in boron carbide are a direct result to the structural variation, disorder, distortions within the material, and polytypism that comprised the previous section of this dissertation. An image of nominal B_4C's Raman spectra is shown below in Figure 5 and will be further elaborated on in the proceeding text.

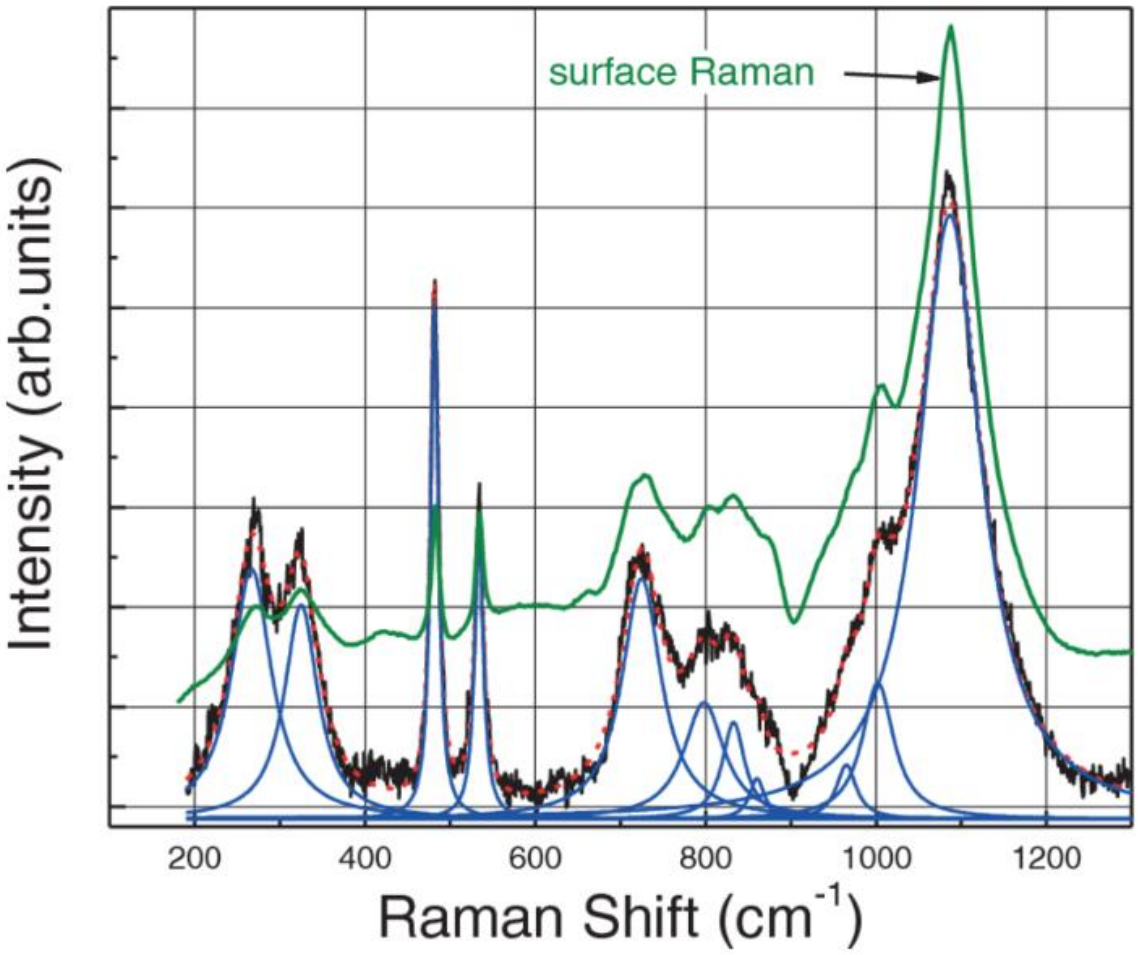

Figure 5: Representative Raman spectra of B_4C. Deconvoluted constituent peaks are shown in blue.[34]

The doublet first found at 270 and 320 cm^{-1} still has an unknown origin.[4] Theoretical studies predict no boron carbide peaks below 360 cm^{-1} [35, 36], yet these features are always seen experimentally, and have been confirmed by multiple laser sources, although they vary in intensity depending on the incident beam energy. Werheit [33, 37] denotes these as evidence of chain rotations, from either CBC or CBB chains, and supports their stance with modeling by Shirai and Emura [38]. Conversely, Vast [36] and Lazzari [35] believe these peaks are a result of disorder-induced acoustic phonons. However, it is important to note that this is in conflict with the fact that these peaks were shown to exhibit anti-Stokes spectra.[33] Additionally, these peaks are seen in not only hot pressed material, but single crystal B_4C as well.[4] This brings into

question both the importance of defects inherent to the boron carbide structure, and the resulting effects on its observed properties and material performance, but also brings into question whether or not single crystals truly exist in such a complex structure.

Two peaks also observed together at 480 and 530 cm^{-1}.[4] These peaks have been initially designated as modes predominantly relating to the chain structure.[18] The 480 cm^{-1} mode is due to chain rotations about an axis [18, 35], but it is generally understood that this peak is relevant to the chain structure in B_4C. More specifically, that peak denotes a CBC chain. The peak seen at 530 cm^{-1} has a varied history, with Lazzari [35] and Vast[36, 39] noting this features relevance to the icosahedra's liberation mode, similar to what is seen in α-boron, in contrast to claims by Tallant [18] and Aselage [40] that is denotes a chain-related peak.

A pair of peaks found at 720 and 740 cm^{-1} are never discussed much in literature, but nonetheless are seen in experimental boron carbide spectra. They are lower in intensity and could be a result of surface scattering. However, they do show a similar pressure dependence and intensity change to the 480/530 cm^{-1} pair, noted by Hushur et. al. [34], who studied $B_{4.3}C$ single crystals under pressure, due to their relevance to semiconductor applications.

Raman peaks are lastly seen in the region of 900-1100 cm^{-1}. The most prominent peak in the spectrum is located around 1080 cm^{-1}, and it is well established that this peak pertains to the breathing mode of the icosahedra, or the icosahedra breathing mode (IBM).[4] A large shoulder can be seen on the left side of the IBM peak, and can be comprised of smaller peaks, with some variation expected. A small contribution can come from a small peak at 950 cm^{-1} as a result of surface or bulk defects.[35] All peaks seen in this region (above 600 cm^{-1}) are well established as varying icosahedral peaks.[4, 18, 36, 40]

This explains the Raman spectra seen in boron carbide. Regardless as to the exact nature of boron carbide, these peaks are experimentally seen where a mix of polytypes should

exist in an experimental material. Thus, whether a ($B_{11}C$) or (B_{12}) icosahedra exists, peaks representing the cage structure remain unaffected. This is also true with chain structures, which can exist as CBC and CBB, and their associated Raman peaks. As a general rule of thumb, one can generally assume that Raman peaks below 600 cm^{-1} are related to the chain, while peaks observed above that are belong to icosahedral-related modes.[18]

This assumption comes from looking at the α-boron raman spectra, where only boron-boron bonds exist in a rhombohedral structure. It was be deduced that most rhombohedral borides will have similar peaks, albeit with some atomic substitutions. α-boron has peaks from approximately 600-1200 cm^{-1}, an only comprises boron clusters without chains present, so it is believed that these peaks are associated with icosahedra modes in similar materials. Newer peaks seen in similar rhombohedral borides come from other atoms being present, usually in a connective chain structure, which is seen with boron pnictides and boron carbide. It is with this information that any peaks below 600 cm^{-1}, in boron carbide specifically, are assumed to be related to the chain structure.[18]

Again, as boron carbide is discussed in greater detail as this dissertation progresses, and doped boron carbides and amorphous phases of boron carbide are brought into play, those sections will also address the changes or new spectral information given by Raman spectroscopy.

Raman Spectra Peak List	
Peak (cm^{-1})	Possible Origins
270/320	Chain/ Disorder Phonons
480	Chain
530	Chain/Cage
700s	Unknown
1080	Icosahedra

Table 1: Raman spectra listed by peak position along with their most likely origin noted in literature.

2.1e. Limitations of Boron Carbide in Ballistic Performance

In 1994, Grady evaluated high temperature ceramic materials on their performance under shock-wave loading techniques.[1] The findings were also published in subsequent reports.[41, 42] When subjected to shock loading, boron carbide shows a very different response than comparable ceramics, a primary example being silicon carbide. Both are ceramics with high hardness and high Hugoniot limits, so both are expected to perform similarly in the same experiments.

The boron carbide used here has a grain size of 3 um and a density of 2.50 g/cm^3, so a 1% porosity is assumed. Since this sample has porosity, as it does not have a 100% theoretical density, some degree of structural variation or substitutional disorder from the last section can be assumed here.[1]

A projectile gun is used to impact samples with a maximum projectile velocity of 2.5 km/s, and a backing plate is composed of either the same material being studied, or a high density metal.[1]

Figure 6 shows the elastic precursor wave responses of silicon and boron carbide, respectively. While boron carbide can withstand a higher Hugoniot limit of 18-20 GPa, corresponding to an impact of 0.7-0.8 km/s, compared to silicon carbides 15 GPa, allowing a

0.55 km/s impact, boron carbide exhibits a post-yielding softening mechanism which drastically hinders the materials performance from that point on in the study. The Hugoniot elastic limit is defined in this study as the break in the slope, past which the material shows some aspect of work hardening/softening.[1]

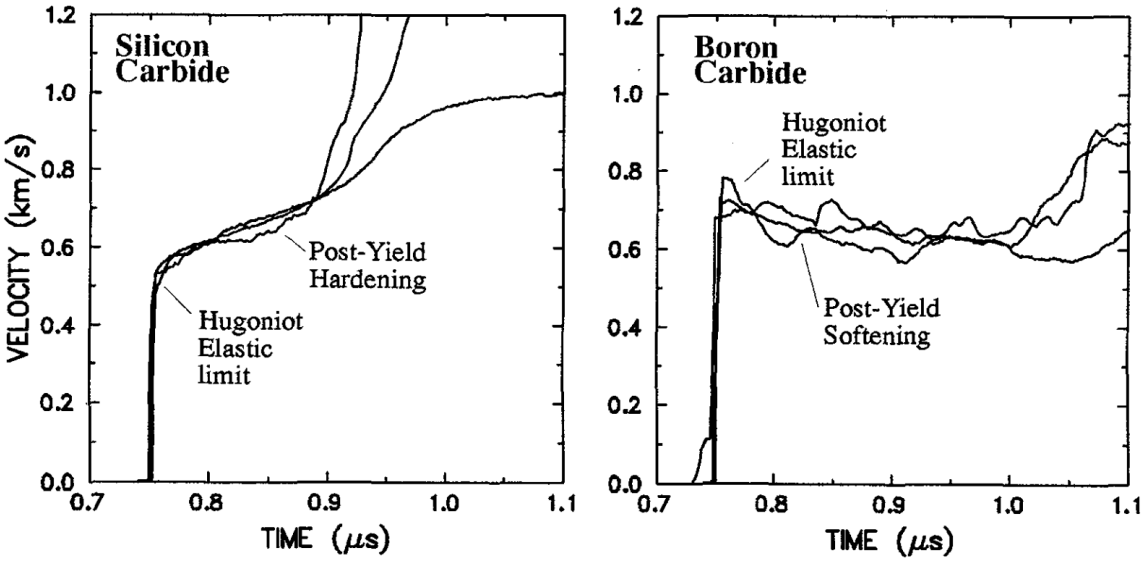

Figure 6: Elastic precursor shock-wave profiles for silicon carbide (left) and boron carbide (right).[1]

In further investigating boron carbides post-yield softening, it is also found that boron carbide has a lower shock velocity than its bulk velocity, and it is suggested that the material has no shear strength at the Hugoniot state. Boron carbide also shows a large increase in its compressibility past the HEL, again pointing to a dramatic loss of shear strength for the material. This would be a critical deficit for boron carbides applicability in defense applications.[1]

Further elucidating boron carbides failure, an enhanced volumetric compression can be expected. This increased lattice compression can occur under shock-impact due to its more open lattice structure. This also brings up the possibility that a possible phase change can occur if the volumetric compression is large enough. A heterogeneous deformation process is also observed on the mesoscale, which in turn brings up the possibility that a micron-level deformation process can coalesce in discrete localized zones as a result of possible melting.[1]

All of these ideas are precursors to first discovering “amorphization” in boron carbide, as a means to identify what is causing boron carbides anomalous performance in dynamic impact testing. Amorphization will be discussed in extravagant detail in the following section (Section 2b) of this dissertation.

2.2. Amorphization of Boron Carbide

This section is dedicated to amorphization in boron carbide (B_4C). Amorphization is commonly understood as the main instigator behind boron carbides failure and lack of strain-hardening after a high-velocity impact. Amorphization refers to localized nano-meter sized bands in the material that lack structure, and hence, are amorphous. There is not a fully comprehensive understanding of amorphization. Many aspects of it, such as its atomistic-mechanism and conditions under which amorphization occurs, are still highly debated and studied, to the extent that it can be described as seemingly different phenomena when viewed through different lenses. There are several ways this “amorphization” occurrence can be stated, and such terminology was used throughout the literature and will be used throughout this thesis as well. Such terms and terminology for amorphization can be read interchangeably as: a transition to an amorphous phase/phase transformation, structural disorder/collapse/destabilization, a loss of crystallinity, and even as a meta-stable high-pressure phase.

2.2a. Origins and Characteristics of Amorphization in Boron Carbide

Several groups were circling around discovering amorphization in boron carbide in the early 2000s. These different studies were completed around the same time, but were done in very different ways, although they both concluded that amorphization was occurring in boron carbide under similar loading instances.

Structural changes in boron carbide were first observed within indented areas of (0001) and (10-1-1) single crystal $B_{4.3}C$ by Domnich et. al.[43] Nanoindentation was used to measure hardness and moduli, but post-indentation Raman spectroscopy revealed that vast damage and possible structural changes were occurring beneath the indented regions.[43] The load-displacement curves from indentation showed no noteworthy features that could be indicative of slip systems activating or phase transformations taking place to explain what was happening. This is in stark contrast to what is seen with similar materials, where such transformations show a marked difference in corresponding load-displacement curves.[44]

New bands in the Raman spectrum appeared between 1200-1900 cm^{-1}, predominantly at 1330 cm^{-1}, with a weaker shoulder observed at 1520 cm^{-1}, and a hump at 1810 cm^{-1}. Peaks at this frequency are not expected to be seen in boron carbide, nor elemental boron. These features have been observed with multiple laser sources in order to confirm their existence, and to rule out the possibility of them being a fluorescence effect from a specific laser wavelength.[43] Images of pre- vs. post-indented boron carbide Raman spectra can be seen in Figure 7.

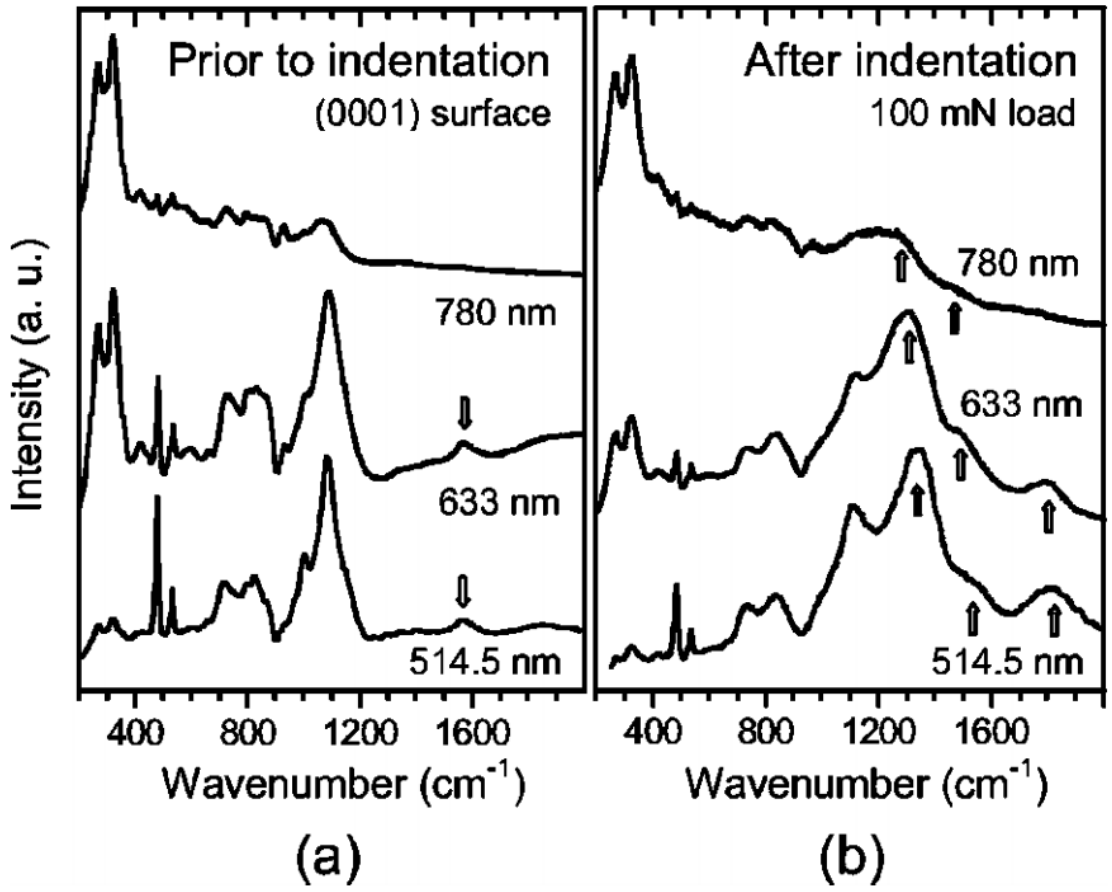

Figure 7: Raman spectra of $B_{4.3}C$ before (a) and after (b) 100 mN indentation at several excitation wavelengths.[2]

Ge *et. al.* followed Domnich's initial study with a more comprehensive look into a possible phase transformation in boron carbide as a result of high-pressure instances. This transformation was observed as a result of contact loading, depth-sensing nanoindentation, and scratching techniques, all of which were confirmed with high-resolution TEM imaging.[45] It is in this work that the formation of a high-pressure amorphous phase was first formally stated.

The initial explanation offered for the new Raman peaks are described as being a result of carbon clusters or aromatic rings coming from the disordered carbon-rich chain structures. This also explains their similar positioning relative to graphitic carbon's D- and G-bands, at 1350 and 1590 cm^{-1}, respectively.

TEM imaging underneath indented and scratched specimens revealed local disordered regions consisting of amorphous material. Also observed were features relating to lattice shearing and deflection, as well as nanocrystalline features. Electron energy loss spectroscopy (EELS) showed no chemical deviations within the disordered regions, compared to the crystalline boron carbide regions. This implies that no chemical reaction is taking place as an instigator or result of amorphization, and that the resultant bands are still comprised only of boron and carbon.

Nanoindentation was used for its similarity to impact conditions, where the indentation is capable of reaching initial contact pressures of 40 GPa.[45] The formation of nanoscale amorphous bands are believed to be a result of deviatoric stresses facilitating a high pressure phase transition. This phase forms to accommodate shear strains in the material after the loading or scratching. Since no distinct changes occur in the nanoindentation load-displacement curves, it is believed that the material exhibits a purely elastic loading and unloading response. The orientational preference seen with amorphous bands could be a result of the lattice having a limited number of dislocation slip systems.

Concurrent to these studies, Chen et. al. was doing TEM investigations on boron carbide fragments that were recovered from ballistic impact testing. Boron carbide was subjected to ballistic testing to determine if the material showed a softening or melting of some sort under shock loading. Postmortem boron carbide fragments were studied using high-resolution transmission electron microscopy (HR-TEM).[3] It was found that projectiles with a large enough impact velocity were causing a phase change in the boron carbide fragments. In addition to the expected cleavage during fragmentation, and planar defects found on the specimens, there were damage zones consisting of nanoscale-sized bands of amorphous material.[3] This was confirmed by TEM because the bands did not yield a diffraction pattern, instead showing a

diffuse halo, an observation indicative of amorphous material. This was the first time such a mechanism was imaged in boron carbide. The images are shown below in Figure 8. The bands were shown to be a few nanometers in width, but hundreds of nanometers in length.

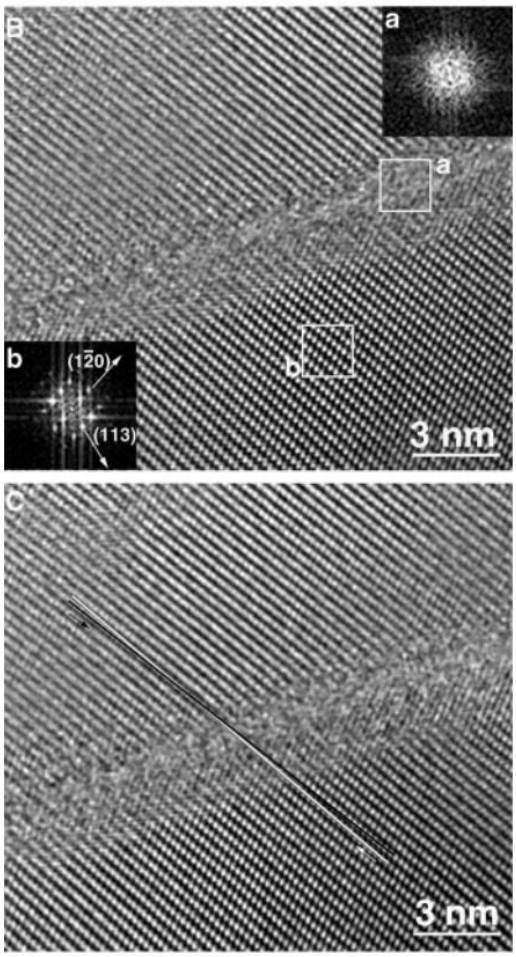

Figure 8: High-resolution microscopy images of an amorphous band in boron carbide. In the top image, the (a) and (b) regions show amorphous and crystalline diffraction patterns, respectively.[3]

The critical impact velocity was approximately 850 m/s. So, an impact velocity of 907 m/s, correlating to roughly an impact pressure of 23.3 GPa, yielded amorphous bands in postmortem characterization. However, an impact velocity of 793 GPa, correlating to 20.3 GPa, did not show the formation of any bands.[3] This critical impact pressure needed to form amorphous bands agrees well with the established Hugoniot limit of nearly 20 GPa, past which boron carbide is expected show decreased ballistic performance.

Once again, the amorphous bands did not show a composition change with electron energy loss spectroscopy (EELS) measurements, so it is not believed that a chemical reaction is taking place. Chen also ruled out the formation and rebonding of cracked surfaces and saw no evidence of melting. This means that this was a solid-state phase transition as a result of the high-impact ballistic event. Chen also saw that the bands had an orientational preference, as is also the case with twins and stacking faults in boron carbide. The bands aligned with the (-101) direction. Dislocations can also form to accommodate the amorphous phase. A 1° lattice displacement was also seen around the amorphous regions. This can also support the claim that a phase change is occurring, and that the crystalline phase transitions into a more dense amorphous phase. This is an anomalous finding for an amorphous phase, which are typically less sense, and is similar to that seen in silicon dioxide and ice.[46, 47] In specimens below the critical impact velocity, where no amorphous bands were seen, they instead saw a high degree of stacking faults and microtwins present.

All of these earlier works [2, 3, 45] were crucial to discovering and characterizing amorphization in boron carbide. While the means to induce amorphization in the different studies varied, all surmise that amorphization is more of a direct result from the pressures reached during the indentation or impact. All works are in agreement that the bands do not have a different chemistry than the starting boron carbide, and interestingly, both cite a still-unpublished work by Manghnani that states that boron carbide undergoes a phase change at 20 GPa. This idea was initially thought to be important to understanding amorphization at the time, but the work remained unpublished and otherwise unverified, although some works still point to it being a possibility that warrants further investigations.

2.2b. Experimental Observations of Amorphization in Boron Carbide

In the years since amorphization was first observed in boron carbide, there has been a considerable amount of research done to understand more about this phenomenon. There are many ways that amorphization can be induced in boron carbide, and there are many experimental observations detailing the extent of amorphization as a result of those occurrences.

Boron carbide was studied under plate-impact conditions, with different forms of shocking, reshocking, and shock-releasing.[28] It was shown experimentally that boron carbide fails when the HEL limit is exceeded, where the HEL is defined as the point where the material just begins to yield. Unlike silicon carbide and aluminum nitride, B_4C shows no form of strengthening past this limit. In all instances of plate-impacts past the HEL, boron carbide fails, and as such, no data for intact strength beyond this point exists due to the materials failure. A phase change is believed to be occurring to account for this loss of strength past the critical HEL.[28] Boron carbide also exhibits a very large elastic anisotropy, which can contribute to the material fracturing during ballistic testing.[32]

Raman spectroscopy was carried out on amorphized boron carbide by Yan et. al. at elevated temperatures.[48] Pressure-related amorphization was induced by Berkovich indentation, predominantly on single crystal (223) single crystal B_4C.[48] It was noted that a higher intensity of the amorphous Raman signal was seen at the center and corners of the indented area as a result of higher contact and shear stresses from the indenters tip and edges. Early on, boron carbides amorphous phase was thought to consist of D- and G-band carbonaceous features, due to the presence of carbon in the material as well as the overlap of the amorphous boron carbide peaks with the D- (1330 cm^{-1}) and G-bands (1550 cm^{-1}) of carbon. Carbon bands at those frequencies are denoted for their features relating to sp^2 carbon

aromatic rings, as well as C=C double bonds, which are found within aromatic rings.[2, 48] This lead to the belief that since no chemical reactions were taking place as a result of amorphization, the cause of the amorphous bands and new Raman peaks could be explained by a collapse of the C-B-C chain structure, as they predominantly consist of carbon atoms.[48] The boron present in the chains are believed to be able to substitute into the aromatic rings, and also explains a lack of Raman-active peaks relating to any form of boron (α-boron, β-boron, or amorphous boron). Yan's explanation is insightful because boron carbide is predominantly composed of boron, yet no boron peaks are observed during structural collapse. Thus, relating collapse to mainly carbon-based chains was helpful early on.

The boron carbide sample was analyzed with Raman spectroscopy at temperatures between 83 and 873 K. At elevated temperatures (approx. >600 K) the amorphous signature disappears from the Raman spectrum. This can be seen in Figure 9. This is likely due to a sufficient level of thermal energy to allow the structure to recrystallize. It is important to remember this finding later when other literature details the thermal energy released in boron carbide as a result of pressure or ballistic impacts.

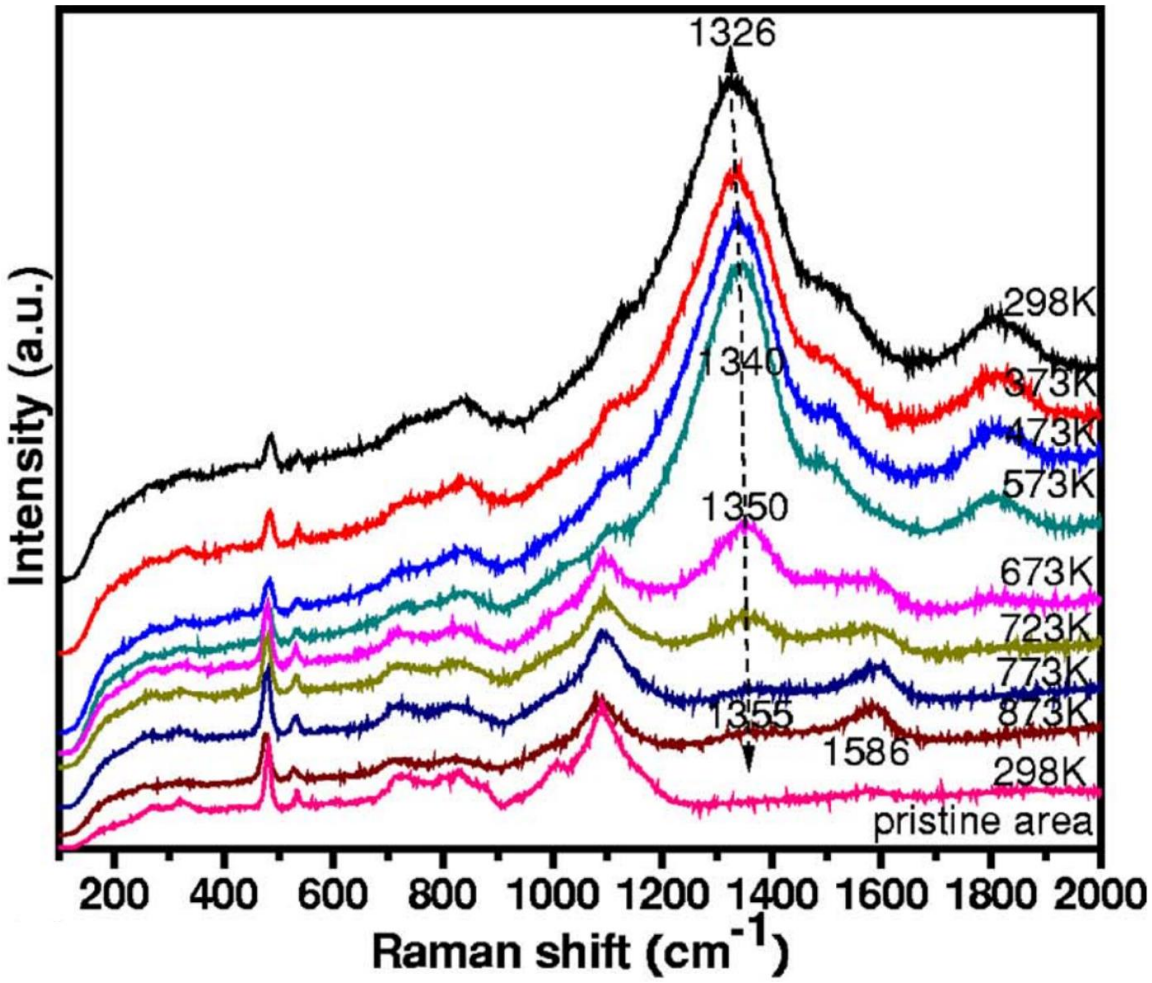

Figure 9: Raman spectra of B_4C from room temperature to 873 K.[48]

In addition to mechanical methods of inducing amorphization, like indentation and scratching, which were previously discussed, it was observed that a sufficiently large electric field can cause a similar phase change in boron carbide.[49] Boron carbide can also be amorphized by means of laser shock compression [50] and radiation [51].

In studying amorphization as a result of indentation techniques, the amorphized zone created by a Vickers indentation is approximately 7 times larger than the indentation depth itself.[52] This was the result of a study where the depth of the amorphous zone was determined as a function of incident indentation load.

It is theorized by Subhash et. al. that the amorphization process begins when the indenter makes initial contact with boron carbide. The sharp tip initially creates a very high pressure on the material, causing structural collapse which then penetrates and continues into the sample as the indenter imparts its load into the weakened amorphized boron carbide.[52] Indentation is used because the pressure created is similar in magnitude to the HEL of boron carbide, which is sufficient to induce and study amorphization in boron carbide without requiring a ballistic or dynamic impact.

Up to this point the amorphous zone created by an indentation has not been studied, and in this study the spatial distribution and intensity of the amorphous zone created by Vickers indentation is determined.[52] This was done by inducing amorphization in boron carbide via indentation, and subsequently mapping the indented area with Raman spectroscopy. The amorphized zone beneath an indentation was determined by successive polishing steps to remove sub-micron-level amounts of material and mapping the newly exposed subsurface. Registration indents were used to determine the depth removed at each successive step.

This work also states that the maximum intensity of the 1330 cm^{-1} amorphous peak is not at the apex of the indentation, but rather slightly below the surface, and then diminishes at greater depths. There is also a correlation between indentation load and the size of the amorphized zone created by it. As the indentation load increases, the amorphized zone created by the indentation also increases. It is also seen that the maximum intensity for the 1330 cm^{-1} peak is approximately the same for different indentation loads, which agrees with Hertzian contact theory, which states that self-similar stress fields exist from Vickers indentation, irrespective of the indents depth or load. This means that the amorphization intensity would be approximately the same at a given depth regardless of the indentation load used.[52]

At a load of 4.9 N, an amorphous zone approximately 8 um deep is created in standard boron carbide. Initially, the width of the amorphous zone is almost that of the indentation size, but reduces conically beneath the surface.

It is believed that the critical stress to cause amorphization is much greater than the stress required to begin plastic deformation.[52] The amorphized zone is also thought to be much smaller than the presumed size of the plastic zone for boron carbide.

Tabor defines hardness as a materials resistance to a localized permanent deformation.[53] Taking the assumption that the indenter tip amorphizes boron carbide, and the indentations load and penetration pushes this into the material to nucleate and propagate, it is believed that with Vickers and Berkovich indenters, the true hardness of boron carbide is never actually measured. Instead, this paper postulates that the hardness of the amorphized material is being measured, and that the true hardness of crystalline boron carbide would be greater, if it could be measured without inducing amorphization.[52]

Confinement stresses from the material and the indenter also account for the large shear stresses caused by indentation, which can also aid in the formation of amorphous bands. Without confinements under pressure, as with uniaxial compression, plastic deformation happens through defect modes such as twinning and stacking faults.[3, 52, 54]

In a subsequent study by Parsard, 3D models of amorphized material beneath indentations were made using Raman spectroscopy.[55] This was done by inducing amorphization in boron carbide via indentation, and subsequently mapping the indented area with Raman spectroscopy, similar to the previous study.[52] The 3D volume of the amorphized zone was determined by successive sub-micron polishing to remove material, and re-mapping the new surface. Registration indents were also used to determine the depth removed at each

step. It is suggested that amorphization can activate from von Mises stresses above 6.6 GPa and equivalent plastic strains above 0.026.[55]

The fact that amorphization only occurs beneath the indentation in a localized region confirms amorphization requires high levels of stress to occur. The amorphous signature does not surpass the limits of the indentation imprint, regardless of whether the indentation was quasi-static or dynamic; surrounding crystalline regions always yielded a crystalline Raman spectra. It is also seen that the amorphized zone is larger with increasing indentation loads, which is expected, and that strain rates do not have a large effect on the depth of the amorphous zone.

Figures 10 and 11 show an example of a 1 N load indentation is used to induce amorphization and determine the depth of the amorphized zone created by it, and the process of obtaining Raman spectra from indented boron carbide, and the subsequent intensity maps and 3D amorphized volumes generated from the data, respectively.

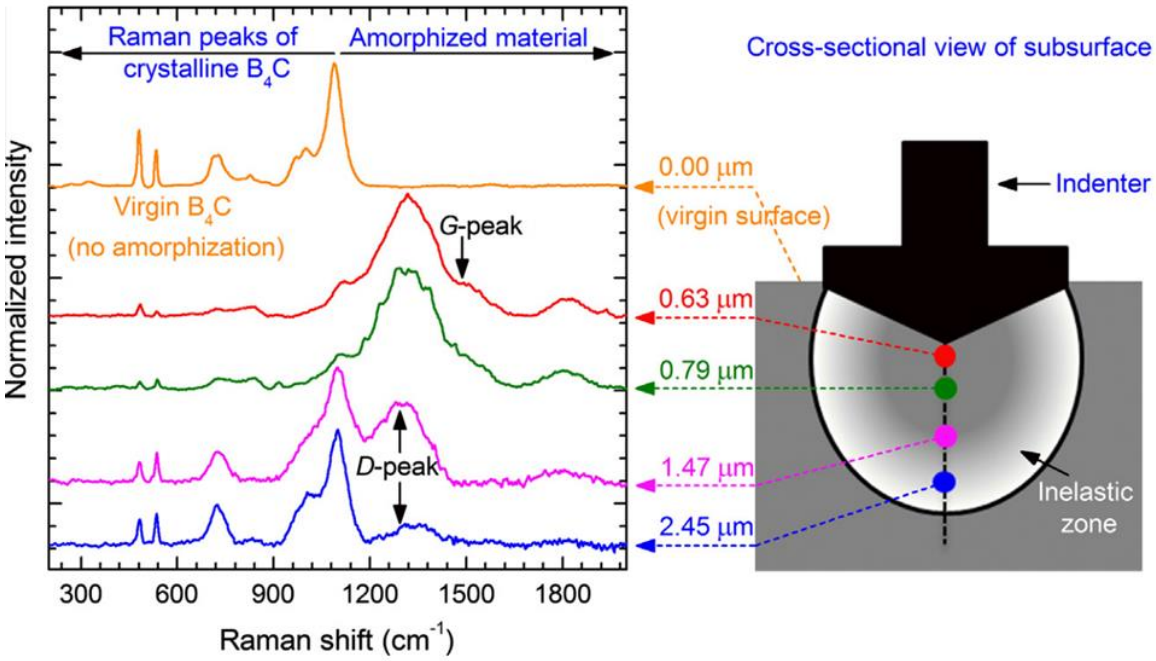

Figure 10: Raman spectra from virgin B_4C (top spectra) and subsurface amorphization from a 1 N indent.[52]

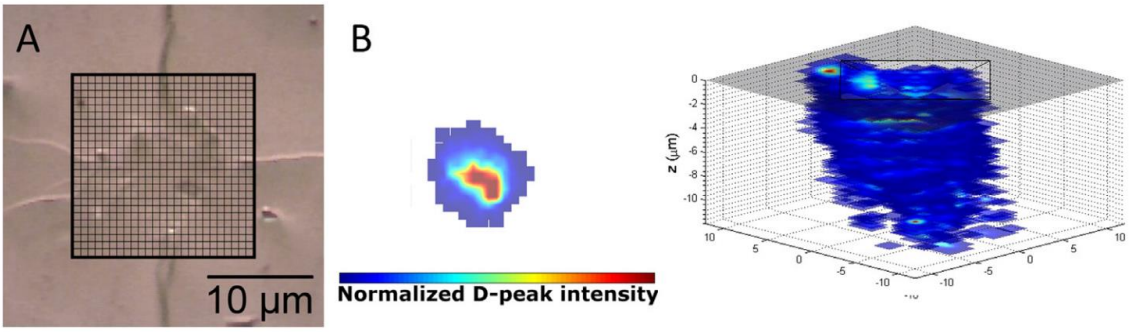

Figure 11: 11(a) shows an optical micrograph of a 5 N indent, (b) shows a normalized pseudo-color map of the indent, and (c) shows the 3D depth profile of amorphized material beneath the indent.[55]

With larger loads, larger indents are placed, creating a larger amorphized volume beneath the material. Past a critical loading point, however, larger crack formation begins to occur, which can alleviate some of the stresses necessary in forming amorphous bands, limiting the extent of the amorphization seen and the volume of the amorphized zone created. The critical loading point observed is at loads greater than 9.8 N, and past this point appreciable lateral cracking is seen in lieu of amorphization. Past this critical point the measured hardness also decreases with increasing indentation load as a result of more energy going towards crack formation and propagation.[15] This alludes to the idea that the amorphized zone resides within a larger zone comprised inelastic damage also associated with the indentation.[55]

In 2013 aberration-corrected TEM was employed by Reddy to study the atomic structure of amorphous shear bands in boron carbide.[56] In theory, for light elements, it is possible to achieve an ultrahigh spatial resolution of 0.1 nm. Cross-sectioned specimens of nano-indented amorphized B_4C were prepared using FIB lift-out procedures and were sufficiently thinned for TEM analysis. Shear bands and micro-cracks are seen, but within the amorphous region there are no voids or gaps observed. Distorted icosahedra are also imaged within the amorphous band, such that a Burgers vector analysis reveals obvious lattice

displacement within the band.[56] The strain that results from this is equivalent to a partial dislocation, thus giving rise to shear displacements. It is also stated that bending of the 3-atom chain can readily bend and deform by means of shear, and, while icosahedra are distorted within the amorphous band, they are ultimately retained.[56] This study is questionable, in that there is come confusion as to whether the icosahedra are destroyed, or intact albeit distorted, but nonetheless this study provides direct experimental images of the amorphized bands, in agreement with simulated results. Figure 12 shows the simulated and experimental images of crystalline and amorphized boron carbide.

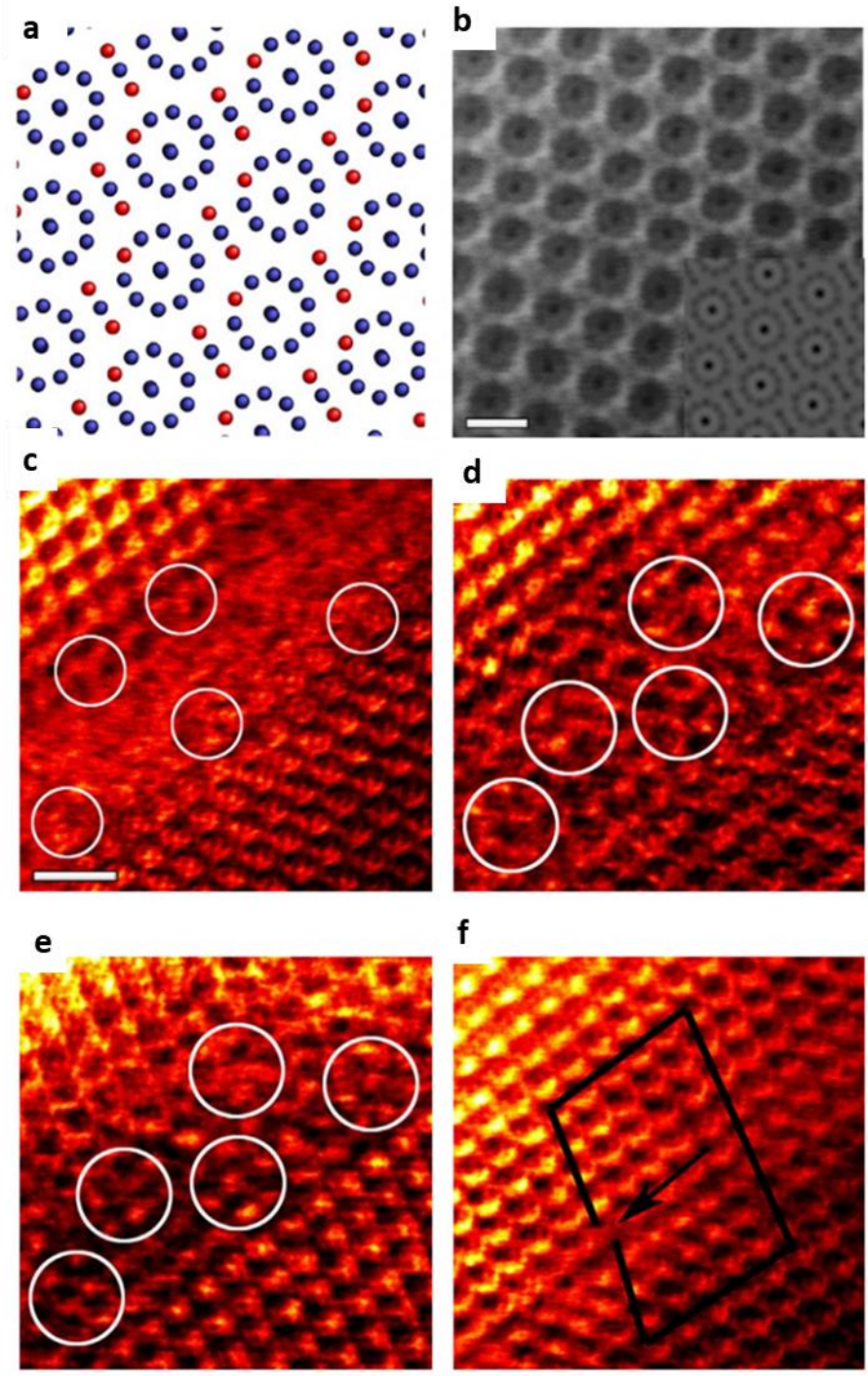

Figure 12: 12(a) Projected atomic structure of B_4C, (b) Experimental ABF-STEM image of B_4C, (c) An off-axis image of displaced icosahedra, (d & e) Images of retained icosahedra, and (f) Shear displacement.[56]

In 2016 Xie et. al. studied the stability of the icosahedra and chains in the boron carbide structure using a laser-assisted atom probe.[57] This high-energy probe was able to atomize a specimen of boron carbide, and atomic-resolution detection can determine which element is being ejected from the structure first. It was found that the icosahedra units were atomized first, and as such, are less stable than the chains, likely due to their electron-deficient bonding. This result was unexpected, but showed the structural integrity of the strong covalently bonded chain units. This information points to tailoring of the icosahedra in boron carbide to address and suppress amorphization in future materials.

2.2c. High Pressure Studies of Boron Carbide

Since boron carbide amorphizes under high pressures, there has been an extensive amount of work done in understanding boron carbides structural evolution under large pressures in situ. To do this a diamond anvil cell (DAC) is used. A DAC is a tool capable of reaching large pressures while still allowing the sample material to be probed as pressure is applied and held. The general working principle is very similar to a pressure-assisted sintering tool, such as a hot press. A DAC is just dealing with much smaller size-scales. Where a hot pressed sample can be on the order of millimeters or centimeters, DAC samples are on the order of 10s of microns in length. Similar to graphite punches, a DAC uses diamonds, the hardest known material, to compress the samples to reach large pressures. Since pressure is defined as a force per unit area, and the area of the diamond tip, called a culet, is so small, only a moderate force is required to generate large pressures during experiments. Pressure can be applied by means of gas pressure, or by a series of screws or levers being tightened or turned. Samples are held in place by a steel ring with a hole drilled in the middle, inside of which the sample is placed, giving the gasket a donut-shaped appearance. Thus, the sample chamber is comprised of the diamond anvils above and below the sample, and the surrounding walls are from gaskets

drilled hole. Pressure is measured by determining the shift of a standard ruby line, something that is commonly used and well understood in high-pressure research. A DAC is used while the sample material is being probed by means of X-ray or Raman techniques to determine structural evolution as the pressure is varied or increased in the chamber. Salt, inert gases, and alcohols are sometimes placed in the gaskets sample chamber with the sample to give hydrostatic loading conditions, otherwise quasi-uniaxial, or non-hydrostatic, loading occurs. DACs have been helpful in studying boron carbide and its amorphization at elevated pressures.

Studies of boron carbide at elevated pressures are useful for applications other than amorphization. This is because at higher pressures, boron carbide can exhibit metallic behavior, and can have applications as a semiconductor or superconductor.[29, 34] At 600 GPa the boron carbide structure is computed to be stable, and the indirect bandgap of boron carbide can fully close, allowing the material to exhibit metallic properties.[29]

Yan et. al. was able to observe amorphization *in situ* in single-crystal boron carbide while unloading pressure in a DAC, after first reaching critical pressures during the loading regime.[5] While boron carbides amorphous signature Raman peaks are found at 1330 cm^{-1}, with a shoulder at 1500 cm^{-1}, and at 1800 cm^{-1}, only the 1800 cm^{-1} peak was considered in this study. This is due to the strong carbon peak present at 1330 cm^{-1} from probing through the diamond anvil, effecting visibility in this Raman spectral range.

In this study Raman characterization was performed as pressure was gradually increased and decreased to and from 50 GPa. During experiments where sodium chloride was used as a pressure transmitting medium (PTM) to achieve quasi-hydrostatic loading, no amorphization was seen during loading or unloading. However, when NaCl was replaced with powdery boron carbide, allowing for non-hydrostatic loading, amorphization was seen during the unloading

regime. The critical loading pressure needed to activate amorphization upon unloading is approximately 25 GPa. If this point is reached or exceeded during loading, amorphization will be seen in the Raman spectra during unloading below approximately 15 GPa. The loading and unloading cycles for hydrostatic and non-hydrostatic loading are shown in Figure 13. This threshold pressure agrees with other literature, and is also consistent with the HEL limit of boron carbide.[3, 52] If higher pressures are reached during loading, a larger degree of amorphization is seen during unloading.[5]

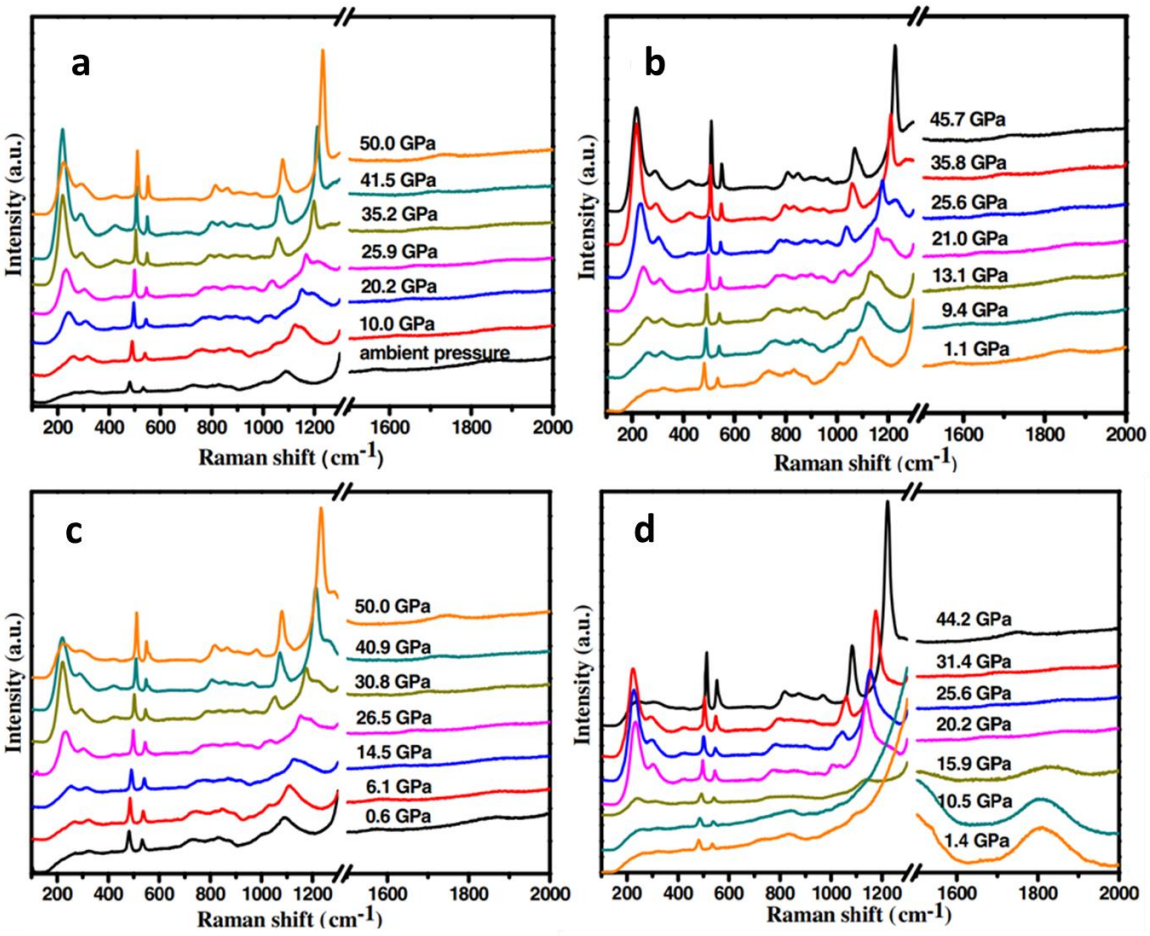

Figure 13: 13(a) shows hydrostatic loading to 50 GPa, (b) shows hydrostatic unloading from 50 GPa, (c) shows non-hydrostatic loading to 50 GPa, and (d) shows unloading from 50 GPa under nonhydrostatic conditions.[5]

It is thought here that amorphization consists of individually nucleated events, not as a continuous transformation throughout the amorphous zone. Amorphization is once again

thought to be the reason behind boron carbides sudden loss of shear strength at high pressures. The DAC experiments carried out by Yan *et. al.* are also in good agreement with boron carbides response to both static and dynamic impacts.[5]

There is a limited amount of literature where boron carbide was studied in a DAC and amorphization was also considered in that study. Shear deformations were applied to boron carbide while the material was being subjected to large pressures.[58] This was done in a rotational diamond anvil cell (rDAC or RDAC), where, once pressurized, one diamond anvil can rotate while the other stays stationary, thus creating shear deformations on the material in the gasket hole. Boron carbide powder with a 15 um grain size was used. Samples were loaded up to pressures ranging from 25-55 GPa, and once max pressure was reached for a given run, one anvil was rotated 90 °. Samples were post-characterized with TEM to observe any change in structure.[58] At lower max pressures, lattice distortions and defects were present in post-characterized specimens, as well as some evidence of cracking. At larger maximum pressures, TEM post-analysis revealed the appearance of strain bands as a result of the large pressures and shearing. The strain bands are never formally described as amorphization, nor is Fourier transform analysis done on the bands to confirm crystallinity, or lack thereof, within the bands, as other works have done.[3, 58] However, it is noted that similar features in other literature are in fact shown to be amorphous regions.[3, 58] Annenkov et. al. also assume that icosahedra simply distort under deformation, and do not fully fracture.[58]

Due to the unique bonding of icosahedral boron-rich solids, it is hypothesized that materials such as boron carbide can undergo a unique form of compression called inverted molecular (IM) behavior. This means that features like the icosahedra, typical to boron-rich materials, can compress to a larger degree than the structure as a whole. This means the icosahedral units shrink more than the resulting crystal lattice as a whole, a phenomenon that is

not seen in normal molecular solids. This arises from the electron deficient nature of an icosahedra, where valence electrons are distributed between several boron atoms. This almost-delocalized bonding nature is reminiscent of what is seen in metallic bonding and is believed to be a weaker form of bonding when compared to covalent bonding between icosahedra and chain structures. This can lead to icosahedra being more susceptible to compression or deformation under loading. Inverted molecular behavior is believed to occur in boron carbide and can ultimately play an important role in the determination of the material's intrinsic properties.

When loaded in a high-pressure cell to over 10 GPa, boron carbides (B_4C) icosahedra units are shown to be nearly 25% more compressible than the entire structure.[59] This is the first time this has been observed in boron carbide experimentally. At the time, the experimental data was in good agreement with models attempting to further understand the complex bonding of icosahedral borides, and the effect that behavior has on material properties and performance.

High pressure x-ray diffraction studies of B_4C were done by another group up to maximum pressure of 126 GPa.[60] Lattice parameter confirmation suggests that $(B_{11}C_p)$CBC was the specific form of boron carbide being studied. A mixture of various alcohols and water were used as a pressure transmitting medium, with Ruby fluorescence being used to measure pressure. Upon application of pressure, X-ray peaks right-shifted, indicating compression, and also showed clear evidence of peak broadening. All peaks representing crystalline B_4C remained intact throughout the entirety of loading up to 126 GPa, and no signs of amorphization were observed.[60] Again, it is important to note that unloading measurements were not recorded, and post-characterization was not completed on the sample. This work compliments Yan et. al.

[5] showing no amorphization during any type of loading. The *c/a* ratio of B_4C decreased with an increase in pressure, a result that is not seen with α-boron.

X-ray diffraction was used to study spectral evolution of peaks in situ while boron carbide was loaded to 74 GPa under quasi-hydrostatic conditions.[61] This work found that the icosahedral units were less compressible than the volume of the entire unit cell, in contrast to inverse molecular theory.[61] This is also in stark contrast to other experimental work by Nelmes et. al. [59] showing that boron carbide does indeed exhibit inverse molecular behavior under compression. Dera used B_4C and determined that the sample did not contain any twinning prior to experimentation. 2 separate high-pressure experiments were carried out, and neon was used as a pressure transmitting medium to achieve quasi-hydrostatic compression during loading, and ruby calibration was used to determine the pressure inside the cell. Ultimately, amorphization was not observed during loading, as expected, and the structure was not studied during the unloading regime, nor postmortem, for signs of amorphous band formation.

Single crystal $B_{4.3}C$ is studied up to 70 GPa in a DAC to look at the atomic distance spacing under pressure and to observe changes in the Raman spectra. The sample was loaded into a DAC with a rhenium gasket and uses argon as a PTM and the R1 ruby line as a pressure estimator. A 514 laser was used.[34]

Interesting observations were made in terms of boron carbide changing color and transparency as pressure was applied. Went from opaque to lighter and lighter color until it was nearly transparent, or white, at 60 GPa. This is interesting because boron carbide is supposed to be transparent if there are no defects.[34]

Most bond lengths decrease as pressure is increased. Additionally, a phase transition at 40 GPa is once again suggested, citing possible structural changes in the chain, while the icosahedra appears to be less effected in this study.[34]

2.3. Models to Explain and Eliminate Amorphization in Boron Carbide

In an effort to atomistically explain amorphization and seek improvements to create amorphization-resistant boron carbide, many theoretical models have been developed over time. Some of the models used are ReaxFF, Molecular Dynamics (MD), and Density Functional Theory (DFT), among others. These models are closely coupled with experiments, and both are being continuously developed and improved over time, almost as if in an iterative loop together. Models can further explain what researchers are seeing in their experiments and can also direct experimental research. Experiments are important to models, as they confirm the information coming from the models, so they can be properly refined and utilized. This section delves into the modeling efforts to explain amorphization in boron carbide, while offering suggestions to rid boron carbide of amorphization. Models point to several dopants that, if introduced into the boron carbide matrix, can rid boron carbide of amorphization. As such, doped boron carbide materials will be mentioned here only in theory and will be discussed experimentally in forthcoming sections.

2.3a. Early Modeling Efforts

Early modeling on boron carbide used the Gibbs free energy method to estimate the relative abundance of several stable polytypes that exist in practical materials.[6] In addition, the polytypes considered were studied as a function of their relative resistance to amorphization. The weakest polytype in boron carbide was identified as $(B_{12})CCC$, requiring only 6 GPa pressure to collapse. Once collapsed, the material segregated into B12 and amorphous graphitic sheets/inclusions. $(B_{12})CCC$ is considered a minority polytype in boron carbide, with

($B_{11}C_p$)CBC still cited as being most abundant. Nonetheless, (B_{12})CCC is responsible for the formation of amorphization in localized regions, even though both structures show similar elastic constants and vibrational spectra. The bands formed also show a directional dependence, orthogonal to the (113) lattice. It is also hypothesized that ($B_{11}C_p$)CBC can transition into (B_{12})CCC under pressure to also instigate a collapse of structure through a mechanism of atom swapping. Having free carbon from the chain act as a glass-like material would also inhibit boron carbide from showing any elasticity under pressure or impact.[6] Silicon doping is also suggested to reduce the formation of the (B_{12})CCC phase.[62]

Yan et. al. also modeled the failure and amorphization of boron carbide after identifying that non-hydrostatic stresses are critical in single crystal B_4C's collapse.[5] They found that CBC chain bending under large pressures distorts the lattice irreversibly as a result of the central B atom in the chain bonding with adjacent icosahedra. That bond persists as pressure is removed from the structure, causing the distortions and collapsed B_4C structure to remain.[5]

Other modeling work by Taylor et. al. looked into many configurations and stoichiometries of boron carbide to learn more about amorphization in the material.[7] Larger calculations included 960 atoms to properly accommodate larger stresses and strains and their effect on the system. Boron carbide ranging from 6.7-26.7 at. % C were modeled to determine the effect of stoichiometry on atomic structure as well as mechanical properties under various loading schemes. While boron carbide does adhere to R3m symmetry, having a carbon atom in the icosahedra causes slight monoclinic distortions in the lattice, reducing the overall crystal symmetry, in addition to introducing slight strains within the material. The DFT calculations used in this study assume a 15-atom unit cell; possible vacancy structures were not considered. Thus, the four different carbon compositions in this study are 26.7, 20, 13.3, and 6.7 at. % C, although both limits in that range are not practical.[7]

The stress-strain response of each configuration is studied as a result of hydrostatic, uniaxial, and shear loading. All materials show a clear lack of strength to shearing loads and the response from all various materials studied are similar.[7] These shearing strengths are much lower than the uniaxial compressive strengths observed in these tests. This is important because shearing strains are believed to be a key contributing factor in the formation of amorphous bands in boron carbide.

The C44 shear modulus can also attest to the sudden drop in shear strength of boron carbide, as well as the anisotropic elasticity that is also seen. This elastic anisotropy difference can be as much as an order of magnitude different in boron carbide. All samples exhibit softening of C44 modulus. This allows for new bonds to form between the chain and equatorial sites in the icosahedra, something that is discussed elsewhere as well.[5, 8]

The main takeaway from Taylors work is the bending of the 3-atom chain that enables its interaction with nearby icosahedra. Their work gives an early indication into considering boron-rich boron carbides being less susceptible to amorphization compared to B_4C. CBC chains are shown to be favorable over the CCB configuration in $B_{13}C_2$, indicating a preferential boron substitution to occur in the icosahedra. Also, no collapse of structure is seen for (B_{12})CCC and (B_{12})CBC during continuous loading. It is worth noting that these claims are contradictory to those of Fanchini [6]. Lastly, it can be noted that the (B_{12})CBC structure showed the largest yield strength during shearing, which shows the importance in studying boron-rich boron carbides as a means of reducing amorphization.

It is important to note the fact that the computed stresses that samples are subjected to in Taylor's work [7] do not result in a collapse of structure, but this cannot be confirmed under the same conditions experimentally. This may be due to large shear stresses that can lower

phase transformation pressures. This shows that there is a large gap between theoretically modeling and experimentally tested boron carbide. It is a testament to how complex the boron carbide structure is, and how this can be extremely difficult to accurately model.

The Sjakste group introduces different ideas to determine what plays a critical role in structural collapse and amorphization of boron carbide.[63, 64] This group cites vacancies in the CBC chain structure as being critical to collapse of boron carbide. It is a boron vacancy, giving a C-V-C chain, where V denotes a vacancy. They state that under pressure the B atom can be removed or ejected from the chain. This allows a C-C bond to form between the carbon atoms that usually reside at the end of the chain. They cite a lack of literature determining the role of defects and defect structures in boron carbide, and how defects can affect the performance of boron carbide. Ultimately, they determine that boron carbides mechanical properties are not hindered by these defects, but that they do play a role in its failure under dynamic testing. They also note that “chain bending,” a term commonly used by modelers, is in fact incorrect, and what they presume is chain bending is in fact a C-C bond forming from a C-V-C chain under pressure.[63, 64] This models agree with other work that cite a significant number of chain vacancy unit cells present in boron carbide.[29]

Kunka et. al. fits simulated Raman spectra to experimental spectra to determine hundreds of stable polytypes in synthesized boron carbide.[30, 31] From the same group, Subhash *et. al.* gives multiple suggestions to tailor boron carbides structure and improve its resistance to amorphization.[65] One suggestion includes doping nickel atoms into the free spaces within the icosahedra to stabilize the material. Nickel was chosen because its atomic size, electronegativity, and thermodynamic stability allow it to be stable within the boron carbide matrix.[65] Another recommendation includes attempting to control processing parameters to favor certain polytypes over others.[65] This would necessitate extreme precision in processing,

but could allow for a material that can be tailored to also improve selected or desired mechanical, electrical, or thermal properties. Lastly, creating nano-sized grains in boron carbide could lessen the degree of amorphization if grain growth is limited during sintering. This limits the strains that can be accommodated by grains, instead leading to crack formation or dislocations in place of amorphization. In nano-grained boron carbide, Raman mapping showed a lower amorphous phase intensity compared to boron carbide with a grain size of 10 um.[65] This would also likely increase hardness of the material, since hardness follows Hall-Petch behavior in relation to grain size, such that as grain size is decreased, an increase in hardness is seen.[66]

2.3b. Models from Caltech and the University of Nevada, Reno

Many insightful models came from Caltech and later the University of Nevada, Reno. It is established that boron carbide fails atomically through the formation of nanoscale amorphous bands. These bands form through the mechanism of strain being applied to the $(B_{11}C_p)CBC$ configuration of boron carbide. First, the inter-icosahedra B-C bond breaks, leading to an icosahedral C bond interacting with the boron atom in the middle of the chain structure, which is thought to bend under strains. This interaction ultimately forms a bond after the strain is removed, collapsing the icosahedra.[8] This interaction is shown pictorially below in Figure 14, where strain is applied to the system in increasing amounts.

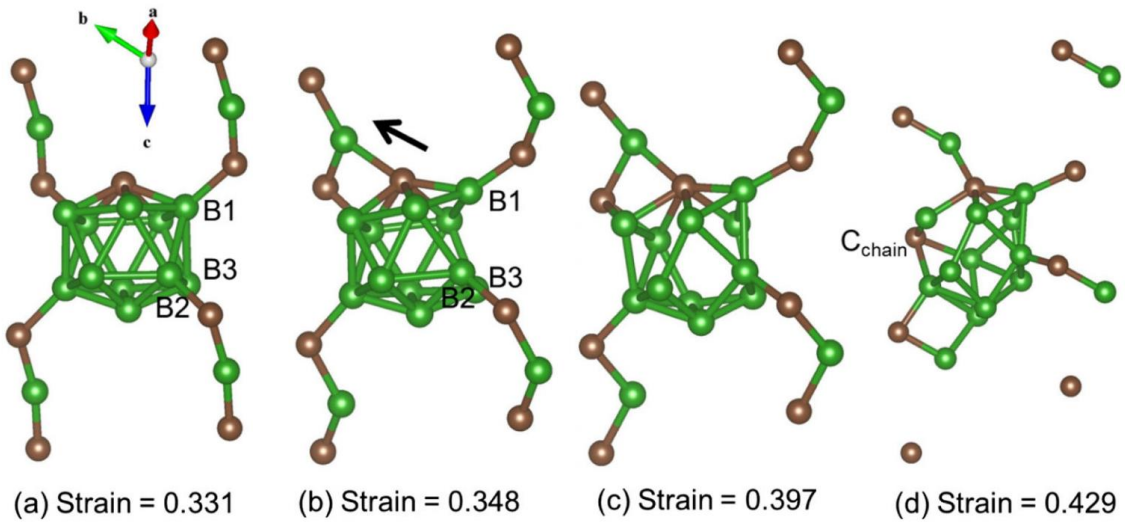

Figure 14: Structural evolution along the (01-1-1)/<-1101> slip system. 14(a) shows critical failure strain, (b) the middle boron atom interacts with the icosahedra carbon atom, (c) the icosahedron carbon atom bonds with the boron atom, and (d) the icosahedral B-C bond is broken.[8]

So, the $(B_{11}C_p)$CBC polytype is responsible for amorphous band formation, since there will be no icosahedra-C and chain-B interactions from the $(B_{11}C_e)$CBC or (B_{12})CCC polytypes. This result differs from Fanchini's claims [6], although both or either argument could still be possible.

Additionally, shear-induced amorphization takes preferentially takes place along the (01-1-1) plane. It is also found that the (01-1-1)/<-1101> slip system exhibits the lowest shear strength in B_4C. These models show that through minimizing the $(B_{11}C_p)$CBC polytype in boron carbide, the formation of amorphous bands can also be minimized.

The previously mentioned susceptible slip system is observed in a larger simulation environment, comprising hundreds of thousands of atoms using reactive-molecular-dynamics simulations. Now, the formation of amorphization can be studied from a larger size-scale. At this point discrete twinning is observed. Within these twinned regions, amorphous bands are formed by means of the atomistic mechanism previously mentioned. These amorphous bands have a higher density than crystalline B_4C, leading the structure immediately surrounding the bands to experience negative pressure. This leads to a free volume that leads to cavitation, and

finally crack opening.[9] Amorphous band formation begins in twinned regions due to the presence of already-distorted icosahedra. The band formation is able to reduce shear stressed and pressures built up from twinning.[9]

An and Goddard, who previously suggested making boron-rich boron carbides to address amorphization by minimizing icosahedra-chain interactions, now compared boron-rich $B_{13}C_2$ to B_4C. Boron-rich boron carbide shows a higher intrinsic shear strength under shear and biaxial shear deformations. However, nanotwins present in $B_{13}C_2$ lower the shear strength compared to B_4C. This differs from the effect nanotwins have on $(B_{11}C_p)$CBC in B_4C, which strengthen the material. In B_4C, the twins suppress B-C interactions between the chain and icosahedra.[67] Failure of boron-rich boron carbide occurs from the CBC chain interacting with twin boundaries. Twinning in $B_{13}C_2$ also serves to soften the material, giving it a lower overall shear strength.[67] Biaxial shear strength is similar for perfect B_4C and $B_{13}C_2$, but lower for twinned $B_{13}C_2$. Ultimately a boron-rich boron carbide is still suggested, although there are tradeoffs to be considered when tailoring the boron carbide structure.

Other ideas from this group include replacing the CBC chain with an Si-Si chain structure to increase ductility and allow for shear stresses without amorphous band formation seen in B_4C. This ideally allows for a rotation of the chain when subjected to shearing.[68] Also, an alloy of B_4C-B_6O can allow for a large strains or shears without the formation of amorphous bands.[69] These ideas are insightful, but less influential on this dissertations work, compared with other models from this group.

2.3c. Awasthi Model

In 2019, Awasthi and Subhash proposed a new model to explain the process of amorphization in boron carbide.[10] In doing so, they present a comprehensive review of the

literature to date, and argue several valid points against theories the community has long held onto as fact. This work builds off initial ideas and models by Fanchini [6] as well as experimental data from Yan [5].

The main takeaway from this model is that amorphization is instigated mainly at defect sites, where there can be large stresses there are built up and can lower the melting point of boron carbide. Under shock, compression, or indentations, the large compressive pressures reached can cause a large increase in thermal energy, causing boron carbide to reach temperatures at or even exceeding its melting point of approximately 2000 K. At that point the material melts, and, if not given sufficient time to recrystallize when the stress is removed, can quench, forcing the material into a locked amorphous state of unbonded atoms.

The assumption with this model is that the amorphous bands are made up of unbonded atoms that ultimately have the same density as crystalline boron carbide (2.52 g/cm^3), but due to their unbonded state, result in large repulsive forces. This results in their main assumption that the amorphous band is less dense (i.e. requires a larger volume), than the surrounding crystalline matrix, as a direct result of the repulsive forces, a statement which is still heavily debated. As this expanded material presses against the crystalline material, very large stresses (~100 GPa) at the interface between the crystalline and amorphous material result, causing the immediate surrounding area to be subjected to large compresses forces. Using DFT and MD models, simulated Raman spectra for ($B_{11}C_p$)CBC is determined at elevated pressures, such that the pressurized peaks overlap with the experimental amorphous signal that is seen. This specific polytype is well understood as being the most prevalent in boron carbide, which is why it was studied here. It is noted that boron carbide can take on many different polytypes in an experimentally made material, and thus leave room for some discrepancy, as other polytypes can possibly also play a role in the amorphization process.[10]

Thus, the unique amorphous signal seen in the Raman spectra is ultimately not from the amorphous material itself, since it is a confined matrix of amorphous unbonded atoms, and as such would not be Raman-active, but rather as a result of the boron carbide that is compressed at the interface, which is subjected to pressures ranging from 80-105 GPa.[10]

The argument is made that flaws and defects are the main nucleation sites for the amorphization process to occur, because that region can already exist at an elevated stress state, thus resulting in a lower localized melting temperature for the material in that area.

DFT calculations were used to generate their simulated Raman spectra. First, simulations at ambient pressure were matched to experimental hot-pressed boron carbide that was indented to induce amorphization. Both pristine and amorphized spectra were generated. Then, using experimental data from Yan's [5] DAC data, spectra were generated at elevated pressures to fit the high pressure spectral peaks to the amorphous peaks seen experimentally in indented regions. This can be seen below in Figure 15, where the simulated Raman spectra at elevated pressures is fitted to an experimental spectra of amorphized boron carbide.

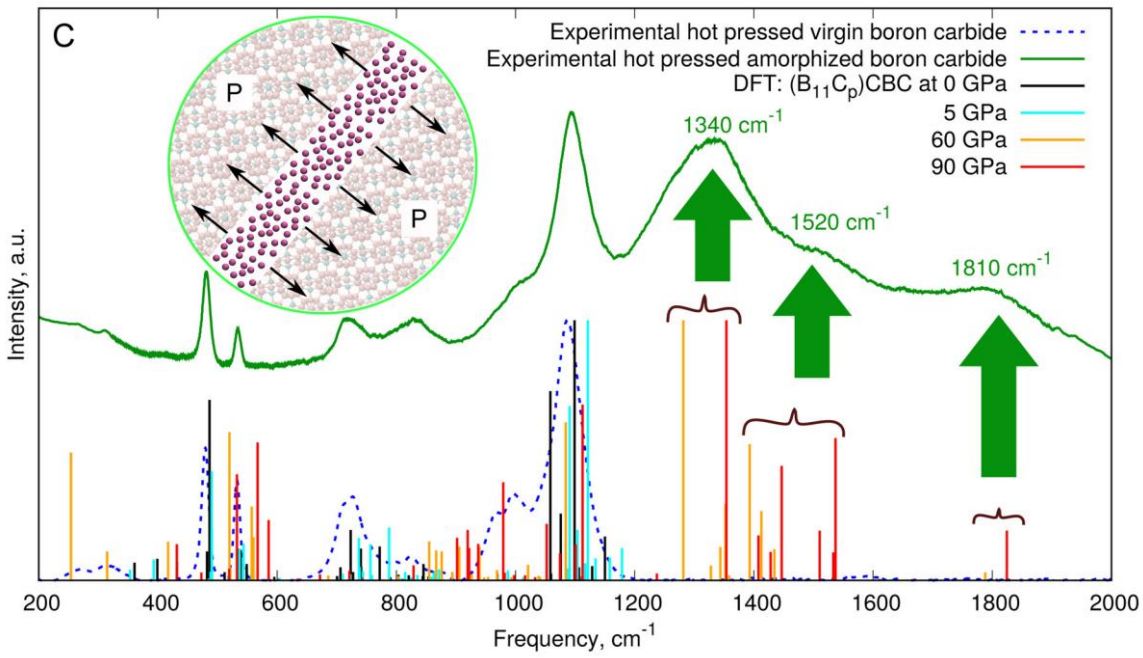

Figure 15: Experimental hot pressed amorphized boron carbide and DFT-evaluated Raman spectra at varying pressures, denoted in the image by color. The inset "P" notes the compressive pressures at the interface between amorphous and crystalline material.[10]

MD simulations were also carried out to study the effect of temperature, and the temperature rise of bulk material under compression. MD simulations allow for large bulk simulations to be carried out, in this case consisting of 18,000 atoms, which was periodic in all directions.[10] Again, this simulation also utilized the $(B_{11}C_p)CBC$ configuration for B_4C.

Awasthi and Subhash also related the volumetric compression to the resulting pressure increase and temperature rise resulting from such a compression. A 15% volumetric compression led to a compressive pressure (P) of 30 GPa and an elevated temperature (T) of 725 K, at 20% compression, a P ~ 34 GPa and T ~ 1100 K was seen, and at 25% compression, a P ~ 45 GPa and T ~ 1400 K is noted. At 30% compression, P ~ 70 GPa and T ~ 2100 K are experienced by the material.[10]

These ideas evolved from Fanchini's work, which stated that intermediate products were formed from $(B_{12})CCC$, such that the amorphous phase consisted of that polytype, along

with disordered carbon sheets and alpha-B clusters.[6] But Awasthi claims this in inherently flawed, as both constituents would not exhibit Raman peaks at such a high frequency, unless they are under very large pressures, which is not stated nor suggested. It was from this that it was hypothesized that boron carbide constituents could be presenting themselves as higher frequency Raman spectra seen in experimental amorphized boron carbide.

The authors also question that if such compressive forces were seen in an amorphized region, where would such forces originate from? This is further brought into question if one assumes the amorphous region is more dense, because then the surrounding crystalline matrix would be under tension, which could lead to crack formation, something that has never been found in experimental TEM analysis of such zones.[3, 45, 57]

Awasthi further asserts that in previous DAC work [34, 60, 61, 70] unloading rates were sufficiently slow, such that the high pressures results in increased temperatures that allow the material could recrystallize, and the system ultimately reaches a state of equilibrium between temperature rise and recrystallization, which explains why the material can remain intact while being kept under a constant pressures in excess of 100 GPa.[10]

This model ultimately gave a vast insight into a new possible explanation of the amorphous phase of boron carbide. It was able to validate itself using a wide variety of pre-existing literature and knowledge to further assert their claims, while also re-evaluating older literature that, in the face of more recent developments, appears to be more limited in its usefulness.

2.3d. Summary of Modeling Suggestions to Suppress Amorphization

While many various suggestions are given to explain the atomistic mechanism that causes amorphization, most assumptions and models revolve around either the (B_{12})CCC or the

($B_{11}C_p$)CBC polytype. Also, there is a debate as to whether these polytypes are susceptible to collapse through their chains or icosahedra, although many cite interactions between them both such that permanent bonds are formed under loading or strain. Regardless of either polytype or explanation given, a boron-rich boron carbide, assuming a (B_{12})CBC structure, would be able to suppress amorphization, because either susceptible polytype in B_4C will no longer be present in the material. So, creating these materials utilizing the boron-rich side of boron carbides homogeneity range in the B-C phase diagram will minimize the tendency of amorphous bands to form, allowing a better performing material for use in defense applications.

2.4. Experimental Work on Boron-Rich Boron Carbides

The previous section dug deep into the best modelling approximations of the amorphization problem in boron carbide. Ideas were discussed of what conditions need to be met to make boron carbide amorphize, how it amorphizes from an atomistic perspective, its impact on the material and its performance and properties, and suggestions to get rid of amorphization altogether. One suggestion was to create boron-rich boron carbides. This suggestion successfully addresses the suggestions from modeling, even if models differ on the exact mechanism that causes amorphization. In making a boron-rich boron carbide, such as, for example, (B_{12})CBC, interactions between the chain and icosahedra under any loading condition will be minimized, and this is regardless of whether the polytype responsible for collapse is (B_{12})CCC or ($B_{11}C$)CBC. If that key interaction between the chain and icosahedra is minimized, or those predicted weak polytypes are eliminated, an amorphization-resistant boron carbide will exist. This section details what work has been done in processing and characterizing boron-rich boron carbide. A fair amount of work done with these materials previously was done to better develop the B-C phase diagram, and for scientific understanding, and have only recently been studied as they relate to amorphization in boron carbide. Some of these boron-rich materials,

which will be discussed in detail, form the basis of this dissertation, where they were extensively studied in terms of understanding their differing composition, and how this effects amorphization in the boron carbide system.

2.4a. Theory, Processing, Characterization, and Properties of Boron-Rich Boron Carbides

Creating a thorough understanding of the B_4C structure is difficult, and going to the more boron-rich side of B-C's homogeneity range makes this matter even more complex. Models and experiments have been studied to understand boron-rich boron carbides since the 1970s, and the exact structure of boron-rich boron carbide is still subject to scrutiny and debate.

Icosahedral boron-based solids all have an α-rhombohedral structure. This holds true for α-boron, B_4C, and boron-rich boron carbide. It has always been a question of whether B_4C consisted of B_{12} clusters and CCC chain structures, or a ($B_{11}C$) icosahedra and a CBC chain. It is now been shown that both are stable structures that can be found within a processed material. There is still much debate as to what specific structural changes preferentially occur going more boron-rich than B_4C (20 at.% carbon).[18]

Early models developed by Yakel suggest that boron-rich boron carbides exhibit expanded lattices compared to B_4C. It was also initially postulated that the boron-rich structure consisted of (B_{12}) icosahedra, while the CBC chains were gradually replaced by planar (B_4) units that linked icosahedra. The carbon-rich end is said to consist of ($B_{11}C$), (B_{12}), and ($B_{10}C_2$) icosahedra with CBC chains.[71]

Tallant, based on vibrational spectroscopy, also believed that the initial B substitution into B_4C was taking place in the chain, though he also states that ($B_{11}C$) and (B_{12}) icosahedra can exist in boron carbide. This initial substitution would change the CBC chain to a CBB chain. This would create an asymmetry in the chain. This substitution would gradually take place until all

unit cells have been substituted, creating a $B_{13}C_2$ structure, which correlates to 13.3 at.% C. Further substitutions would go into the icosahedra, making (B_{12}) clusters, similar to those seen in α-boron.[18]

With Raman spectroscopy, spectra can consist of broad and narrow bands, where broader peaks represent a slightly more amorphous or disordered mode. This is important for boron carbide materials since structural disorder can explain peak broadening in the boron-rich materials spectra. Also, since boron-rich boron carbides have larger lattices, most, if not all, of the Raman peaks can be expected to show some extent of a downshift to lower frequencies. Mode broadening can create confusion when trying to determine subtleties between similar possible Raman peaks in the boron carbide spectrum, to such an extent that one broad peak can result from contributions from multiple peaks that represent similar configurations. Peak broadening can also be due to disorder and unit cell variation, in addition to the effect of twinning and stacking faults.[36]

A follow-up study to Tallant's work [18] was completed by Aselage, where the lattice constants of varying boron-rich boron carbides were determined through X-ray diffraction techniques, using high-purity boron carbides that ranged from 8-20 at. % carbon.[72] An increase in boron content does not have a noticeable effect on the length of the chain, although bonding distances for inter- and intra-icosahedral units tends to increase. This is seen as an increase in the *c* axis of the rhombohedral unit cell, as much as 40% when comparing B_4C and $B_{13}C_2$. As initial boron content increases, a boron atom substitutes a carbon atom in boron carbide. At the time, the initial substitution was believed to occur in the chain structure, transitioning from CBC chains to CBB chain. Further boron addition was thought to go into the icosahedra, creating (B_{12}) cages. Primary and secondary substitution preferences for boron atoms are still under intense debate. This paper does observe an increase in lattice parameters

going to the boron-rich side of boron carbides homogeneity range. However, past the critical point where $B_{13}C_2$ is reached, the *a* and *c* parameters tend to level off.[72]

Nihara has studied the hardness and fracture toughness of boron-rich boron carbides and discovered a large amount of scatter in their data.[73] Boron-rich boron carbides, as well as standard B_4C, can also lose their rhombohedral structure and assume a tetragonal or orthorhombic structure as the lattice expands.[74] The structures and properties in boron-rich boron carbides can vary greatly.

Powder diffraction data on boron-rich boron carbides shows a large percentage of chain structures with vacancies.[75] Reitveld refinements were used to understand the diffraction data. This study again suggests initial boron substitution taking place in the CBC chain, and that $B_{13}C_2$ is made up of B_{12} icosahedra and CBB chains. This mostly supports previous work my Yakel and Tallant.[18, 71] It is also presumed that at extreme boron-rich limits, rather than a planar (B_4) unit, a non-linear BBB chain can potentially exist.[75] Again, chains with vacancies can also promote initial chain substitutions.

Roszeitis et. al. also investigated boron-rich boron carbides, and observed large grain grown in the boron-rich materials.[76] The lattice parameters calculated in this work agreed well with Aselage. [72, 76].

Newer studies were recently done to determine the structure and properties of boron-rich boron carbides.[13, 14] The challenge is that even as recent at 2017, there is still a debate as to whether boron substitution into boron carbide preferentially occurs in the icosahedra or the chain. Xie uses his current [14] and previous work [57] to come to the conclusion that boron first enters the icosahedra, becoming (B_{12}), until $B_{13}C_2$ is reached. Past this point, the chains become altered. Contrarily, Cheng [13] asserts that initial substitution modifies the chain

structure up to the 13.3 at. % carbon stoichiometric change, past which the icosahedra accepts the additional boron atoms. Hardness values and trends vary between the study, as well as between nano- and micro-hardness. Characterization techniques only addressed the precise stoichiometry of the samples and their accompanying mechanical properties, amorphization was not considered or probed.[13, 14]

As far as Raman spectroscopy is concerned, both studies previously mentioned agree on their findings. Both notice downshifting of the IBM 1080 cm^{-1} peak, and at extreme boron-rich limits, notice the appearance of a new peak at 375 cm^{-1}, though neither have a specific claim as to its origins.[13, 14] It is presumably a new or modified chain structure, since icosahedral peaks tend to reside at higher frequencies.

Figures 16, 17, and 18 detail some of the various lattice parameters, hardness values, and Raman spectra, respectively, from various works investigations of boron-rich boron carbides.

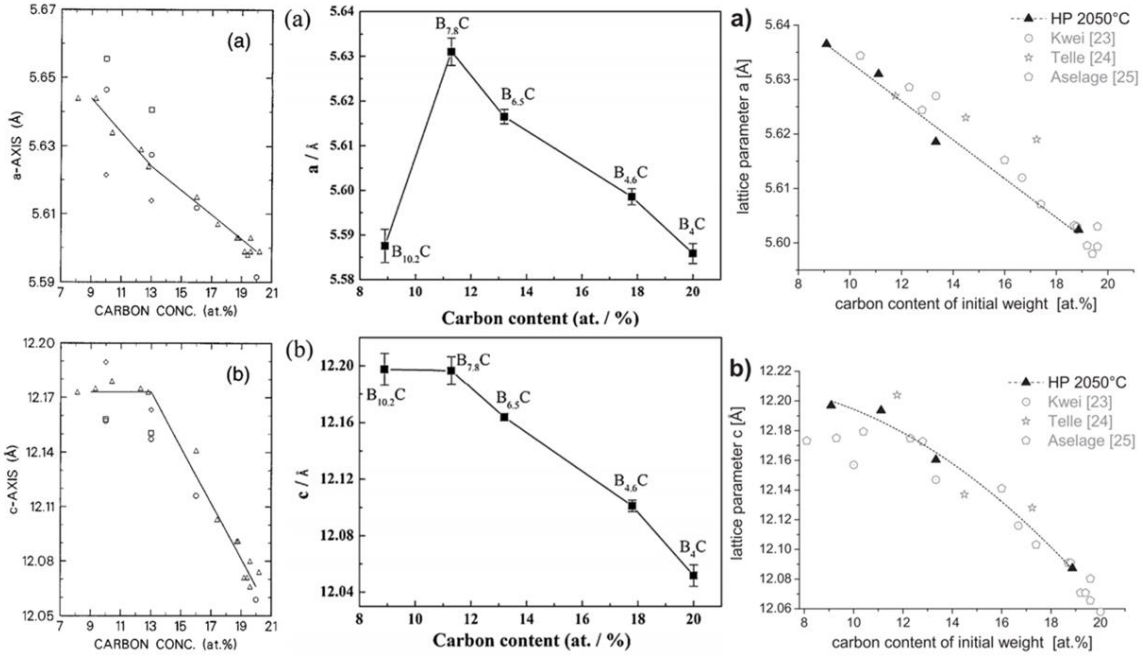

Figure 16: Various examples of boron-rich boron carbide lattice parameters plotted against carbon concentration.[13, 76, 77] a-parameter vs carbon content is plotted on the top, and the c-parameter vs carbon content are plotted on the bottom row.

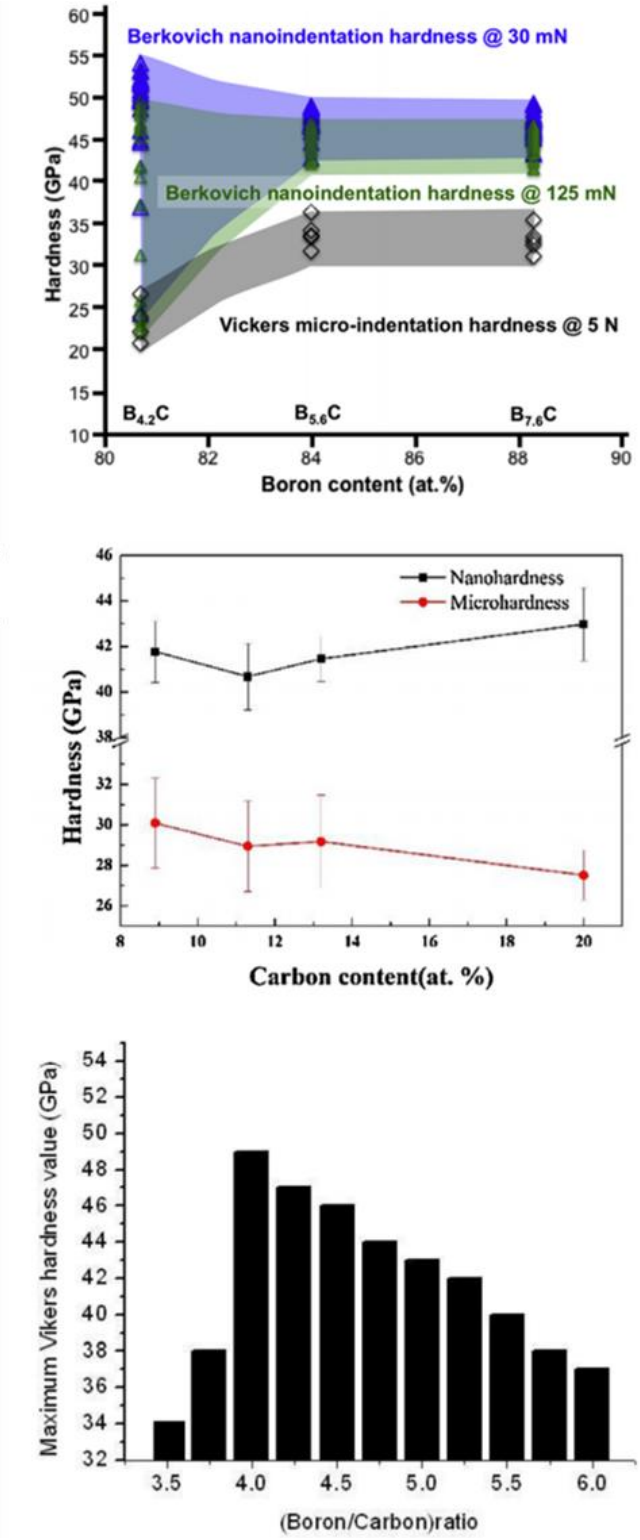

Figure 17: Hardness values from various literature on boron-rich boron carbides.[13, 14, 74]

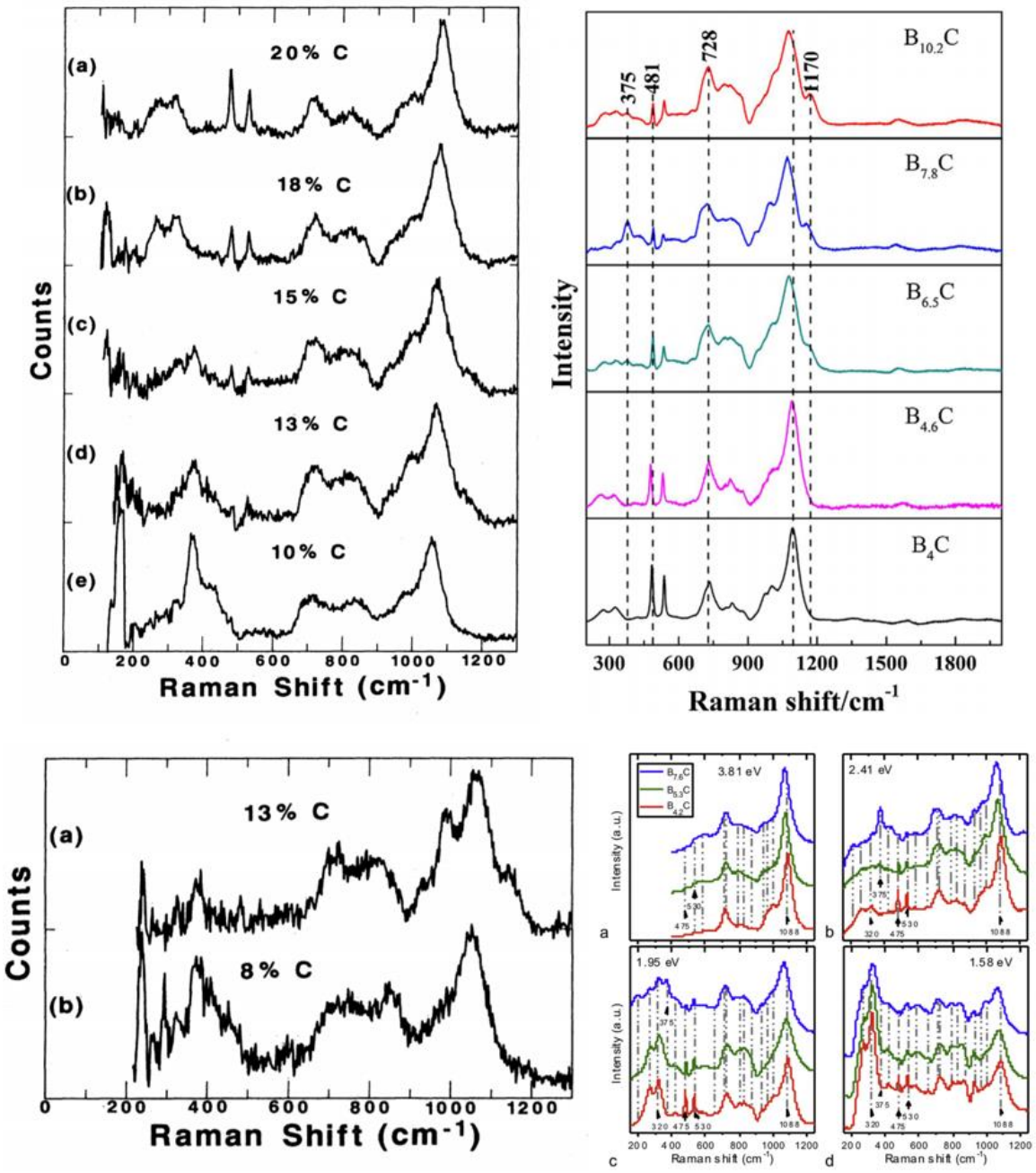

Figure 18: Various examples of Raman spectra of boron-rich boron carbides from the literature.[13, 14, 18]

2.4b. Boron-Rich Boron Carbides Studied in This Dissertation

This dissertation was done as part of a larger program, which utilized past work completed and expanded upon towards a common goal. To that end, this thesis focused primarily on characterization, with a strong focus on amorphization, while previous dissertations

from the same research group have focused on processing the boron-rich boron carbide ceramic materials studied here. This dissertation uses samples from 2 previous dissertations, that of Munhollon and Kuwelkar.[11, 12]

Munhollon's boron-rich samples were prepared by using SPS to sinter Rutgers-made boron carbide powders with amorphous boron. Kuwelkar's boron-rich samples were hot pressed (HP) samples of commercial boron carbide powders mixed with additional boron. There are pros and cons to each set of samples: the SPS samples are nearly fully dense, while the HP samples are more boron rich, with B/C ratios as large as 9 achieved. Samples were characterized in their respective dissertation, but amorphization studies were not completed on these, leading for more experiments to be carried out on them.[11, 12] Since Raman spectroscopy is utilized throughout this dissertation, the representative Raman spectra for both sets of boron-rich boron carbides are shown below in Figure 19.

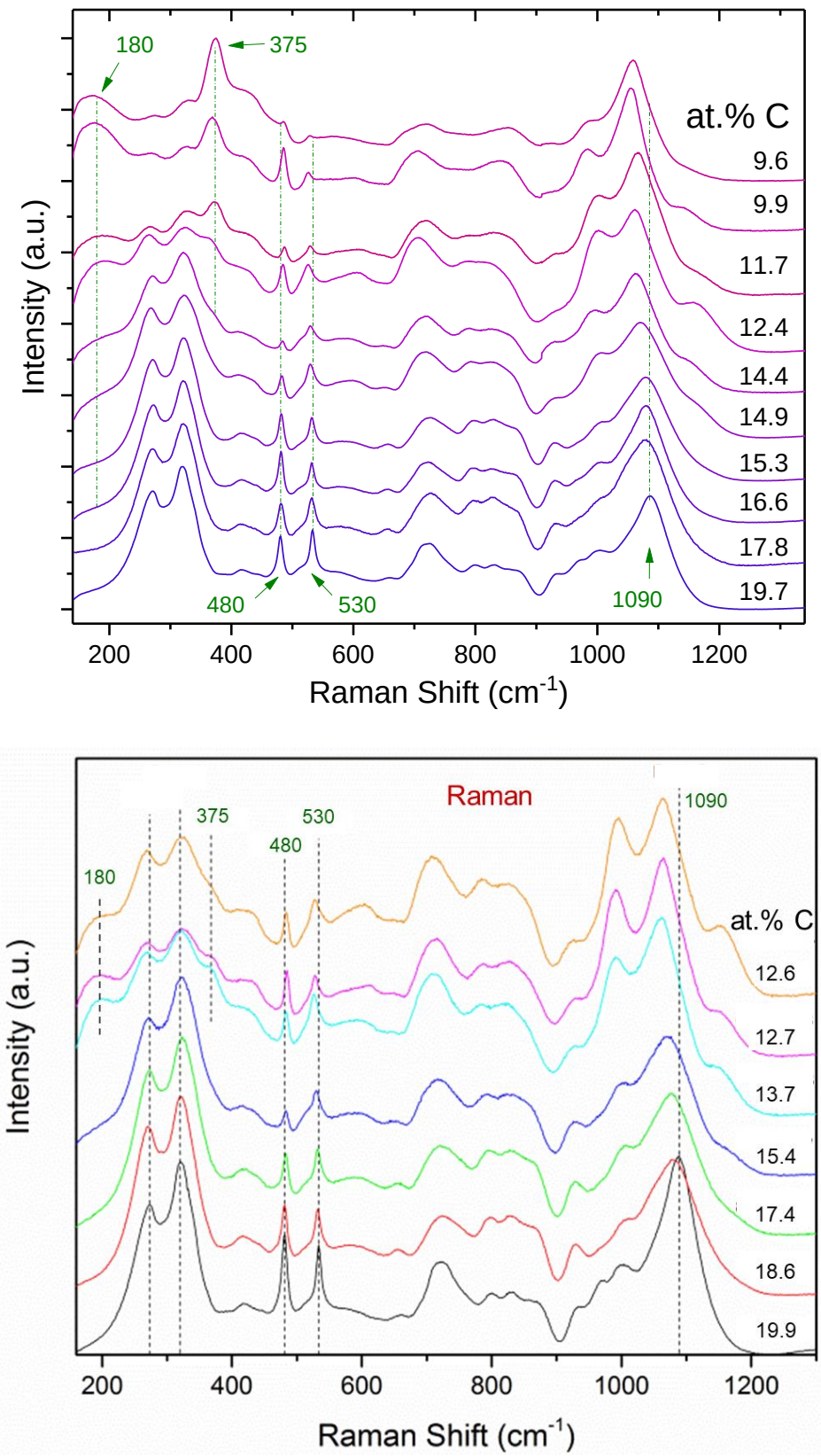

Figure 19: Raman spectra of boron-rich boron carbides prepared by Kuwelkar (top) [11] and Munhollon (bottom) [12].

3. Method of Attack

In an effort to mitigate amorphization-based failure in boron carbide, boron-rich materials were produced in order limit possible chain-icosahedral interactions and possibly improve shear strength. While boron-rich boron carbides have been previously processed to near full density [11, 12], extensive quantification and characterization of amorphization was not completed in these materials to validate models suggesting amorphization mitigation [6, 8]. The goal of this thesis was to gain a better understanding of the role dopants play in altering and mitigating amorphization in chemically varied boron carbides. amorphization in boron carbide and determining the role of dopants in amorphization of chemically altered boron carbides. The onset pressure to induce amorphization, and possible mechanism of amorphization, were also investigated for this thesis, to better understand amorphous behavior in these materials. Relationships between material composition, amorphization intensity, and hardness will also be investigated.

The following 4 objectives show the pathway that was taken to successfully gain the knowledge required to better understand amorphous behavior in the boron carbide system. Indentation was be heavily employed throughout this thesis to quickly and easily induce amorphization in boron carbide in a laboratory setting. The initial impact of the indenter tip is believed to cause a sufficiently high stress in the material, causing structural collapse into amorphous bands, which is then pushed into the material as the indenter penetrates the sample.[52] These regions were then probed with Raman spectroscopy, another instrument that was heavily utilized as a quick, non-destructive characterization technique, in addition to being utilized to carry out in situ measurements needed to accomplish the work included in this thesis.

Note: B_4C is shorthand notation for stoichiometric boron carbide (B_4C, which contains 20 at.% carbon).

Additionally, BC will be the abbreviation of boron carbide.

B-rich BC will be used as shorthand for boron-rich boron carbide.

3.1. Objective 1: Find relationships between amorphization, nano-hardness, and carbon content

The main focus of this first objective was to find relationships between 3 main parameters: nano-hardness, relative amorphization intensity quantified by Raman spectroscopy, and the amount of carbon present in a sample. This served as an indicator of how varying stoichiometry in boron carbide effects hardness and relative amorphization. If doped boron carbide can mitigate amorphization, but sacrifices its high hardness that makes it a desirable armor candidate, this limits the practical applicability of the material outside of the lab. Hardness and amorphization intensity data were gathered from samples spanning the boron-carbon homogeneity range, to compare any relationship present between these 3 parameters. Thus 3 main plots were able to be made, based on 3 important questions:

Question 1: Is there a relationship between nano-hardness and B/C ratio?

Question 2: Is there a relationship between relative amorphization intensity and B/C ratio?

Question 3: Is there a relationship between relative amorphization intensity and nano-hardness?

Berkovich (nano) indentation of a fixed load were placed on pristine surfaces to gather hardness data, as well as to induce amorphization in the material, in samples ranging from 19.7 at.% carbon to the boron-rich side of the phase diagram at 9.6 at.% carbon. The samples studied here were processed by means of hot pressing and were polished to mirror-like surfaces. Hardness from nano-indentation was measured using the actual imprinted area of the nano-indent. To do this, indents were imaged using a field-emission scanning electron microscopy

(FESEM), and their area was measured using ImageJ software. Using the measured area of the indent impression, in addition to accounting for the geometry of the Berkovich indenter tip, hardness values were calculated. Raman spectroscopy was used to take spectra at the center of the indents to get the spectral fingerprint of the amorphized boron carbide, which was then quantified as a ratio of amorphous vs crystalline peak intensities to give the amount of amorphization present from an indent at a specific stoichiometry.

3.2. Objective 2: Observe and quantify predicted amorphization mitigation in boron-rich boron carbides using micro-indentation techniques and TEM imaging.

Extensive Raman data collection revealed the amount of amorphized material detected beneath Vickers micro-indentation. This was completed to determine experimentally if a reduction of amorphization is seen in boron-rich samples, in a manner that was more conclusive than the nanoindentation was in the previous objective. Amorphization was induced by Vickers micro-indentation. Raman data was gathered using a mapping technique that takes thousands of spectra around and within a single indentation area. The results were quantified using a more comprehensive method developed to accurately represent amorphization in boron carbide, using relevant peaks based on the literature and current understanding of amorphization in boron carbide. The relative amount of amorphous material present in indented doped samples were compared based on their B/C ratio. Micro-hardness of these samples was also investigated from indentation.

TEM imaging and analysis of the damage zone beneath indents of varying composition was conducted to study the amorphous bands present beneath boron-doped samples, which has not been done in the literature. To do this, nano-indentation was used to induce amorphization in boron-rich boron carbide, as well as nominal boron carbide for comparison. Cross sections from the nano-indents samples were taken out by means of focused ion beam

(FIB) liftout techniques. This allowed the use of transmission electron microscopy (TEM) to be used to image and study the amorphized regions in both samples.

3.3. Objective 3: Conduct in situ heating of amorphized boron carbides of varying stoichiometry

Another objective of this thesis was to determine the stability of the amorphous phase as the sample undergoes heating *in situ*. During a high-velocity impact, large amounts of energy are dissipated in the form of heat, to such a degree that melting is thought to occur in boron carbide. Since heating within a sample is a major factor during a high strain rate impact as a result of frictional forces and heat dissipation, this objective attempts to replicate and approximate this condition in the lab, to give insight as to the materials behavior under high impact pressure/high strain rate collisions. Previous work had looked at only boron carbide at elevated temperatures.[48] This work will look at boron carbide to confirm this previous work and to compare the response of boron-rich stoichiometries.

Indentation-induced amorphized samples were once again used spanning the homogeneity range of boron carbide. Samples were heated in a closed chamber that is vacuumed down and backfilled with inert argon gas. The chamber was heated while the amorphous signature was recorded using Raman spectroscopy.

3.4. Objective 4: Determine the onset of amorphization in varying boron carbides

Another aspect of this thesis is to determine the onset conditions of stress-induced amorphization in doped boron carbides. Determining the conditions where this phase transition occurs could be the key to generating new and improved boron carbide-based materials that do not fail as a result of amorphization.

A diamond anvil cell is a tool used to generate large pressures in situ, such that stress thresholds can be determined to observe phase changes in situ. In this case, the onset of

pressure-induced amorphization can be observed in situ using Raman spectroscopy. This work will first confirmed previous similar studies by Yan et. al. [5], using boron carbide (B_4C), which showed amorphization under non-hydrostatic loading conditions. There, amorphization was seen during unloading, after a critical threshold was exceeded during the loading phase. Next, samples with increasing B/C ratios were studied in a DAC under extreme pressures to observe any differences in their response to pressure and their tendency to undergo a structural disorder as a result.

4. OBJECTIVE 1: Find relationships between amorphization, nano-hardness, and carbon content

4.1. Experimental Procedures

This objective aims to find any correlations between carbon composition, hardness, and amorphization. Samples used in these experiments spanned the entire homogeneity range of the phase diagram. Carbon compositions used were: 19.7, 17.8, 15.3, 14.4, 12.5, 11.7, and 9.6, as previously processed and characterized by Kuwelkar.[11] Corresponding B/C ratios are given in Table 2.

B/C Ratio	Carbon Content (at. %)
4	19.7
4.6	17.8
5.5	15.3
5.9	14.4
7	12.5
7.5	11.7
9.4	9.6

Table 2: Sample B/C ratios and corresponding carbon compositions used for Objective 1 analyses.

4.1.a. Nano-Indentation

Samples were embedded in epoxy so they could be mechanically polished with a Buehler AutoMet 250 Polisher. Successive diamond-embedded polishing pads and diamond suspensions down to 0.05 um were used to prepare flat, mirror-looking surfaces for testing.

Indentation served a two-fold purpose in this work: 1. To use for hardness measurements, and 2. To induce amorphization in the samples. A Micro Materials NanoTest Vantage System was used for nano-indentation using a Berkovich diamond tip, and a Leco M-

400 Hardness Tester was used for micro-indentation, with a Vickers diamond tip. Many indentations were placed on the sample surfaces, in regions free of any visible residual porosity or pullouts that manifested as a result of polishing. In addition, only pristine indents were considered for further analysis; any with excessive cracking, spalling, or otherwise damaged indents were discarded. Possible damage could have come from pores beneath the surface that led to an unusual looking indent. This is illustrated in Figure 20 where a 5x3 array of nano-indents was placed in a polished sample. 6 out of the 15 indents were deemed unsuitable for further analysis because of their proximity to pores.

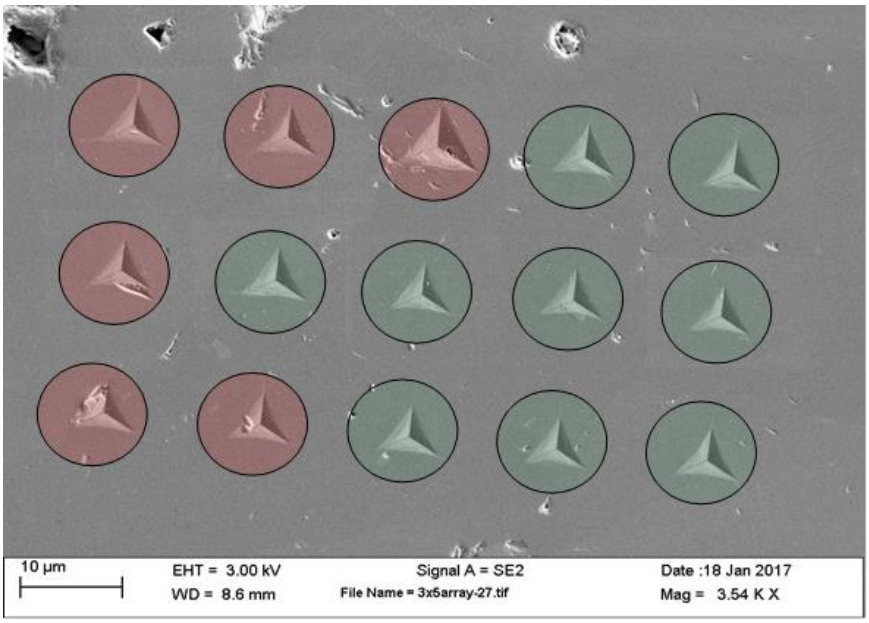

Figure 20: SEM image of 500 mN Berkovich nano-indents in a boron carbide sample. Red-circled indents were discarded from analysis due to their proximity to porous regions.

For nano-indentation, sample pucks were glued to a steel barrel that was then screwed into the nano-indentation unit. The indentation schedule was run overnight in order to minimize any inherent vibrations that could affect measurement quality and precision. This is especially important because of the size of the nano-indents, which are approximately 1 um across, and less than 1 um in depth. Indents were made using 500 mN load, with a loading/unloading rate of 2.5 mN/s and a 2 second hold a maximum load.

Several dozen nano-indents were placed in areas with low residual porosity, such that at least a dozen pristine indents could be used for analysis.

4.1.b. SEM Imaging

A field emission scanning electron microscope (FESEM) by Zeiss Sigma was used to image indents to measure for hardness values. Hardness was calculated from the nano-indents in a similar manner to how micro-hardness is calculated, using total imprinted area from the indents. Graphic depictions of this are shown in Figure 22. To measure the imprinted area of the nano-indents, scanning electron microscopy (SEM) was required to first image indents. An aluminum stud with a 1/2" slotted head and a 1/8" pin from Ted Pella Inc. were used to hold samples, which were covered with carbon tape to prevent charging on samples, since they were left in their epoxy pucks to maintain sample flatness for imaging the shallow indents. The samples were studied using a Zeiss Sigma FESEM. A working distance of around 4 mm was used with a voltage of 5-20kV. Some representative SEM images of indents at various stoichiometries are shown in Figure 21.

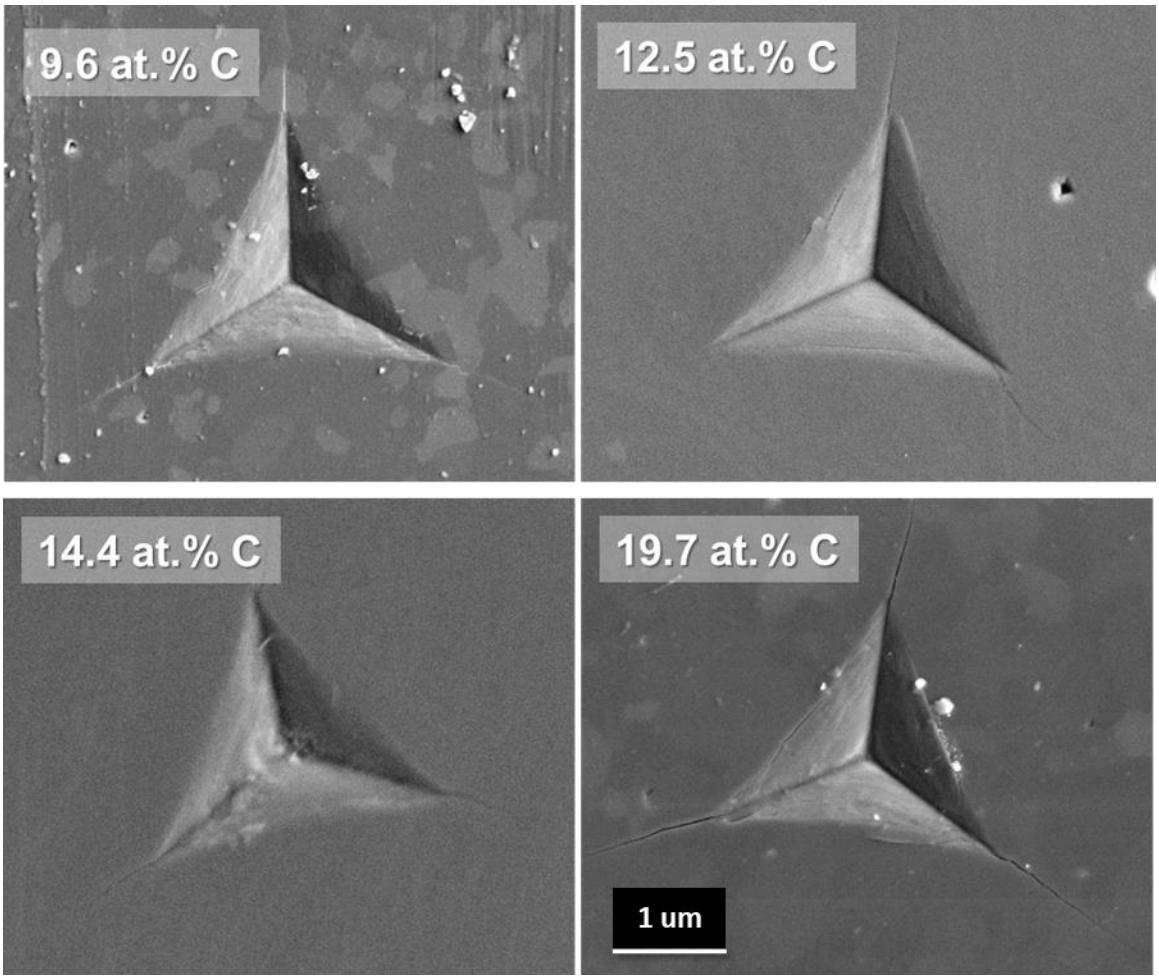

Figure 21: Electron Microscopy image of Berkovich indents of stoichiometrically-varied boron carbides.

For Vickers indentation, a Keyence optical microscope was used to image and measure indents to calculate hardness values.

4.1.c. Hardness Calculations

imageJ software was used for measuring the area of the nano-indents. The scale bar from the micrograph image was used to set the scale for the software, and indents were measured from each corner of the indents impression.

For Berkovich hardness calculations, the total projected area of the indents was evaluated from the measured area of the indent, which was projected on the plane orthogonal

to the indentation direction. The hardness was calculated as the maximum load divided by the total residual area.

Defined in this way, the measured Berkovich hardness can be directly correlated with conventional Vickers hardness. The projected residual area of the indents was measured by counting the pixels of a triangle overlaid on the image of a Berkovich indent and converting the pixel count into um^2, as shown in Figure 22.

Total Area: $A_t = \frac{1}{sin\,(65.3°)} \cdot \frac{\sqrt{3}}{4} \cdot a^2$

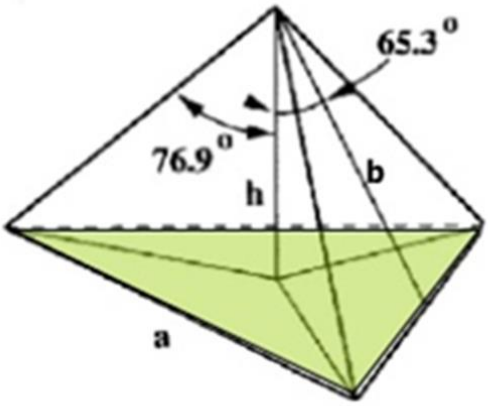

Projected Area: $A_p = \frac{\sqrt{3}}{4} \cdot a^2$

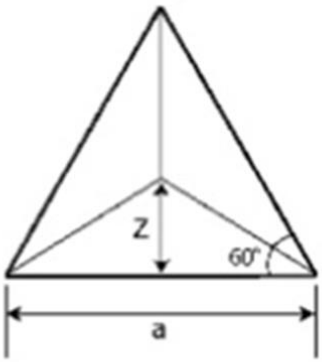

Figure 22: Calculations used to measure total projected area from the Berkovich indentations, to calculate hardness in a manner that is directly comparable to micro-hardness.

4.1.d. Raman Spectroscopy

A Renishaw inVia Raman Spectrometer equipped with a confocal microscope at 100x magnification was used to collect data on the amorphized indented regions in samples. A 40 mW 633 nm laser source with a 1800 I/mm grating was used for signal detection. The laser was focused to the center of each indent to collect data at the apex of the indented area.

Initial methods for quantification of amorphization in the indents were calculated as the ratio of the 1300 cm^{-1} amorphous peak to the IBM icosahedral peak, at approximately 1080 cm^{-1}.

4.2. Results and Discussion

Looking at pristine Raman spectra, several distinctions can be made. While the spectra for B_4C is representative of what has been described elsewhere in literature and this dissertation, several peaks shift in addition to new peaks appearing as the stoichiometry is modified to be more boron-rich. Evident downshifting of the icosahedral peak at 1080 cm^{-1} is observed, and its effect increases with a decrease in carbon composition. Because of this, it is thought that initial boron substitutions occur in the icosahedra, and because of this data, that claim is further asserted and supported throughout the duration of this dissertation, unless stated otherwise. The most boron-rich samples past 13.3 at. % carbon show diminished 480 and 530 cm^{-1} peaks, while a new peak emerges at 370 cm^{-1}, with increasing intensity as samples become more boron-rich. It is believed that this new peak is attributed to new chain configurations, possibly CBB and B-B chains, as suggested by Tallant [18], once all possible icosahedral substitutions are made.

Raman peaks at frequencies above 1100 cm^{-1}, characteristic to the amorphized boron carbide [2, 4, 48, 52], were observed in all in their usual peak positions of 1300, 1500, and 1800

cm^{-1}. For highly boron-rich spectra, the 1300 cm^{-1} peak appears to begin splitting. Some spectra, both pristine and amorphized material, can be seen at varying stoichiometries in Figures 23 and 24. These spectra represent data from one indent at each stoichiometry, and are representative of what was seen in all indents assessed at each given stoichiometry.

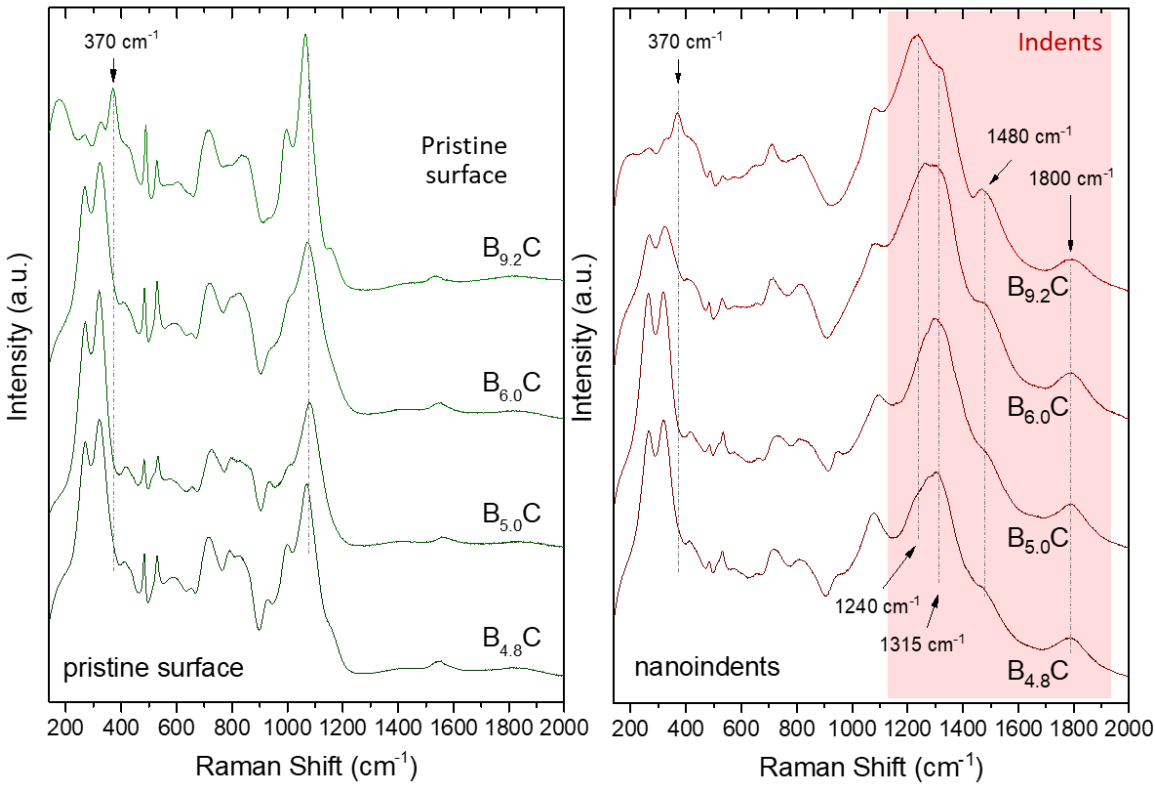

Figure 23: Crystalline and amorphized Raman spectra of boron carbides samples with varying dopant concentrations.

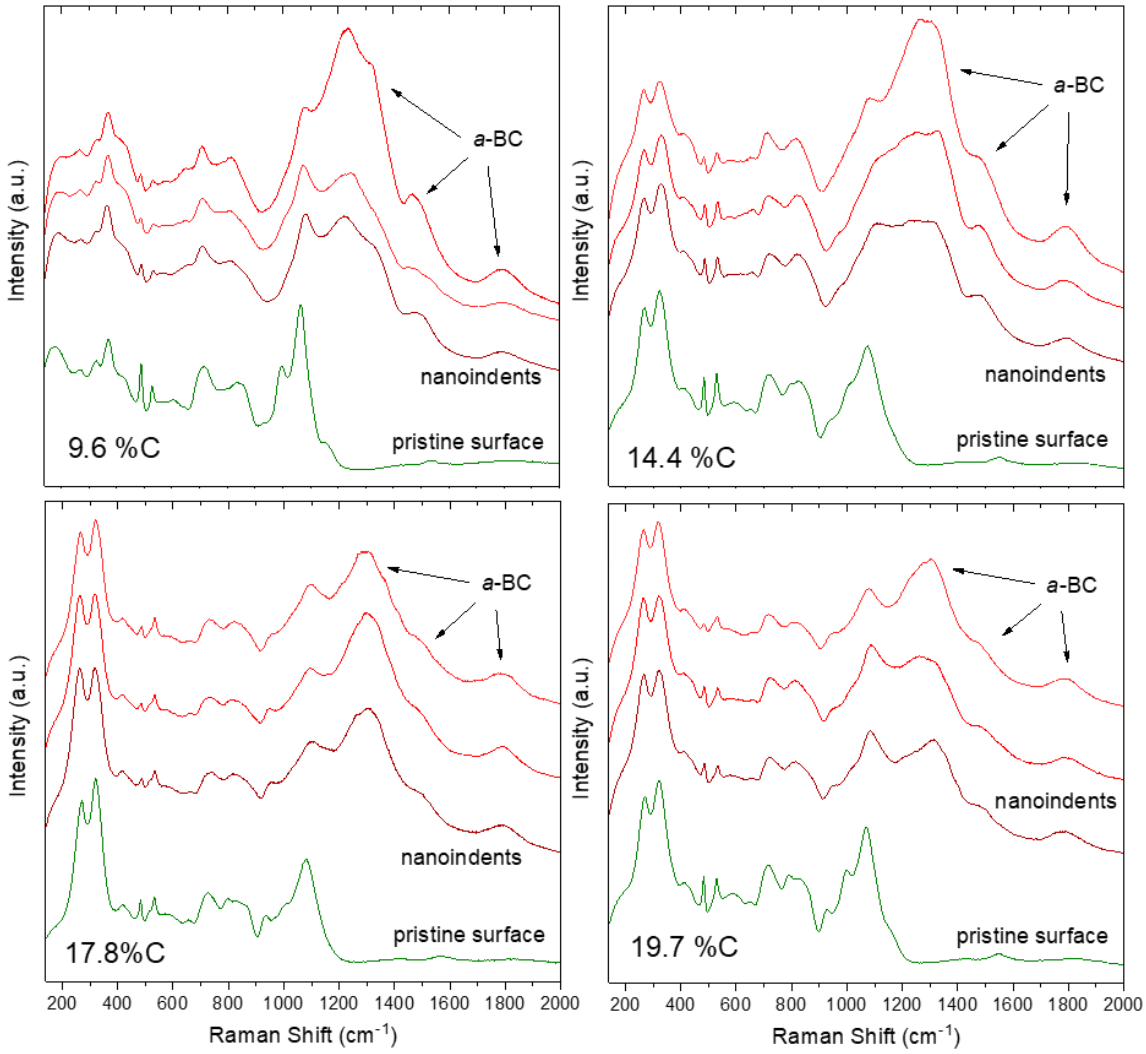

Figure 24: Raman spectra of pristine and nanoindentation-induced boron carbide samples with differing boron contents.

Results for hardness and amorphization values are given in Tables 3-9 below, with each respective table being dedicated to a different stoichiometry studied. These tables show that several indents were analyzed at each stoichiometry so results are statistically significant, although figures only show one representative image of a given indent or spectra.

Indent No	Projected Area (um^2)	Total Area (um^2)	Hardness (GPa)	Amorphization Intensity
1	14.66	16.13	31.0	1.96
3	15.89	17.49	28.6	1.45
4	15.46	17.01	29.4	1.69
5	13.86	15.25	32.8	1.82
10	14.21	15.64	32.0	1.15
11	15.21	16.73	29.9	2.00
13	14.44	15.89	31.5	1.59
14	15.63	17.19	29.1	1.49
19	15.04	16.55	30.2	1.79
21	14.77	16.25	30.8	1.47
22	15.29	16.83	29.7	2.13
23	15.20	16.72	29.9	1.64
24	13.99	15.39	32.5	1.64
		Average	30.6	1.68
		Std. Dev.	1.3	0.26

Table 3: Hardness measurements and indentation-induced amorphization values for boron carbide with 19.7 at.% C.

Indent No	Projected Area (um^2)	Total Area (um^2)	Hardness (GPa)	Amorphization Intensity
1	14.31	15.75	31.7	0.44
2	14.24	15.67	31.9	0.27
3	14.42	15.87	31.5	0.64
4	13.96	15.36	32.5	0.76
6	14.53	15.99	31.3	0.33
7	14.35	15.79	31.7	0.79
8	13.49	14.84	33.7	1.04
9	14.08	15.49	32.3	0.87
10	14.72	16.20	30.9	0.78
11	13.14	14.46	34.6	0.93
12	13.02	14.32	34.9	0.47
13	13.90	15.30	32.7	0.50
		Average	32.5	1.3
		Std. Dev.	0.65	0.25

Table 4: Hardness measurements and indentation-induced amorphization values for boron carbide with 17.8 at.% C.

Indent No	Projected Area (um^2)	Total Area (um^2)	Hardness (GPa)	Amorphization Intensity
12	14.44	15.89	31.5	1.08
13	14.53	15.98	31.3	1.92
14	15.75	17.33	28.8	1.55
15	14.78	16.26	30.8	1.43
16	15.05	16.56	30.2	0.48
17	16.31	17.95	27.9	1.19
18	15.64	17.21	29.1	0.95
19	14.83	16.31	30.7	1.22
20	15.54	17.10	29.2	2.38
21	15.05	16.55	30.2	2.38
		Average	30.0	1.46
		Std. Dev.	1.2	0.62

Table 5: Hardness measurements and indentation-induced amorphization values for boron carbide with 15.3 at.% C.

Indent No	Projected Area (um^2)	Total Area (um^2)	Hardness (GPa)	Amorphization Intensity
4	14.43	15.87	31.5	1.16
5	15.09	16.61	30.1	0.47
6	14.73	16.21	30.8	0.69
7	14.95	16.45	30.4	0.80
8	14.37	15.81	31.6	0.65
9	13.72	15.09	33.1	1.11
10	15.03	16.53	30.2	0.66
11	15.37	16.91	29.6	1.43
12	13.66	15.03	33.3	1.61
13	15.70	17.28	28.9	1.09
14	14.83	16.31	30.7	1.72
15	15.52	17.08	29.3	0.89
16	14.50	15.95	31.4	2.22
17	14.15	15.57	32.1	0.48
		Average	30.9	1.07
		Std. Dev.	1.3	0.52

Table 6: Hardness measurements and indentation-induced amorphization values for boron carbide with 14.4 at.% C.

Indent No	Projected Area (um^2)	Total Area (um^2)	Hardness (GPa)	Amorphization Intensity
4	14.93	16.42	30.4	1.19
5	14.62	16.08	31.1	0.47
6	13.89	15.28	32.7	0.65
8	14.71	16.19	30.9	1.02
9	14.39	15.83	31.6	0.79
10	15.04	16.54	30.2	1.22
11	15.14	16.66	30.0	0.74
12	13.84	15.23	32.8	1.72
13	15.40	16.95	29.5	0.55
14	15.37	16.91	29.6	0.43
18	14.98	16.48	30.3	1.10
19	14.83	16.31	30.7	0.36
21	15.37	16.91	29.6	0.71
22	16.12	17.73	28.2	0.82
		Average	30.5	0.84
		Std. Dev.	1.3	0.38

Table 7: Hardness measurements and indentation-induced amorphization values for boron carbide with 12.5 at.% C.

Indent No	Projected Area (um^2)	Total Area (um^2)	Hardness (GPa)	Amorphization Intensity
1	14.11	15.52	32.2	1.00
2	14.48	15.93	31.4	0.66
3	14.93	16.43	30.4	0.82
4	15.07	16.58	30.2	1.06
5	14.41	15.86	31.5	1.47
6	13.52	14.88	33.6	0.21
7	14.81	16.29	30.7	1.09
8	13.99	15.40	32.5	0.49
9	13.15	14.47	34.6	1.45
10	13.02	14.32	34.9	1.45
12	14.78	16.26	30.7	1.30
13	14.02	15.42	32.4	0.66
14	14.04	15.45	32.4	1.52
15	14.05	15.46	32.4	0.97
		Average	32.1	1.01
		Std. Dev.	1.5	0.41

Table 8: Hardness measurements and indentation-induced amorphization values for boron carbide with 11.7 at.% C.

Indent No	Projected Area (um^2)	Total Area (um^2)	Hardness (GPa)	Amorphization Intensity
1	15.79	17.37	28.8	1.22
2	15.49	17.04	29.3	1.04
3	17.77	19.55	25.6	1.23
4	17.71	19.49	25.7	1.92
5	18.00	19.81	25.2	1.25
6	17.06	18.78	26.6	1.79
9	16.04	17.65	28.3	1.28
10	15.17	16.69	30.0	1.28
11	17.55	19.31	25.9	1.33
14	16.20	17.82	28.1	1.12
15	16.23	17.85	28.0	1.35
16	17.40	19.14	26.1	1.20
17	15.45	17.00	29.4	1.67
18	16.08	17.69	28.3	1.79
		Average	27.5	1.39
		Std. Dev.	1.6	0.28

Table 9: Hardness measurements and indentation-induced amorphization values for boron carbide with 9.6 at.% C.

Thus, plots showing trends between sample composition, hardness, and amorphization were generated. Shown below in Figure 25, nano-hardness plotted against carbon composition is presented across the homogeneity range.

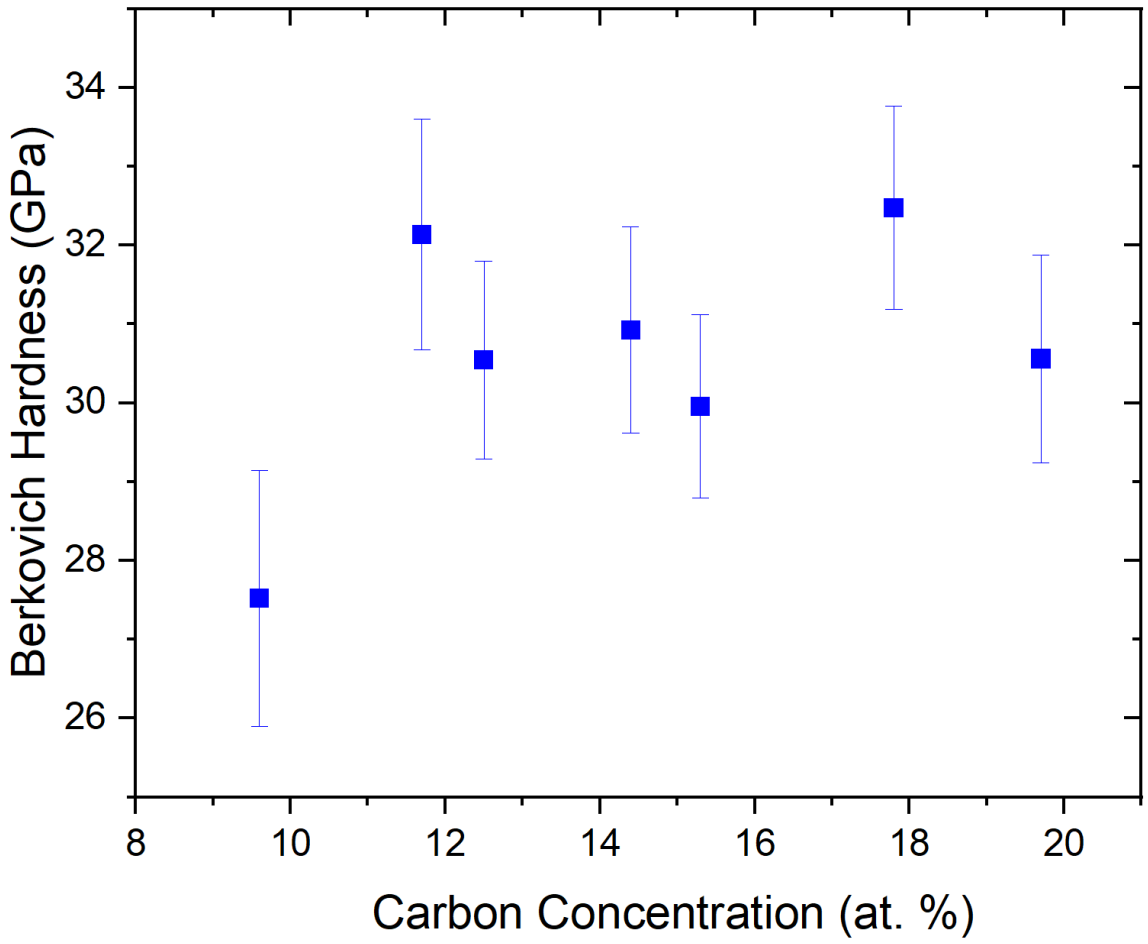

Figure 25: Plot of Berkovich nano-hardness vs. carbon concentration.

The nano-hardness values for boron carbide and boron-rich samples are varied, with no clear trends presenting themselves from the data. The hardness calculated for boron carbide is what is typical of Vickers hardness reported in literature, which is in the range of 29-31 GPa.[4, 16] The most boron-rich sample does show a notable drop in hardness, and no increase in hardness is observed for the stoichiometries close to $B_{13}C_2$ (13.3 at.% C). Large variation was present in all samples, which shows that a given stoichiometry can present a small but varied range of mechanical properties.

Micro-hardness values are not reported or shown in this thesis. In this case, the size of the residual imprint is sufficiently large to accurately align the Raman laser with respect to the

center of the indent. This eliminates possible errors from misalignment, something that was more challenging for nano-indentation. However, because of the high residual porosity of the hot-pressed samples, no reliable Vickers hardness data as a function of carbon concentration were generated. Instead, the selected Vickers indents were used for assessment of the compositional dependence of the temperature stability of the amorphous phase, something that will be discussed in later sections of this thesis.

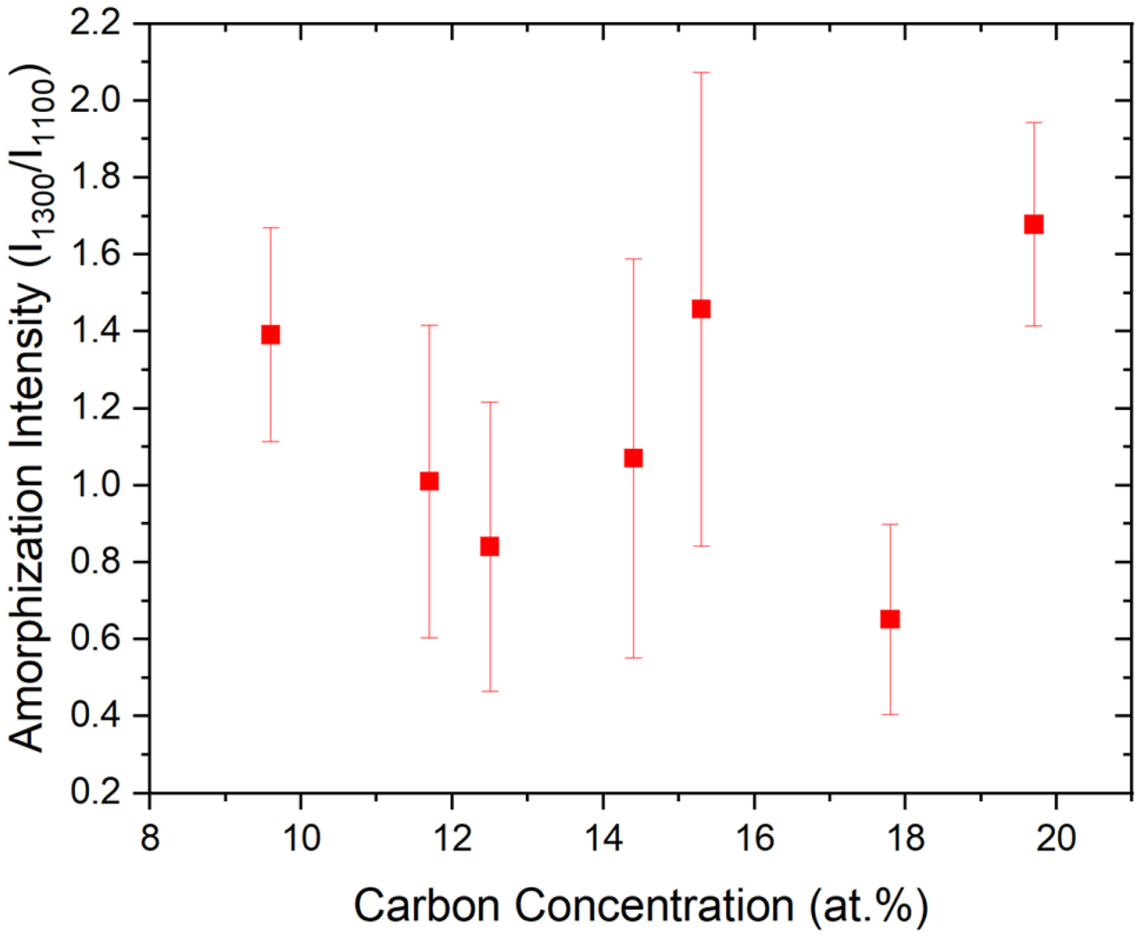

Figure 26: Plot of degree of amorphization vs carbon concentration in boron carbide.

Figure 26 shows the amorphization intensity measured in samples spanning the boron carbide phase, plotted against carbon composition. The intensity of the indentation-induced amorphization did not show an obvious dependence on carbon concentration. Indents with

both high and low degrees of amorphization were observed for all samples. This could be related to the small size of the Berkovich imprints, which are comparable to the size of the laser probe. This means that any slight misalignment from the laser beam relative to the center of the indent could result in significant drop in the intensity of the Raman signal or amorphized boron carbide.

Lastly, hardness and amorphization were plotted together, regardless of stoichiometry, although stoichiometries are differentiated by color. This was done to see if there was a dependence of degree of amorphization as a function of hardness. The scatter plot in Figure 27 shows that no obvious trends can be discerned from the data.

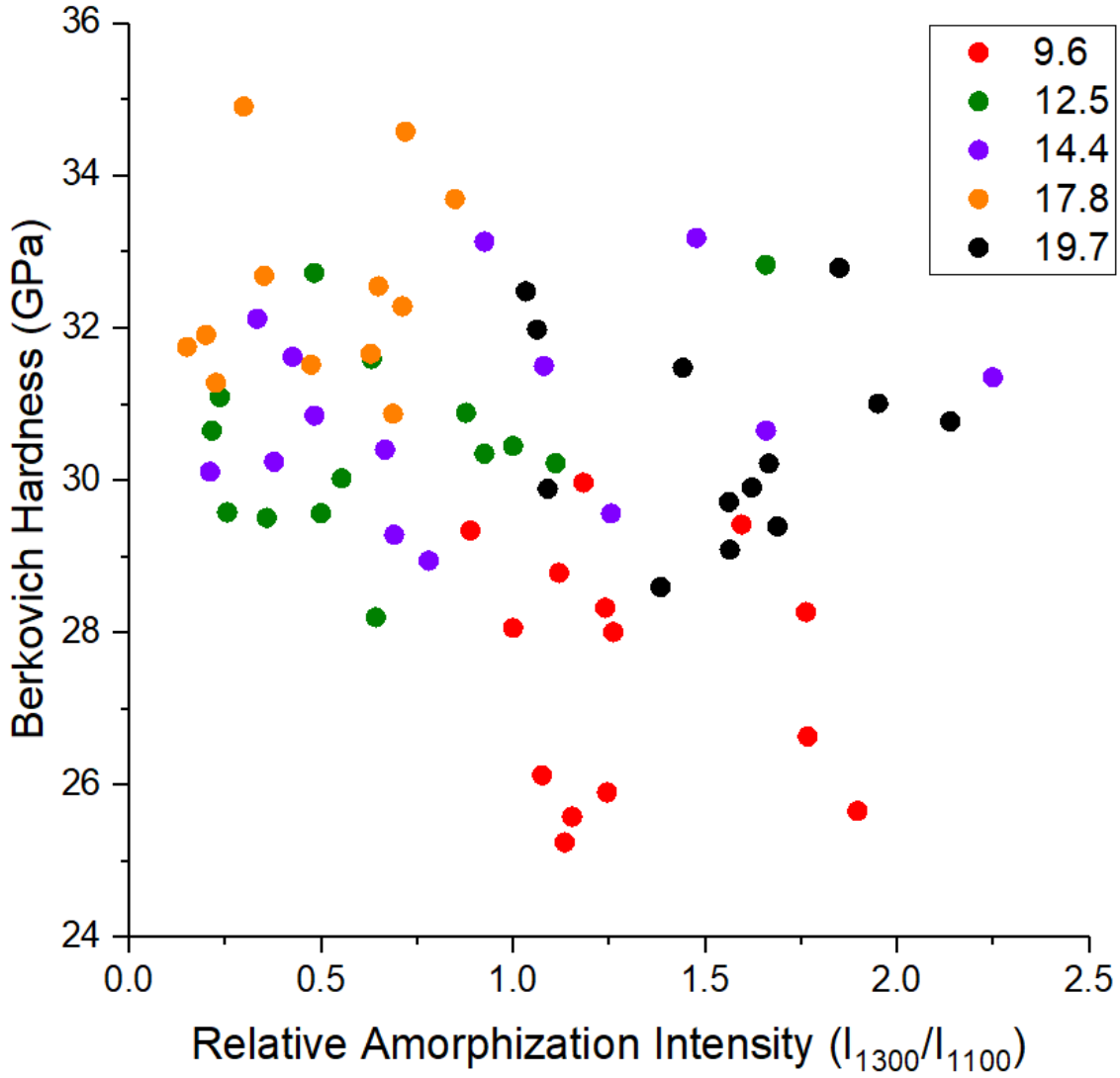

Figure 27: Plot of nano-hardness vs. amorphization intensity. Colors are noted in the key by their carbon composition.

4.3. Summary

Based on the data collected, correlations between the hardness, degree of amorphization, and carbon composition could not be reliably concluded. More in-depth analysis methods for analyzing amorphization from micro-indentation are developed in future sections. Also, as previously stated, micro-indentation also serves to study the amorphous phase at elevated temperatures, which will also be discussed in later sections.

5. OJBECTIVE 2: Observe and quantify predicted amorphization mitigation in boron-rich boron carbides using micro-indentation techniques and TEM imaging

5.1. Experimental Procedures

5.1.a. Micro-Indentation

For this objective, B_4C, $B_{4.7}C$, and $B_{6.3}C$, were studied, and are listed with their corresponding carbon content in Table 10. Samples were previously fabricated and characterized as stated in Munhollon's dissertation.[12] Samples were polished down to 0.05 um using the same regimen employed in the previous section, which utilized a Buehler AutoMet 250 polisher.

Sample Nomenclature	
B/C Ratio	Carbon Content (at. %)
4	19.9
4.7	17.4
6.3	13.7

Table 10: Sample B/C ratios and corresponding carbon compositions used for Objective 2 analyses.

Vickers indentation were used for this study to induce amorphization in boron carbide and determine hardness. Vickers indents, which are larger (~20 um diagonal) than the spot size of the Raman laser (~1 um) and Berkovich indents (~1-2 um across), allowed for extensive probing of the indented amorphized area in greater detail.

Vickers indents were made in selected samples representing different regions of the homogeneity range using a LECO M-400 hardness tester at 5 N maximum loads, 5 seconds loading time, and 5 seconds holding time. Indents were attempted to be made in areas with lower residual porosity.

8-10 pristine indents were used for analysis, free of any porosity, pullouts, or other damage, as a result of indentation or polishing.

Hardness measurements were taken, using Keyence optical microscope (up to 5000x magnification) to image the indents and accurately measure the diagonals. Those numbers were necessary for calculating hardness. This was done to compare any micro-hardness trends present in the samples as a consequence of varied composition.

5.1.b. Raman Mapping and Quantification

Extensive Raman spectroscopy data collection was done for this objective, mapping out Vickers indentations at boron carbide stoichiometries, which are provided in Table 10, to quantify the total amorphization intensity present at each stoichiometry.

The amorphous zone created by Vickers indents should be sufficiently larger than the probing volume of the Raman laser, to ensure that data gathered on amorphization is not over- nor under-represented by a zone that is too small, where possible crystalline regions could be probed. This is because the Raman spectra of amorphized boron carbide is a mixture of amorphous bands and crystalline material, so the resulting spectra is comprised of both types of material. The amorphization intensity probed then depends on the total amount, size, and/or total volume of the amorphous bands/zone, as well as the size of the amorphized zone with respect to the laser probing volume size. So, for larger indents, such as those used here, the size of the amorphized zone is expected to be larger than the laser probe size, based on work by Subhash and Werheit.[33, 52] Therefore in these indents, amorphization mitigation, if seen, should be primarily related to fewer bands, or a smaller volume of total amorphous material, rather than it being a result of probing crystalline material.

The range of 815-1912 cm^{-1} was probed using a 40 mW 633 nm monochromatic laser source with a 1200 l/mm grating. The mapping feature was used to collect data from a selected area, allowing for the investigation of the entirety of the indents imprinted region, along with some of the immediate surrounding crystalline area. The map size was approximately a 20 um x 20 um, at a step size of 0.5 um per scan, so each map yielded nearly 2000 spectra. Mapping was used to get a more thorough picture of what was happening across the entire indented area, since literature suggests that the amorphization intensity maximum is not necessarily found at the apex of a given indent.[52] This total mapping method was able to account for any variation of maximum intensity by accounting for all amorphous behavior as a result of the indent.

Once spectra were acquired, Renishaws WiRE 4.2 software was used to deconvolute the spectra to quantify it. The larger Vickers indents, and the larger number of spectra taken from each indent required a more in-depth method to quantify amorphization, compared to what was used in the previous section, where the ratio of the 1300/1100 cm^{-1} peaks were taken from nano-indents.

To be quantified here, all spectra were first normalized. The total peak area of the 1800 cm^{-1} peak was calculated and normalized to the crystalline contribution from the main icosahedral peaks located around 920-1100 cm^{-1}, which includes the IBM peak at 1080 cm^{-1}. Using peak area accounts for not just peak intensity, but the breadth of the peaks as well, since amorphous peaks can be broader.

Amorphous bands are observed at 1300, 1500, and 1800 cm^{-1}, as first denoted by Domnich [2], but only the 1800 cm^{-1} peak was used for quantification. This is because graphitic carbon bands are seen around 1330 and 1550 cm^{-1}, which means amorphous peaks can be interpreted as either amorphous bands or graphitic peaks, or, most likely, some contribution

from both. If the 1300 and 1500 cm^{-1} peaks are considered, a reduction could be from the fact that less carbon is present in boron-rich boron carbide, assuming those peaks had some contribution from the D- and G-bands of graphitic carbon. Graphitic peaks would be inherently smaller in boron-rich samples, and thus would not prove anything other than the fact that there is less carbon in a boron-rich sample. Only the peak at 1800 cm^{-1} is solely attributed to amorphous boron carbide in the literature[2, 10, 45, 52, 56]. Utilizing this peak to show reduced amorphization is more representative of showing a reduction of amorphization, not a reduction of carbon content. Main peaks for the icosahedral units are located between 920-1100 cm^{-1} and can show point-to-point variation between location and stoichiometry. These were used for normalization as they are the most prominent peaks in the boron carbide spectra, and literature suggests that amorphization can be a result of broken or distorted icosahedra.[8, 56, 57] An example spectra and its highlighted peaks of interest can be seen in Figure 28.

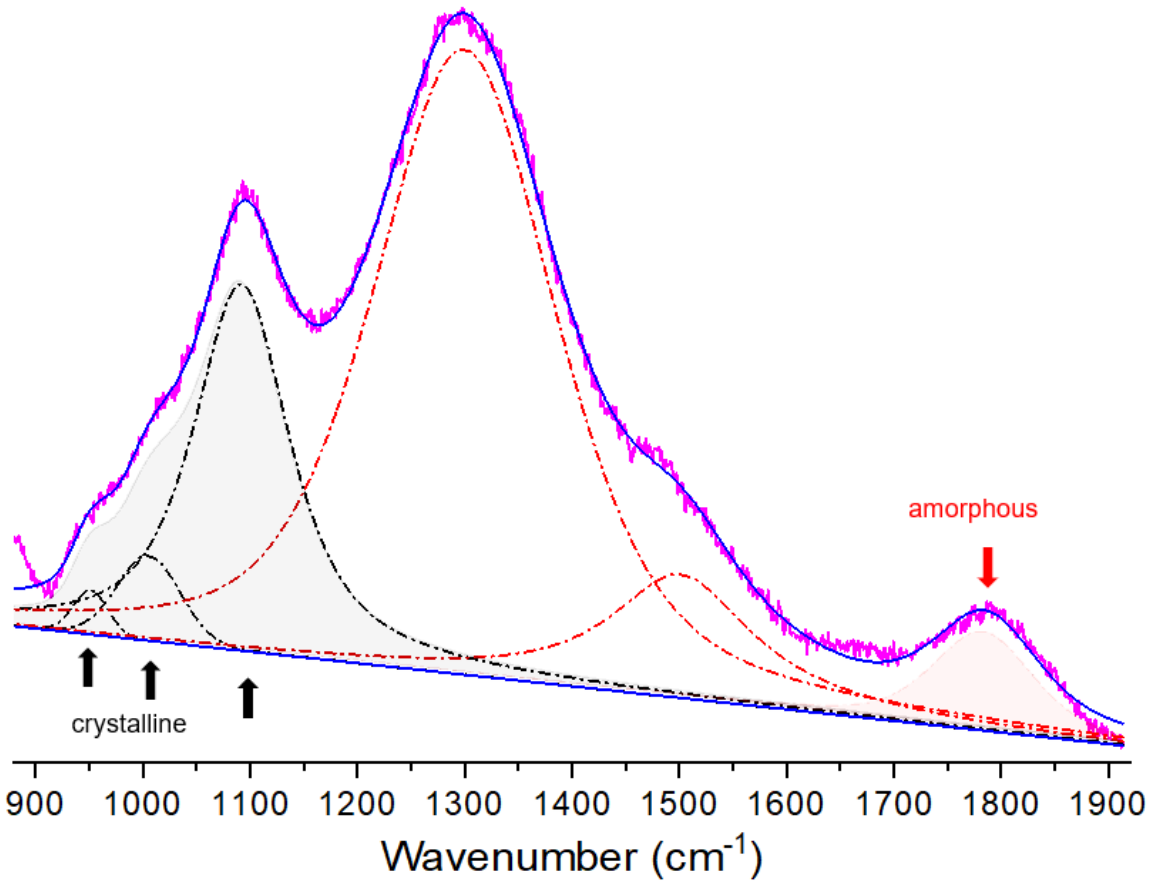

Figure 28: Example Raman spectra probing the IBM peak and amorphous region of boron carbide being deconvoluted into individual peaks.

This quantification method was applied to each spectra taken, and each indent yielded a summation from all values obtained from all spectra taken by each respective map. The results were then normalized with respect to nominal B_4C, so any reduction seen could be directly compared to nominal boron carbide.

5.1.c. Nano-Indentation and TEM Imaging

TEM imaging techniques were also employed to observe amorphization mitigation in boron-rich boron carbides. Amorphization beneath indents were imaged. However, a direct comparison of the indents probed with Raman was not possible. While larger Vickers indents were useful for gathering large amounts of data from Raman, they were too large to be

successfully lifted out from the sample to take images of. Thus, nanoindentation on the same samples was used to induce amorphization to study with TEM.

The Micro Materials nanoindentation unit was used again with a Berkovich indenter tip. A 500 mN load was used with a loading rate of 2.5 mN/s and a 2 second hold at maximum load.

Indented samples were cut out of their epoxy molds using a diamond saw for TEM sample preparation.

Cross-sectioned TEM specimens were taken from the samples using Focused Ion Beam (FIB) liftout techniques. A Thermo Fischer Helios G4 Dual Beam FIB unit was used. A thin protective carbon film was deposited on the sample surface using a 20 kV electron beam. The sample was then tilted to an ideal angle, such that another protective layer, this time platinum, could be deposited onto the samples. This was done with a Ga+ beam that had a 0.79 nA current and an accelerating voltage of 30 kV. The beam then dug trenches on either side of an indent using a higher current of 21 nA. A tungsten microprobe was attached to the platinum layer, and the specimen was able to be lifted out and attached to a copper grid, and the microprobe tip was removed. Lastly, the specimen was thinned down to 50 nm using a lower energy beam. Figure 29 demonstrates the main steps involved in TEM sample preparation.

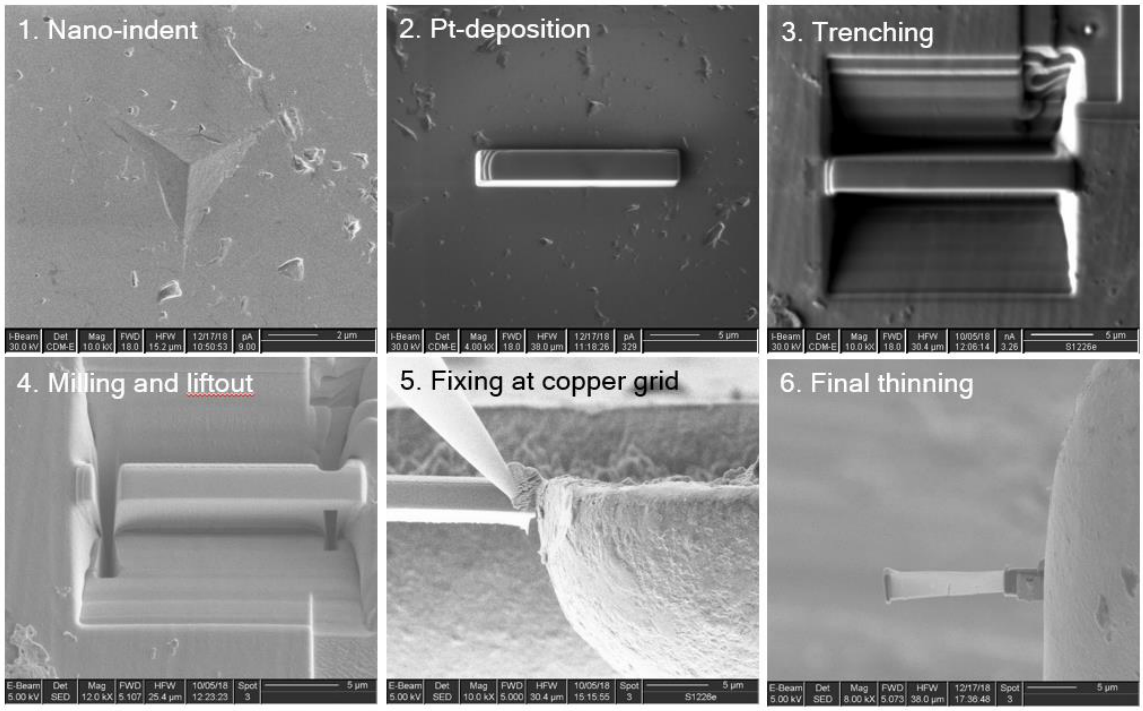

Figure 29: Steps involved in TEM sample preparation: 1. Indentation; 2. Platinum deposition; 3. Make a trench on both sides of the desired material; 4. Mill and liftout the specimen; 5. Attach sample to a copper grid; 6. Thin the sample with more milling.

A Tecnai TF30 Transmission Electron Microscope was used to image the samples at 300 KV. Bright-field (BF) imaging was done on a standard and boron-rich boron carbide. Images were taken on each sample at the same place beneath the indented impression. High-resolution TEM (HRTEM) was completed, and crystalline and amorphous regions were elucidated through the use of selected area electron diffraction (SAED), fast Fourier transforms (FFT), and automated crystal orientation mapping (ACOM). The ACOM data collection required a NanoMegas ASTAR system. Other parameters required in TEM imaging of the subsurface damage zones included spot size 9, gun lens 3, a 4.5 kV extraction voltage, a 30 um C2 aperture, a 1 nm diameter probe, and a convergence semi-angle of 1.4 mrad. The length of the camera was 135 mm to determine diffraction patterns, with a step size of 5 nm. ASTAR software was used to index crystallographic planes, which were then analyzed using OIM Version's electron backscattered diffraction (EBSD) by EDAX, Inc.

The final sample specimen to be studied in shown in Figure 30. The crack in the specimen was a result of sample prep to relive stresses built up from the indent.

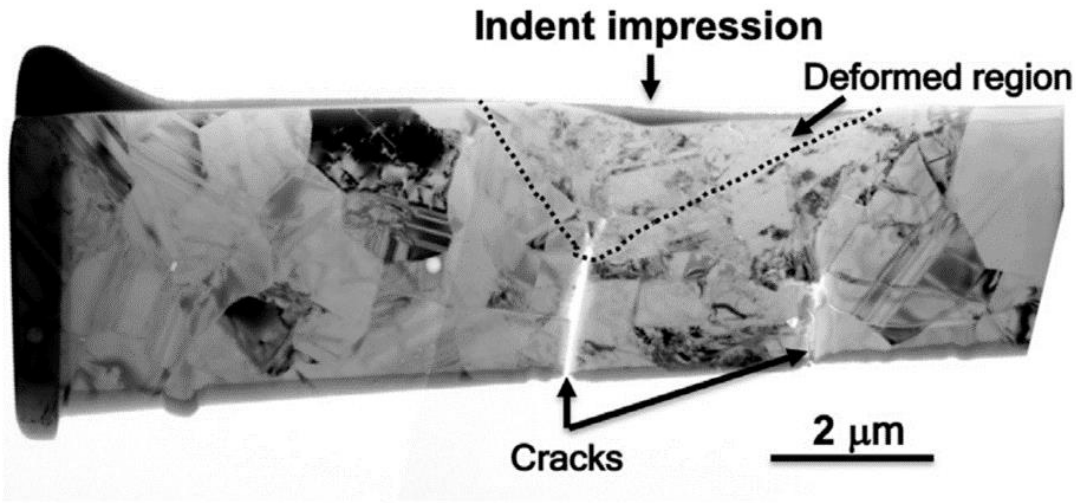

Figure 30: FIB lift out sample of boron-rich boron carbide, thinned to 50 nm.

5.2. Results and Discussion

5.2.a. Micro-Indentation

Looking at hardness values from these Vickers indents in these samples, B_4C had a hardness of 34.6 GPa, $B_{4.7}C$ was found to be 31.9 GPa, and $B_{6.3}C$ was calculated as 32.7 GPa. Error bars on the following figures represent the standard deviations from the data sets. This is shown in Figure 31.

It is difficult to draw any conclusions from these findings, because, as in the previous section discussing nano-hardness values, micro-hardness values determined here do not vary consistently as carbon composition is altered. Additionally, with larger error bars, as was the case here, it can be argued that all samples have a similar hardness with insignificant differences between stoichiometries.

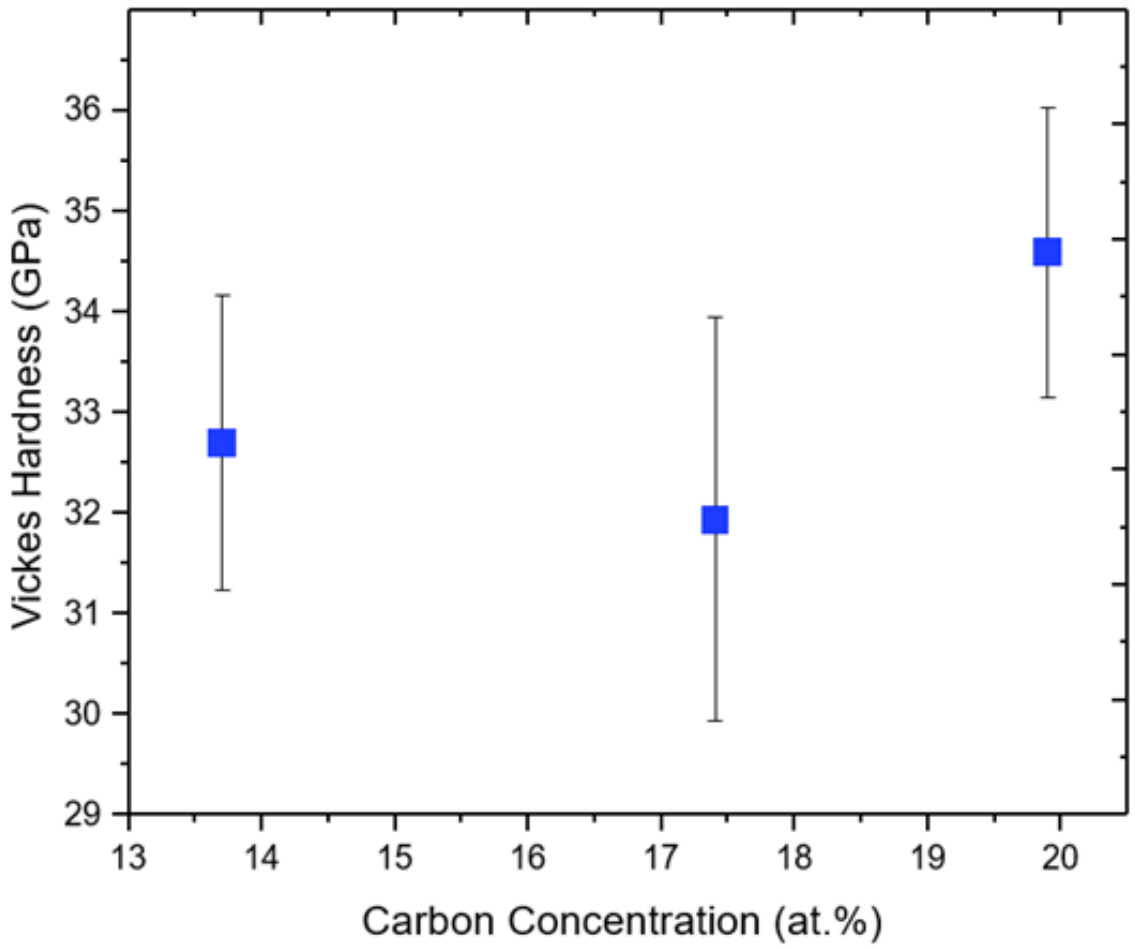

Figure 31: Vickers micro-hardness for B_4C, $B_{4.7}C$, and $B_{6.3}C$.

5.2.b. Raman Mapping and Quantification

The advantage of studying boron-rich boron carbides is that at larger B/C ratios they are mainly comprised of $B_{13}C_2$ units, which would address potential shortcomings and amorphization from any B_4C polytype, whether it be the $(B_{11}C)CBC$ or $(B_{12})CCC$ polytype, as suggested by models [6, 8].

First, it is wise to understand the crystalline Raman spectra of the samples being studied, and determine how their spectra differs, and what that can mean about the samples structures as the B/C ratio is modified. Representative crystalline Raman spectra of the samples are plotted in Figure 32.

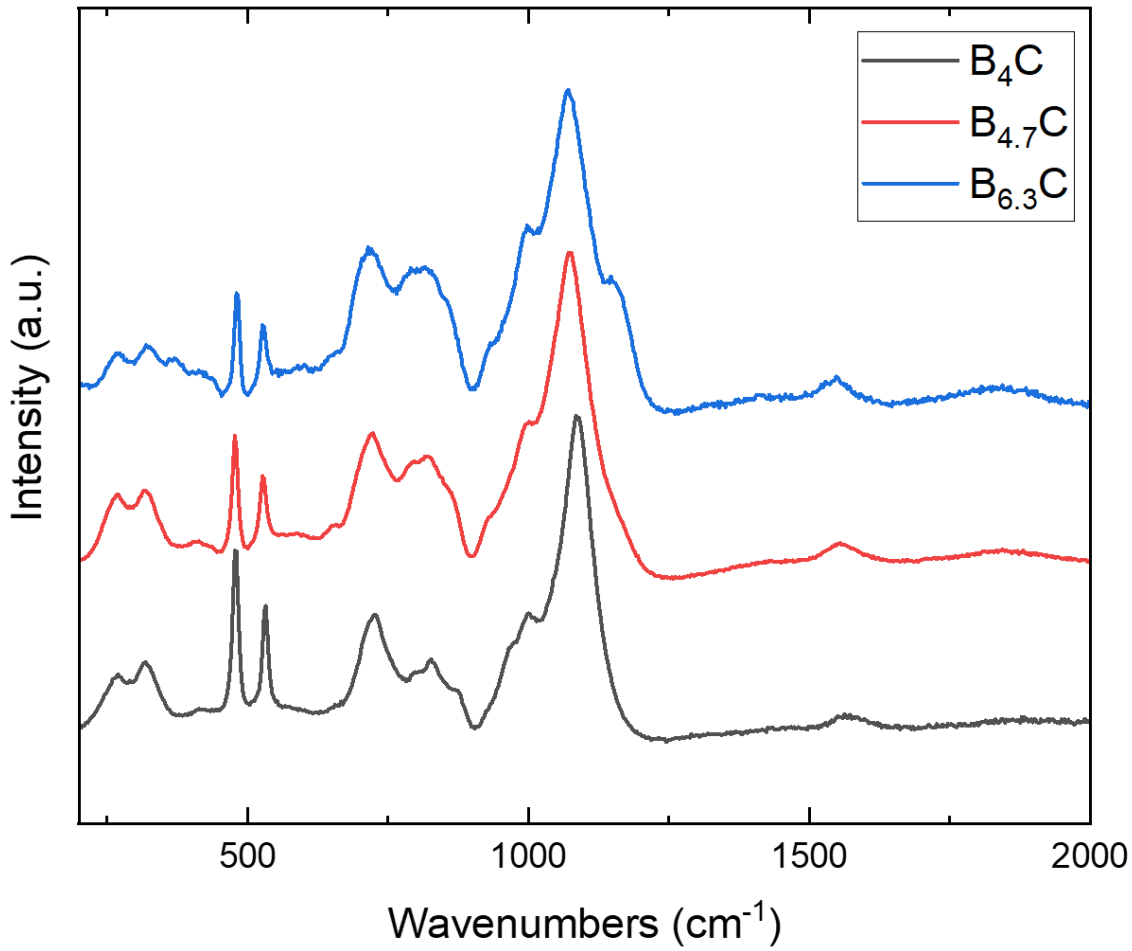

Figure 32: Raman spectra are shown for B_4C, $B_{4.7}C$, and $B_{6.3}C$. The graph is extended to 2000 cm^{-1} to show a lack of amorphous peaks on the virgin surfaces.

Looking at the Raman spectra of the pristine surfaces, a few notable changes are seen going from B_4C to boron-rich materials. The B_4C spectra is in alignment with what has been clearly noted in the literature [4, 18, 38]. However, new peaks at 180 and 375 cm^{-1} are observed in boron-rich samples around the $B_{13}C_2$ (13.3 at.% C) configuration, something seen the most boron-rich sample studied here, as well as the literature on boron-rich boron carbides.[13] The 1080 cm^{-1} icosahedra breathing mode (IBM) shows a consistent downshifting as boron content is increased, which is where the expected lattice expansion for boron-rich samples should be seen. This is indicative of boron-doping initially substituting within the icosahedra. Additionally, some small contributions from peaks between 900-1030 cm^{-1} become more prominent in the

most boron-rich sample, along with a small shoulder on the right side of the IBM peak. All other major peaks, 280, 320, 480, and 530 cm^{-1}, remain fairly consistent and unchanged throughout the stoichiometry range studied here.

Based on the Raman spectra from the samples investigated, it is determined that the initial boron atom substitutes into the icosahedra in B_4C, modifying the icosahedra from ($B_{11}C$) to (B_{12}). This is seen in the Raman spectra to varying extent for all levels of boron-doped samples and is assumed for the duration of this dissertation, as supported by previous work by Xie et. al. [14, 57].

Maps from the three boron carbide samples were analyzed and quantified. Three sets of figures were produced, one for each composition. The first set denotes Figures 33 and 34. Figure 33 shows a color-intensity map for standard boron carbide. The red color denotes intensity from the 1800 cm^{-1} peak. Figure 34 shows more examples of color-intensity maps, where the entirety of those images were probed with Raman, and each colorized pixel once again represents intensity from the 1800 cm^{-1} peak. These maps are pseudo-color intensity maps, and are only for illustrative purposes, since color gradients can be arbitrarily assigned to any range of numbers or intensities. The second set of figures, Figures 35 and 36, are similar in nature to Figures 33 and 34, but for $B_{4.7}C$. Lastly, Figures 37 and 38 follow for $B_{6.3}C$. Similar values were used for color brightness and signal intensities for all maps from all samples. All individual spectra were normalized before any color intensity maps were generated and spectra were quantified.

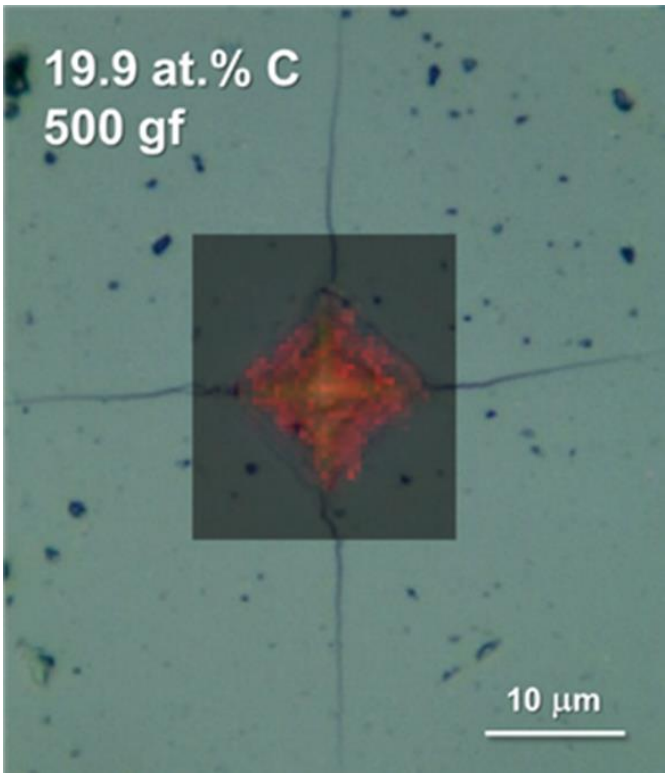

Figure 33: 500 g Vickers indent in B_4C. The darkened region shows the Raman map made, and red coloring indicates degree of amorphization seen at that location.

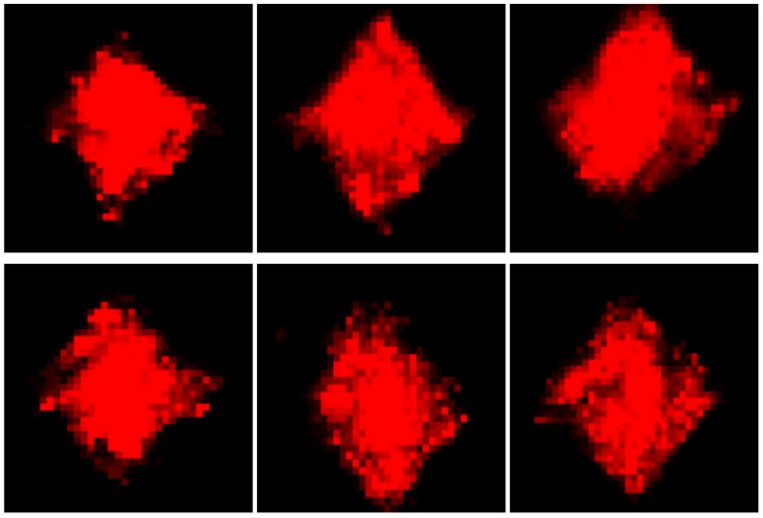

Figure 34: More examples of Raman pseudo-color maps of B_4C.

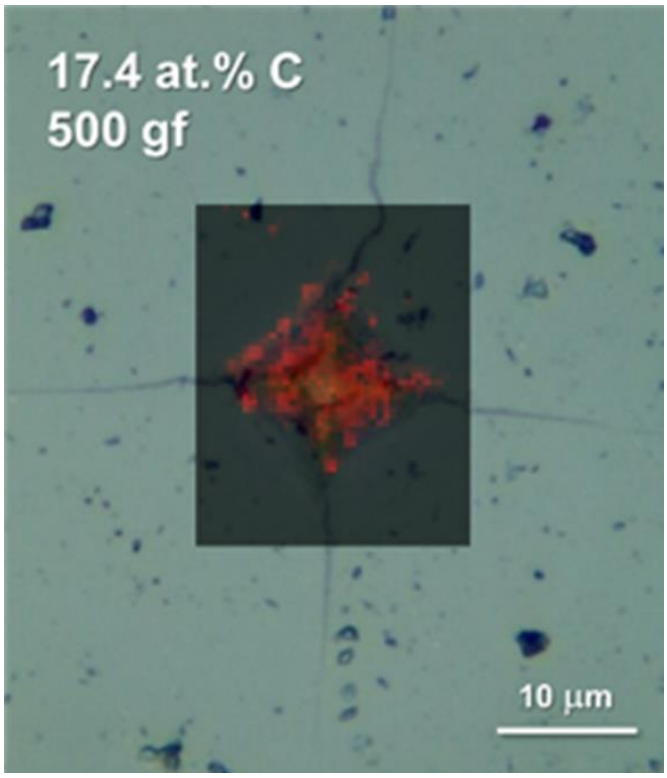

Figure 35: 500 g Vickers indent in $B_{4.7}C$. The darkened region shows the Raman map made, and red coloring indicates degree of amorphization seen at that location.

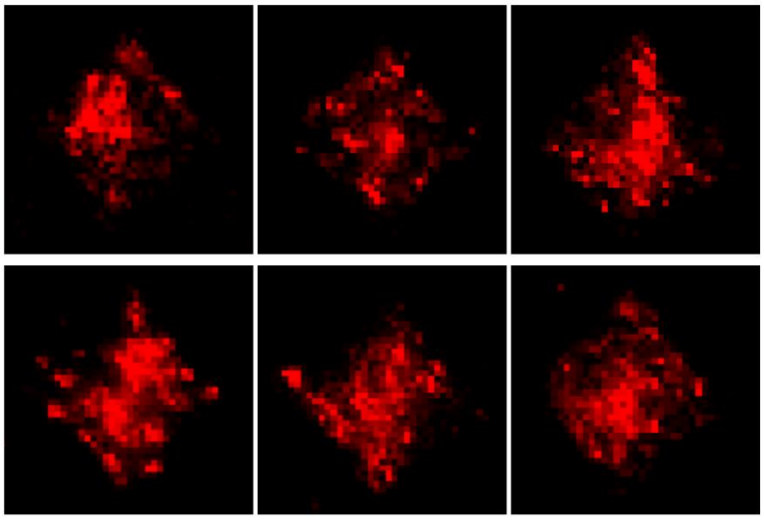

Figure 36: More examples of Raman pseudo-color maps of $B_{4.7}C$.

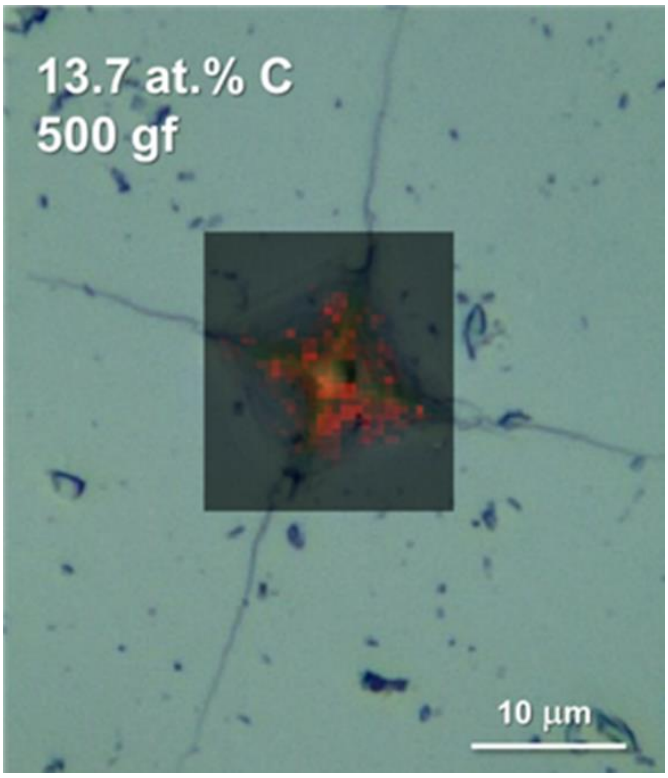

Figure 37: 500 g Vickers indent in $B_{6.3}C$. The darkened region shows the Raman map made, and red coloring indicates degree of amorphization seen at that location.

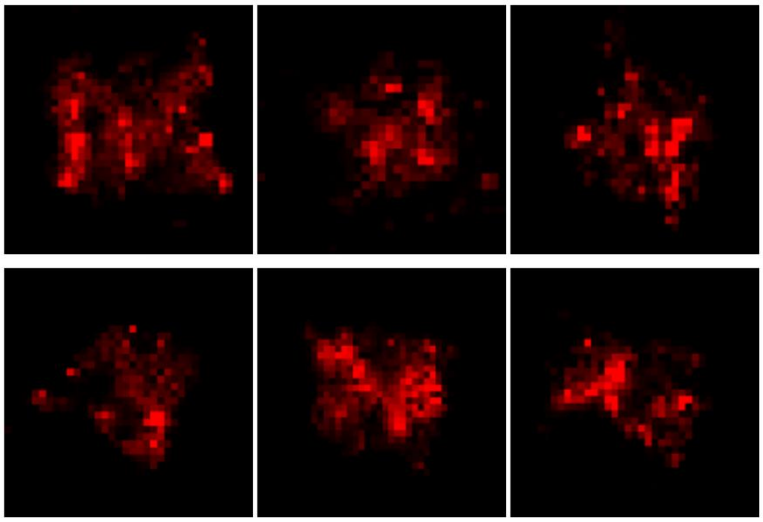

Figure 38: More examples of Raman pseudo-color maps of $B_{6.3}C$.

All maps for all sample stoichiometries show that amorphization is always contained within the contact area of the indenter; amorphization-related signal does not occur in the materials beyond the bounds of the indented region. All damage is in the subsurface of the samples beneath the indents, and amorphization does not extend or propagate laterally in the material. This means that any variations in map size will not add additional amorphous signal from the surrounding crystalline region, regardless of how much or little non-indented material is probed, as long as the entirety of the indent is within the limits of the map.

Each pixel in these darkened mapped images seen in Figures 33-38 represent a site where a spectra was taken, and each spectra has a value associated with it, which is the area of the 1800 cm^{-1} amorphous peak normalized to the crystalline peaks from 900-1100 cm^{-1}. Each spectra from a given map was summed, giving the total extent of amorphization intensity from an indent. Again, 8-10 pristine indents were probed and quantified, yielding the average for a given stoichiometry.

Given that all values were normalized to B_4C, the average total amorphization seen from that sample was set at 1. Relative to standard boron carbide, $B_{4.7}C$ had a total value of 0.45, and $B_{6.3}C$ had a value of 0.30 for total amorphization intensity. This shows a 55 % and 70 % reduction in amorphization intensity for $B_{4.7}C$ and $B_{6.3}C$, respectively. This result is shown in terms of Raman spectra in Figure 39, as well as graphically in Figure 40.

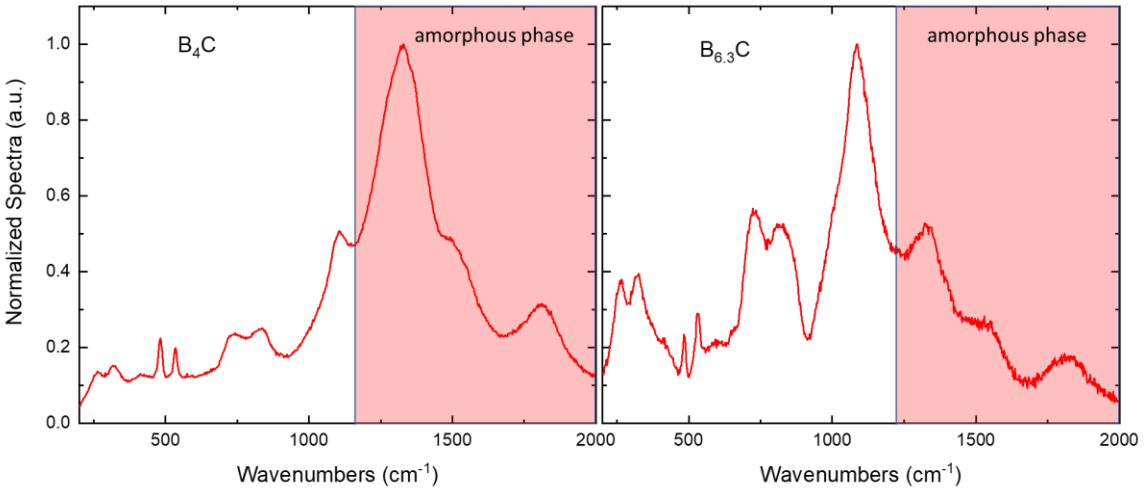

Figure 39: Representative Raman spectra of amorphized boron carbide (left) and boron-rich boron carbide (right). The region where amorphous peaks present themselves are highlighted in red.

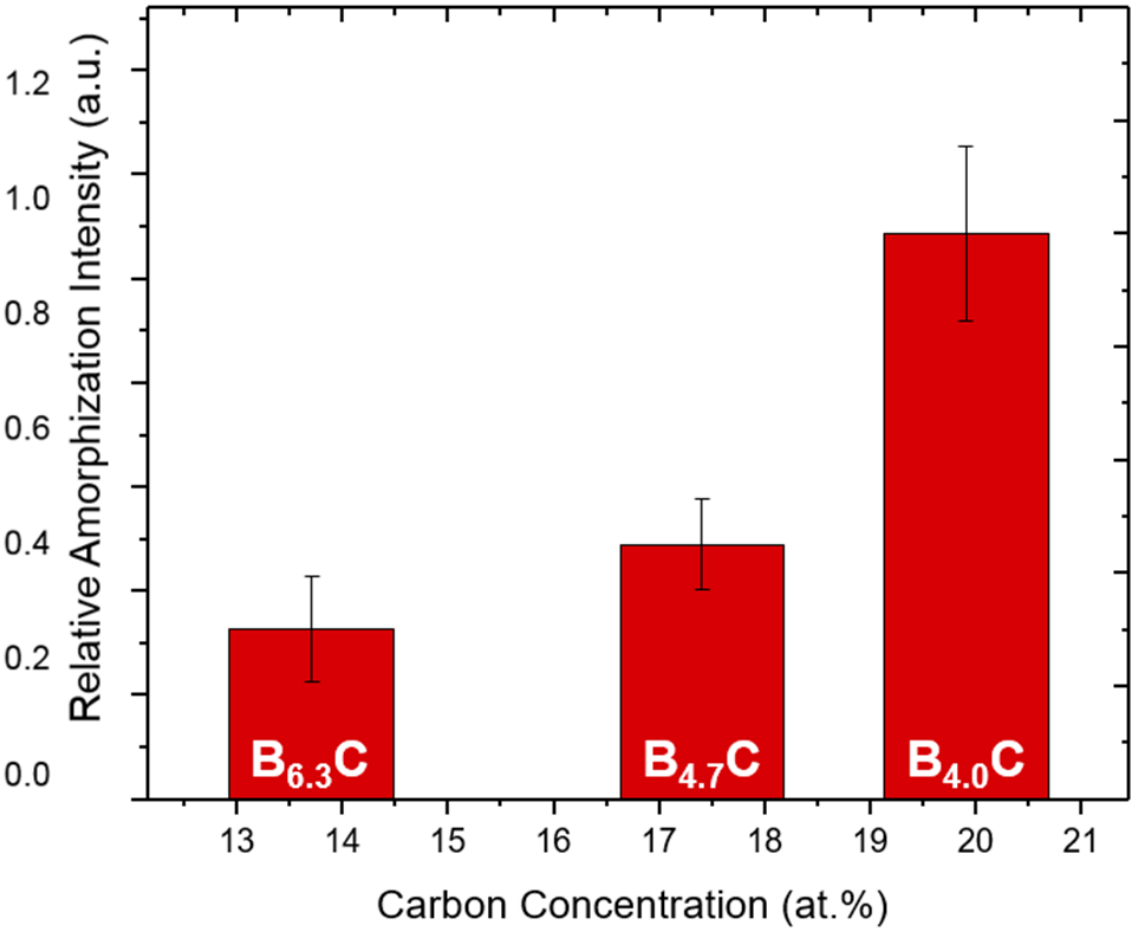

Figure 40: Raman-quantified amorphization intensity for B_4C, $B_{4.7}C$, and $B_{6.3}C$, normalized to B_4C.

These findings of amorphization mitigation are consistent with modeling since any B_4C polytype susceptible to failure will be replaced by a more ductile, although less hard, $B_{13}C_2$ polytype. Even considering an experimental sample can be a blend of polytypes and with different stoichiometries, there are less B_4C unit cells present in boron-rich boron carbides, instead favoring a boron-rich polytype, such as $(B_{12})CBC$. If this is the case, the boron-enriched icosahedra will not lend its carbon atom to interactions with the chain under bending and strain. Conversely, although less likely, if a boron-rich polytype is $(B_{11}C)CBB$, then the chain would be less prone to chain-icosahedra interactions because a CBB chain would be asymmetric and strained.

Yang et. al. [78] uses a similar amorphization-quantification method that accounts for size differences between indents in samples of differing compositions. Although amorphization is seen in the indented region of a sample, because samples with varying composition have different hardness values, as shown in Figure 31, these indented areas will differ. Thus, the amorphized regions created by the indents will vary in size. While it may seem critical to account for indent size variation, is does not change the result that amorphization intensity is reduced in boron-rich samples. Because boron-rich samples tend to have lower hardness values, their indented areas are larger, so, a reduction in amorphization intensity is seen from a larger amorphized area. If size differences were accounted for, a further reduction would be seen in the boron-rich samples.

It is difficult to draw any significant conclusions between a stoichiometries hardness and relative amorphization intensity because the trends between the two parameters differ.

While these results are very promising in reducing amorphization in boron carbide, it is important to note that Raman spectroscopy, while advantageous in its ability to quickly and

non-destructively probe boron carbide to determine amorphous phase transitions, is limited by the fact that it is a surface-sensitive vibrational spectroscopy technique. It is important to confirm a reduction in amorphization by other means. This thesis also identified a reduction in amorphization in boron-rich boron carbide by means of high-resolution transmission electron microscopy (HR-TEM), detailed in the following section.

5.2.c. Nano-Indentation and TEM Imaging

For this, the stoichiometric B_4C was compared to the most boron-rich boron carbide here, $B_{6.3}C$. Cross-sectional specimens were taken from near the center of a 500 mN nanoindentation. This was done to be consistent with initial Raman spectroscopy on the nano-indents taken near at the approximate center of the indent. Although it cannot be quantified the same way as micro-indents, a visual reduction in amorphization intensity can be seen in the Raman spectra from the nano-indents, shown in Figure 41.

While the same samples were looked at with Raman spectroscopy and TEM, the indentations were different. This is because, as stated in this and the previous section, nano-indents can be limiting when probing with Raman spectroscopy, and for TEM analysis, sample preparation is extremely difficult on larger indents. The FIB liftout process attempts to take out a slice of an indented and deformed region of boron carbide, which is still a very brittle material. The indent leaves many residual stresses built up in the region of interest, and that, coupled with the thin sample thickness required for high resolution microscopy, in this case approximately 50 nm, the Vickers indentations were not able to be successfully lifted out from the sample, so smaller Berkovich indents were used for this microscopy analysis.

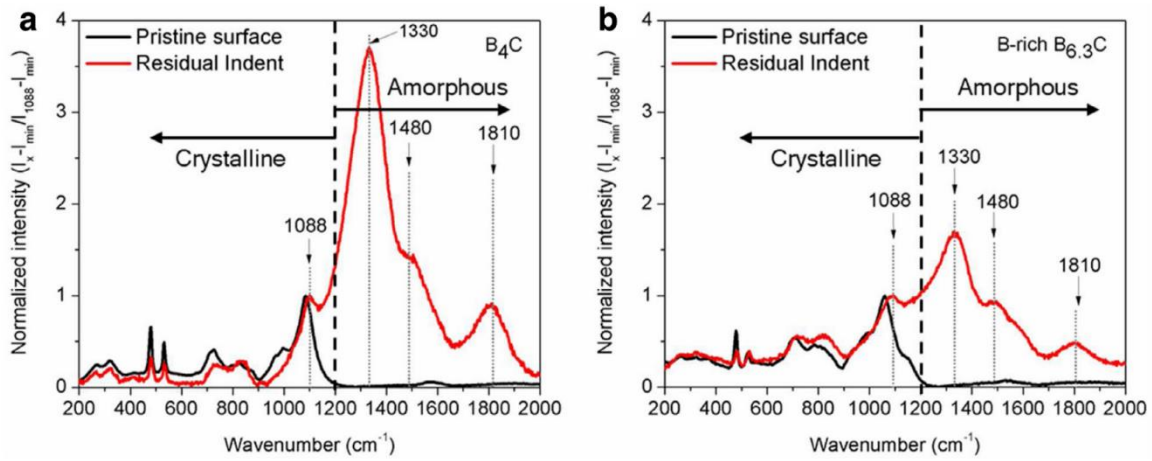

Figure 41: Raman spectroscopy of (a) crystalline and amorphized B_4C, and (b) crystalline and amorphized $B_{6.3}C$.

Nano-hardness values for boron carbide were 40 GPa, with a standard deviation of 2 GPa, while the boron-rich sample was noted at 37 GPa, with a deviation of 1 GPa. As in the previous section, a small drop in hardness is observed for boron-rich specimens. The nano-hardness of boron carbide is consistent with literature values.[4, 14]

The 500 mN nano-indented sample was observed at high-resolution microscopy. Before looking at amorphization in boron carbide and boron-rich boron carbide, the microstructures of the samples were first observed. An image of a microstructural comparison is shown in Figure 42. Both samples studied has a similar microstructure in terms of grain size. While nominal boron carbide appears to have a slightly higher grain size, both stoichiometries have grains on the order of 1-3 um. This makes the comparisons between samples helpful since both have a similar microstructure, the only change between them being carbon content. This also puts the grain sizes on a similar size-scale as the nano-indents used to induce amorphization.

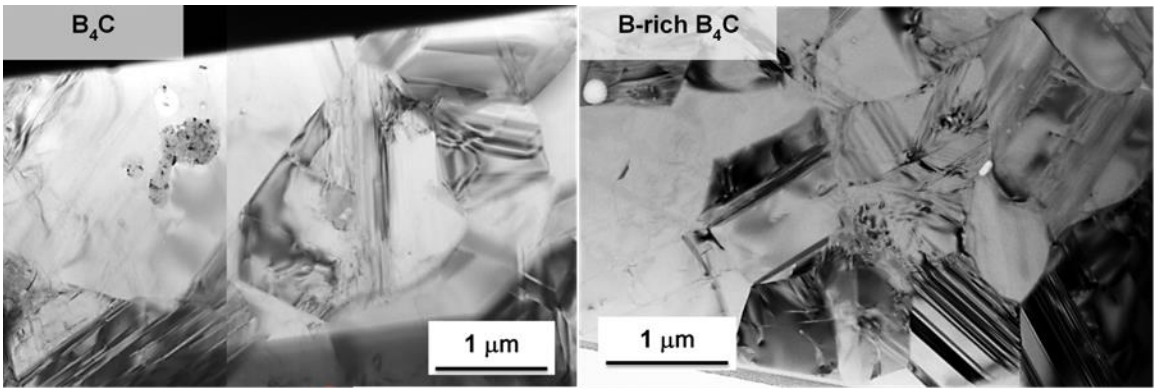

Figure 42: HR-TEM microstructure images of B_4C and $B_{6.3}C$.

A high density of planar defects were observed in the boron-rich sample. Planar defects were mainly comprised of twinning and stacking faults. An example of the planar defects in the boron-rich boron carbide can be seen in Figure 43. These features can also be seen in one boron-rich grain in Figure 42 as well. These features are present in all grains in boron-rich boron carbide, and their visibility depends on the orientation of the sample. It is seen more clearly in some grains due to that particular grains alignment with the zone axis of the microscope. Rotating and changing the orientation of the sample will make these defects more apparent in other grains.

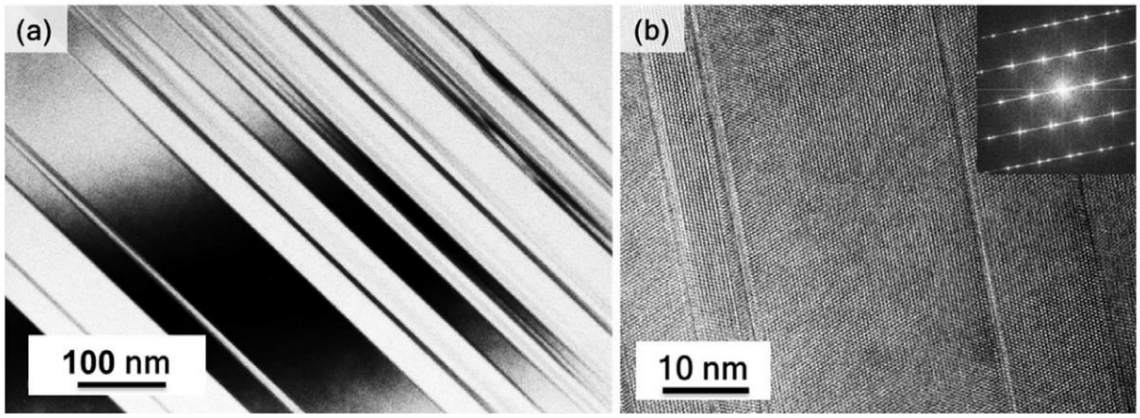

Figure 43: Micrographs highlighting planar defects in boron-rich boron carbide at differing magnifications.

In looking at the polycrystalline nominal boron carbide sample, amorphous bands are seen in the indentation-deformed region, similar to all previous literature that employed high-

resolution microscopy to observe amorphization in boron carbide.[3, 45, 56] There appears to be orientational preference in the formation of the bands, which are trans-granular in nature. The boron carbide indent and magnified view of amorphous bands are shown in Figure 44.

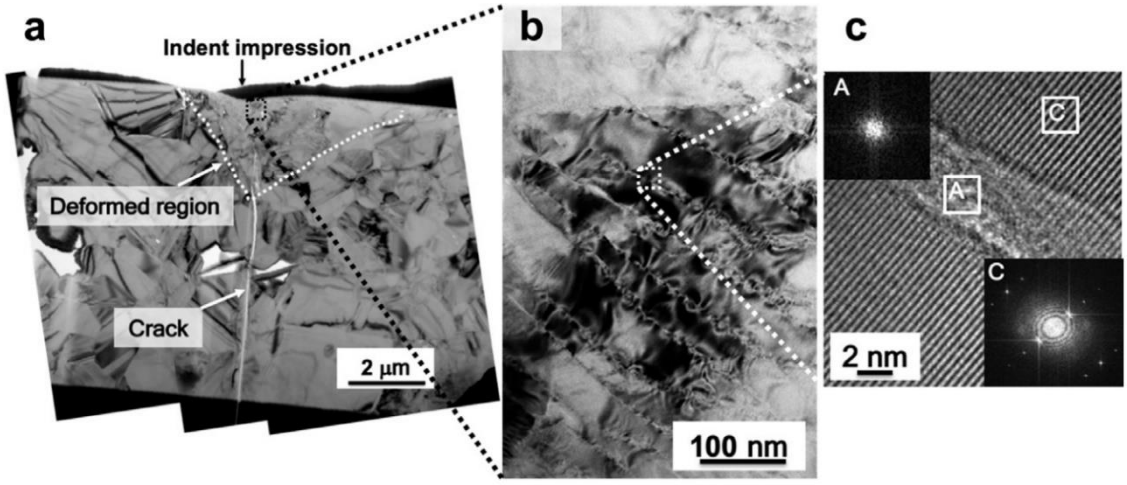

Figure 44: Micrograph of boron carbide, studying the damage zone beneath an indent. A Fourier Transform is shown indicating crystalline, C, and amorphous, A, regions in the images.

Looking into the boron-rich sample, amorphous bands are seen along with the planar defects mentioned earlier. This is the first time TEM has been used to image amorphous bands in boron-rich boron carbide. Images with varying magnification are shown in Figure 45.

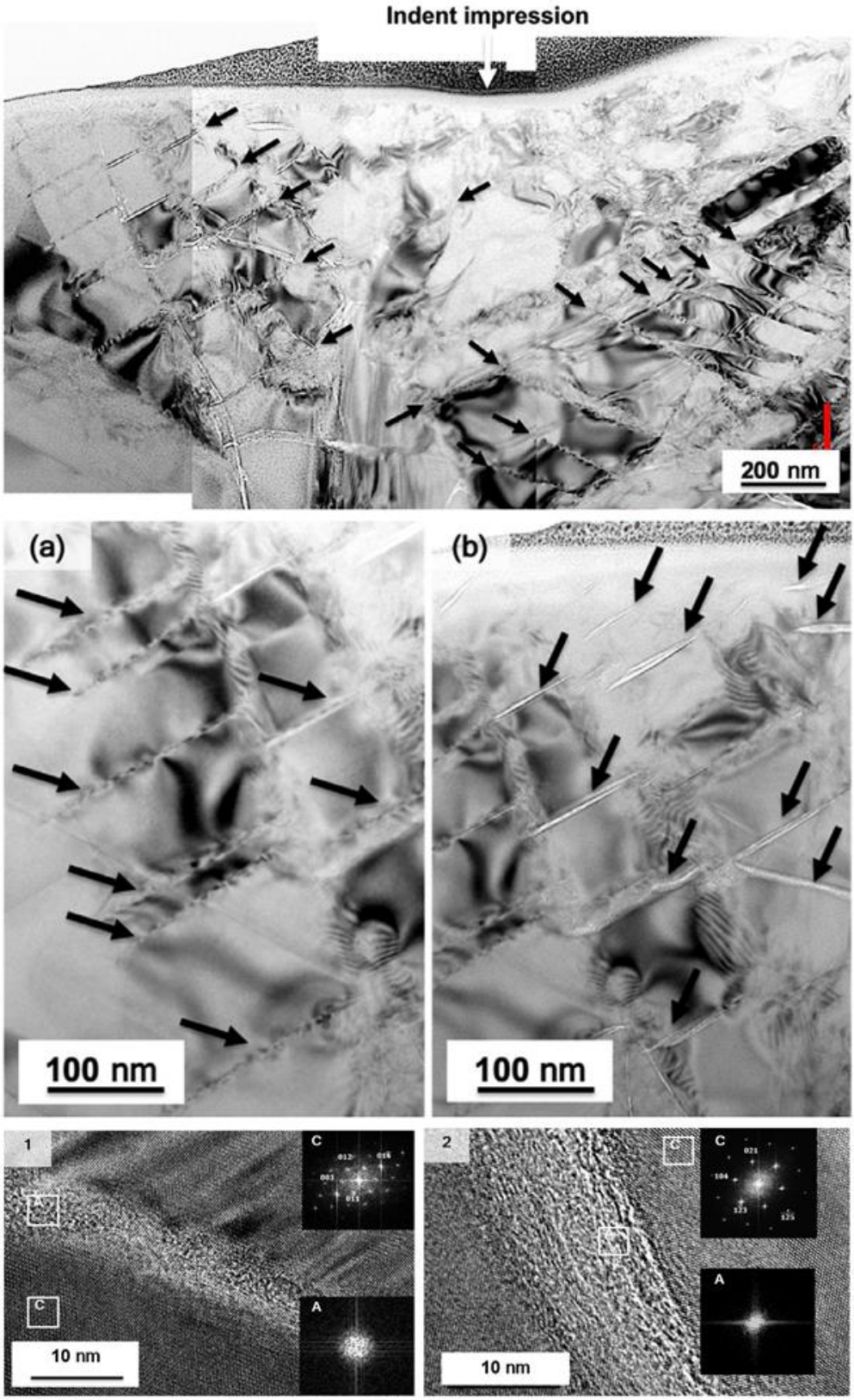

Figure 45: TEM micrographs of amorphous bands in boron-rich boron carbide. Inlaid images in (1) and (2) show Fourier transforms indicating amorphous material and crystallinity, present in and around the bands, respectively.

A direct comparison of the density of amorphous bands in boron carbide and the boron-rich sample was completed, analyzing similar regions beneath the same type of indents. Images are shown in Figure 46. An approximate 30 % reduction is seen in the number of amorphous bands in the boron-rich samples, confirming similar results seen from Raman mapping.

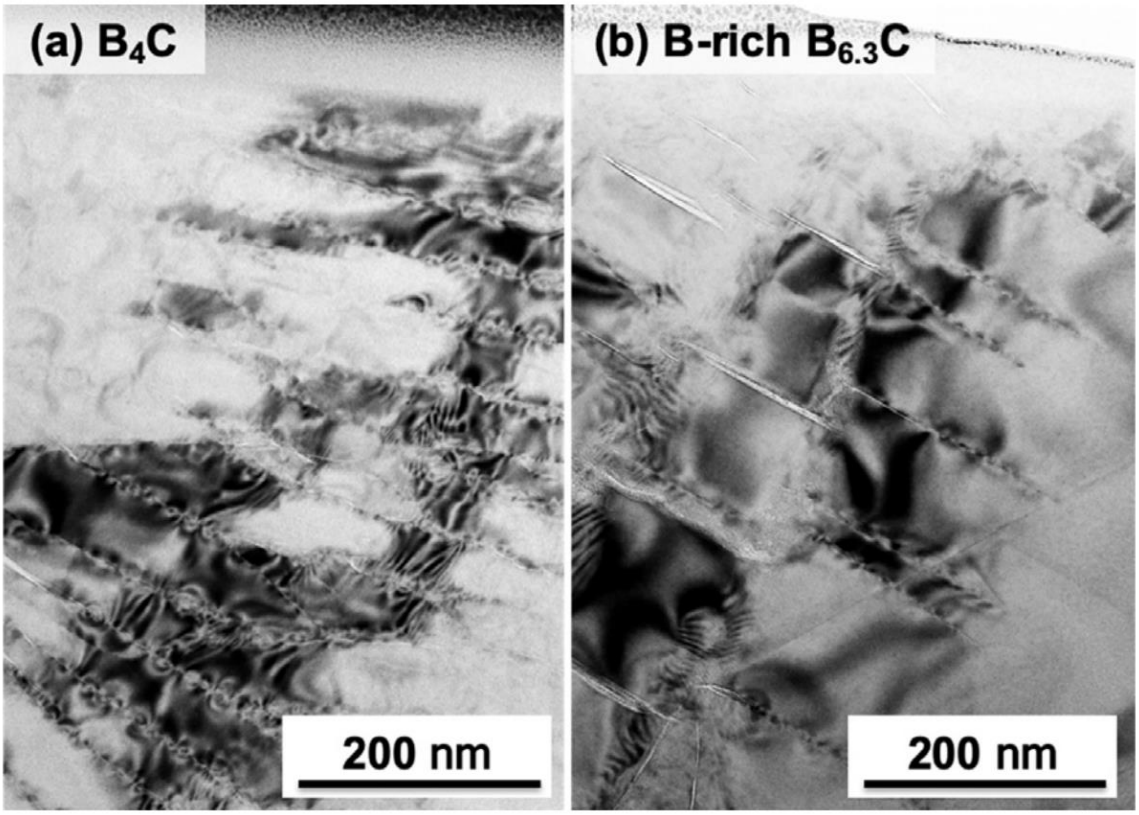

Figure 46: Micrographs of similar areas beneath indentations of standard and boron-rich boron carbides, respectively.

5.3. Summary

A reduction in amorphization in boron-rich boron carbide is determined. While there is agreement between Raman and TEM results indicating a reduction in amorphization in boron-rich boron carbides, Raman showed a 70 % reduction, while TEM results determined a 30 % reduction. This discrepancy does not diminish the results from either method, or their significance. Differences in total reduction between the two methods used can be explained in the following ways: (1) Different types and loads of indentation were used, and the reason

behind that necessity was already discussed. That said, both indentations did yield amorphization in both stoichiometries, with a reduced level of amorphization in the boron-rich sample. (2) With Raman spectroscopy, a volume is being probed with a laser, while with TEM, only a limited number of samples and regions can be similarly probed for comparison, so in that regard, Raman is a more extensive method of gathering a larger amount of data on amorphization from an indent. Since Raman can probe a larger volume than a TEM image, there are more ways to explain the fact that a larger reduction was seen from this instrument: (a) the total volume of the plastically-deformed zone formed by the indent could be reduced from the boron-rich sample, (b) the amorphous bands could be smaller in size, mainly in length, or (c) there are fewer bands created by an indent. Raman results could be a combination of all 3 scenarios (a, b, c). The TEM image only shows a reduction from scenario (c), although scenario (a) and (b) are not disproved as further possibilities and contributions. Thus, between the differing methods, although slightly different in extent, a conclusion can be drawn that boron-rich boron carbide has less amorphization than nominal B_4C, something that can have a large influence on the materials performance and behavior in ballistic events.

6. OBJECTIVE 3: Conduct in situ heating of amorphized boron carbides of varying stoichiometry

6.1. Experimental Procedures

Samples studied for this objective are shown in Table 11.

B/C Ratio	Carbon Content
4	19.7
5.5	15.3
9.4	9.6

Table 11: Sample B/C ratios and corresponding carbon compositions used for Objective 3 analyses.

Samples were previously polished and indented, as in previous objectives. Vickers indents of 5 N load were placed in areas with low residual porosity using a LECO M-400 Hardness Tester. Indents were loaded for 5 seconds and held at maximum load for 5 seconds. Vickers indents were utilized to induce amorphization to study the evolution of the amorphous phase at elevated temperatures. Samples were cut from the epoxy molds using a diamond saw and placed into the hot stage sample chamber for in situ heating.

A Linkam TS1500 hot stage was used to conduct in situ heating of boron carbide samples. The sample chamber was a ceramic cup that was 7 mm in diameter, and 3 mm deep. The system can reach a maximum temperature of 1500 °C with a max heating rate of 200 °C/min. The stage was pumped down using an Edwards E2M1.5 vacuum pump and backfilled with inert Argon gas. The hot stage also has water cooling system running through the device to safely reach elevated temperatures only within the sample cup.

Using Raman spectroscopy, a 633 nm laser probe the boron carbides in the range of 200-2000 cm^{-1} at the center of the Vickers indent. Scans were taken at elevated temperatures up to 900 °C in increments of 50 °C. The heating rate was 50 °C/min, and spectra were taken

every 10 min, which allowed for the stabilization of temperature in the sample, as well as for data collection.

6.2. Results & Discussion

Figure 47 is an example of a typical Vickers indent probed at elevated temperatures. The image, taken with an SEM, is boron-rich boron carbide with 15.3 at. % carbon.

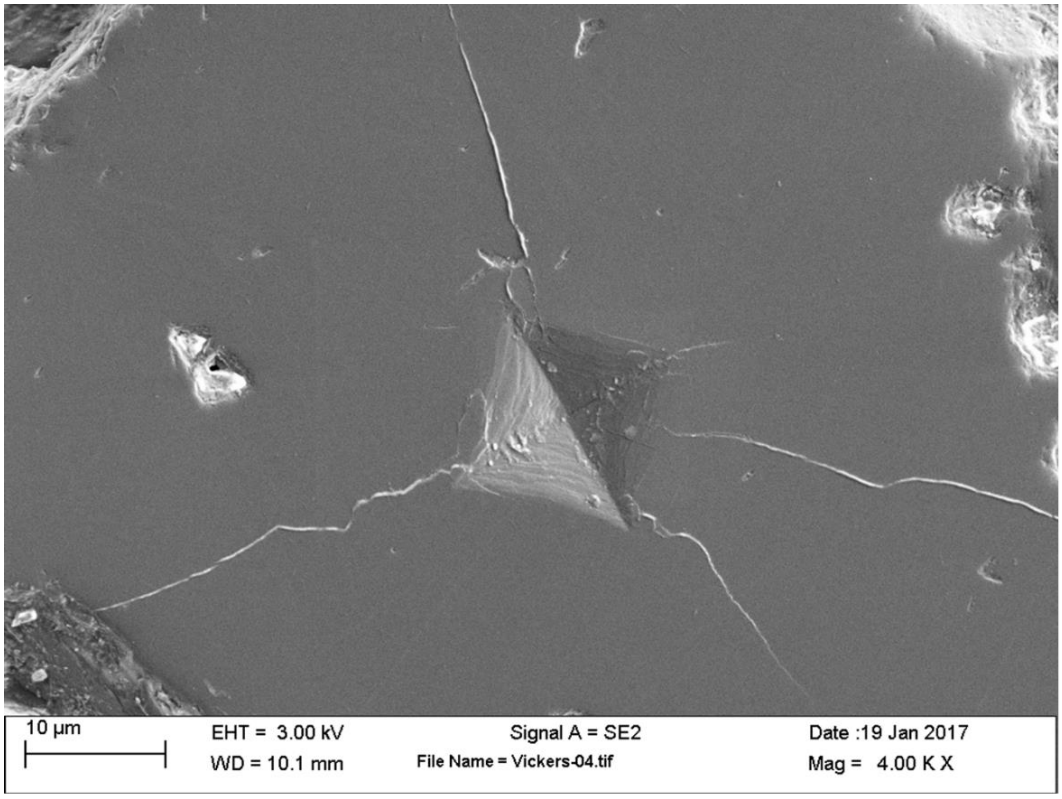

Figure 47: SEM image of a 5 N Vickers indent in a boron carbide sample with 15.3 at. % C.

Figures 48-50 show the Raman spectroscopy results for samples with 19.7, 15.3, and 9.6 at. % C, respectively, up to 650 °C. The amorphous phase signature disappears at elevated temperatures in all samples spanning the homogeneity range. For boron carbide (19.7 at. % C), in Figure 48, the amorphous phase is annealed at 550 °C. This result is in agreement with previous work observing crystalline and amorphous Raman spectra of boron carbide at elevated temperatures.[48]

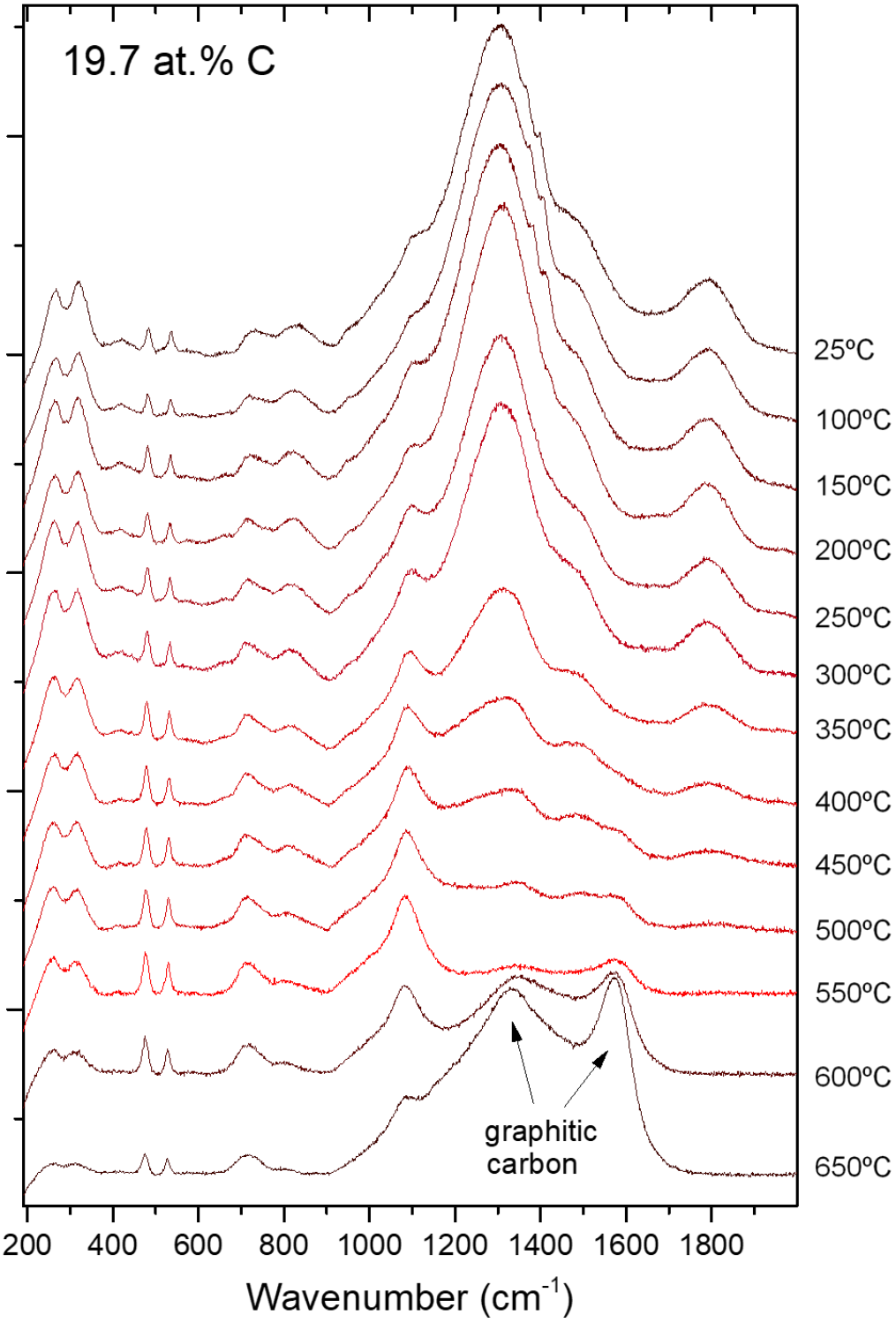

Figure 48: Raman spectra from the center of a 5 N Vickers indent in a boron carbide sample with 19.7 at. % C. *In situ* spectra acquired at elevated temperatures in the hot stage.

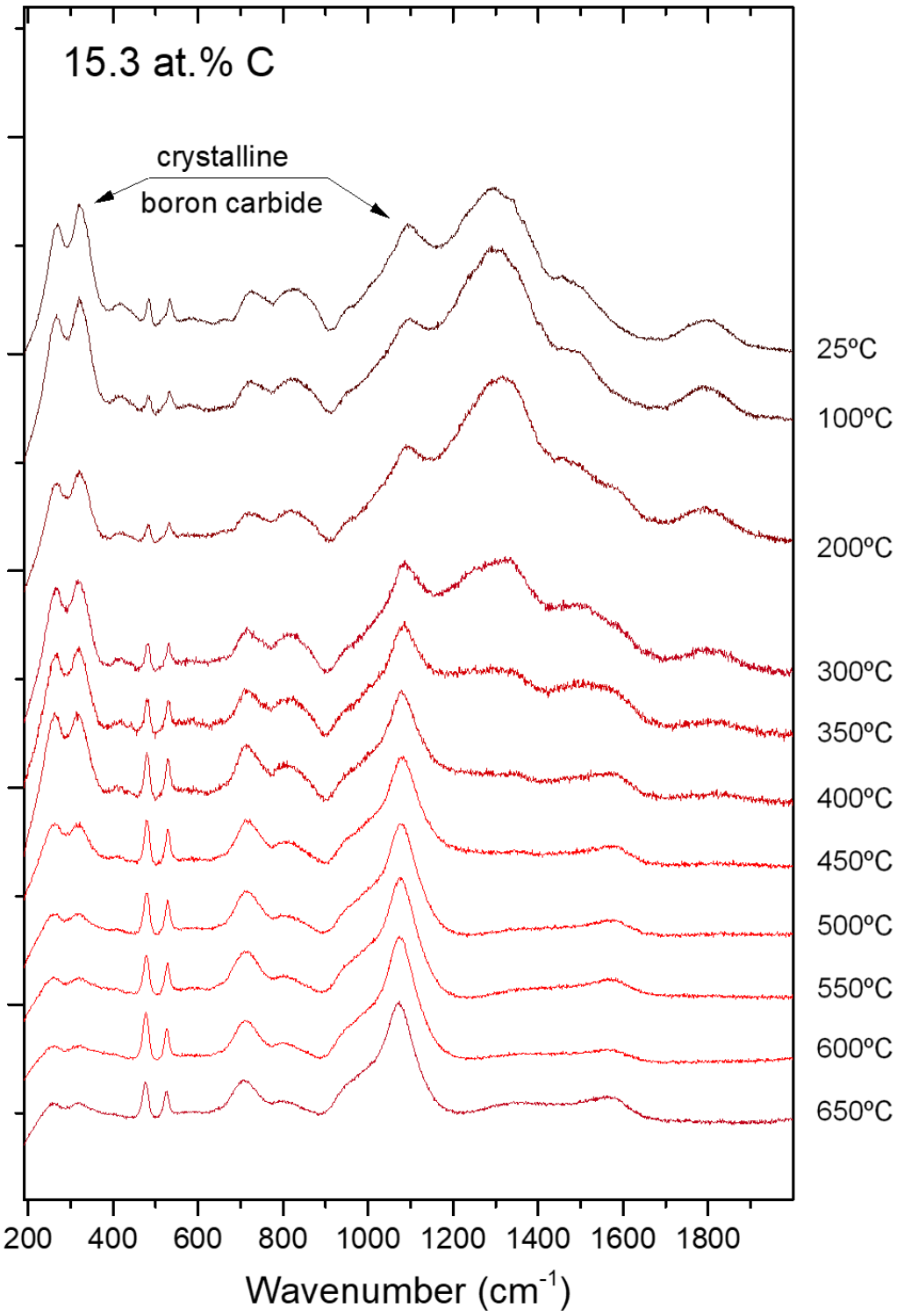

Figure 49: Raman spectra from the center of a 5 N Vickers indent in a boron carbide sample with 15.3 at. % C. *In situ* spectra acquired at elevated temperatures in the hot stage.

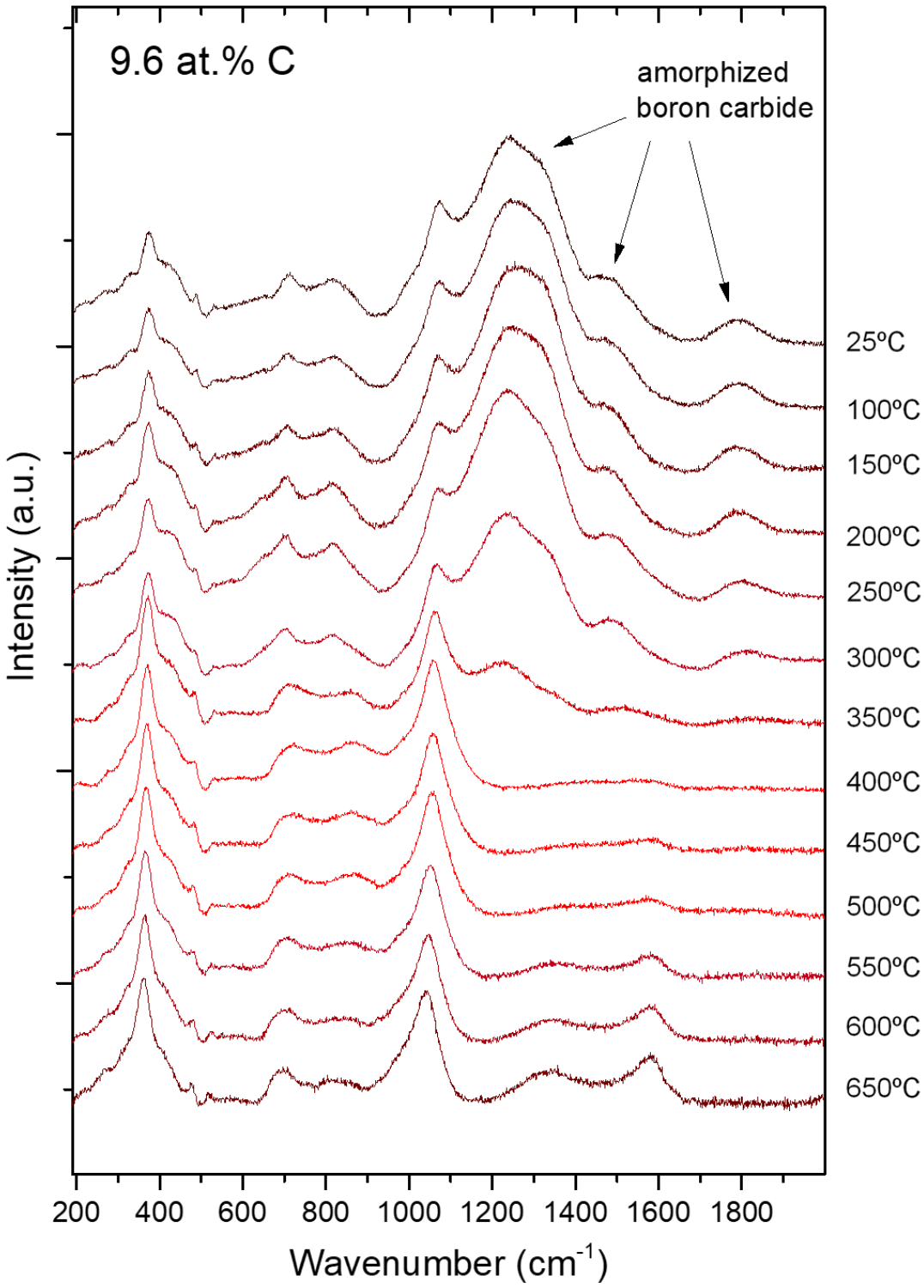

Figure 50: Raman spectra from the center of a 5 N Vickers indent in a boron carbide sample with 9.6 at. % C. *In situ* spectra acquired at elevated temperatures in the hot stage.

For the median sample (15.3 at. % C), in Figure 49, the amorphous phase disappears from the Raman spectra at 450 °C. The most boron-rich sample (9.6 at. % C), shown in Figure 50, showed the amorphous phase disappearing at 400 °C. This can indicate different stability of the amorphous phase at varying stoichiometries. Another possibility is that the amorphous phase is reduced in doped samples, requiring less thermal energy to anneal back into a crystalline state.

Above temperatures of 600 °C, graphitic carbon peaks appear at 1330 and 1550 cm^{-1}. This is indicative of a chemical reaction taking place, presumably between oxygen leaking into the system and reacting with boron carbide to form boric acid (B_2O_3). This resulting material will be a transparent liquid, non-Raman active, and leaves behind graphitic carbon, which is what is detected and shown by the presence of the new peaks above 1200 cm^{-1}. This reaction has been observed and documented elsewhere, and was a result of heating from the intensity of the laser.[79] Oxygen can be present in the chamber after purging, or from a pressure differential in the system allowing atmospheric gasses to enter the system.

Looking further into the appearance of the graphitic carbon peaks, one important thing becomes evident. The peaks formed after the amorphous peaks were annealed; the amorphous peaks did not reduce into graphitic spectra. This could be an indicator that the amorphized peak positions merely overlap with graphitic carbon spectra, and that they were not a result of contributions from graphitic features.

Newer models suggest that boron carbide reaches temperatures such that the material can melt, and that amorphization can result from the quenching of melted amorphous material.[10] The idea of boron carbide melting under impact was also theorized before in trying to understand boron carbides hindered ballistic performance and subsequent large lattice compressions.[1] This work, showing the amorphous phase annealing at lower temperatures,

can support these claims. While the amorphous can be annealed, these tests take place over a timescale of minutes. Ballistic impacts, energy and heat dissipations, and lattice compressions under impact, occur on much smaller timescales, such that quenching can become a good explanation of how boron carbide can amorphize, regardless of the fact that the amorphous phase can anneal at lower temperatures. Furthermore, a chemical reaction taking place and oxidizing the material can also be limited by a lack of presence of oxygen within the bulk material.

7. Objective 4

7.1. Experimental Procedures

Once again, boron-rich boron carbide powders, prepared by hot-pressing [11], were used to complete experiments in this objective. Table 12 shows the B/C ratios of samples used, with their corresponding carbon compositions.

B/C Ratio	Carbon Composition
4	19.9
4.6	17.8
6.9	12.6

Table 12: Sample B/C ratios and corresponding carbon compositions used for Objective 4 analyses.

A diamond anvil cell was used to study the onset of amorphization in these samples in situ with Raman spectroscopy. Before experiments can be run, several preparatory steps need to be taken to ensure the DAC will perform as expected.

Proper alignment of the diamond anvils is crucial for high pressure experiments, so before each high pressure run, alignment needs to be checked and corrected so the culet surfaces are in perfect lateral alignment and are perfectly parallel to one another.

The anvil on the bottom of the cell has 4 screws that can be used to make micron-level adjustments so it can be placed in alignment with the top anvil. This bottom anvil is also placed on a tungsten carbide seat, which allows it to remain perfectly flat. The anvil must be flush with the top anvil, when viewing the top anvil using the camera attached to the Raman spectrometer. Examples of misalignment are shown below in Figure 51. Any misalignment will cause pressure to build up in the diamonds in such a way that the diamonds will fail during the experiment. When properly aligned, only the top anvils culet is visible, since the bottom anvil will be perfectly in line with the top.

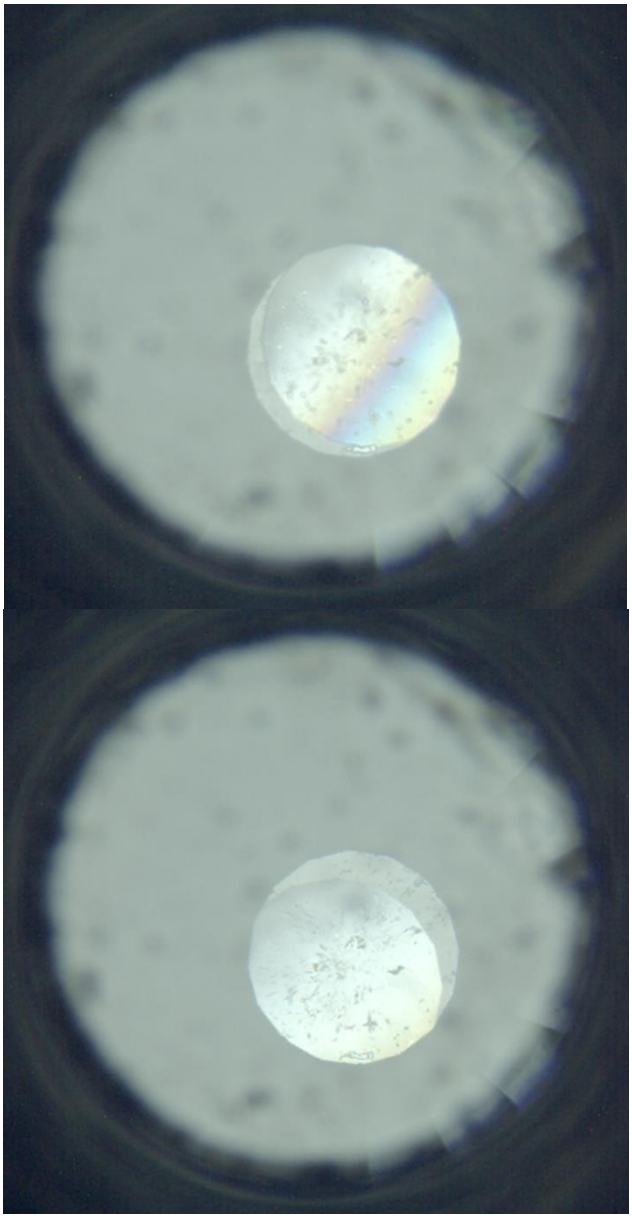

Figure 51: Images of lateral misalignment between the two diamond anvil culets.

Additionally, the anvils must be parallel to one another. Misalignment here will result in improper pressure buildup in the diamonds and will prevent the cell from imparting pressure equally on the sample. This can also cause failure of the diamonds because pressure is meant to be exerted on the diamonds for a preferred orientation. The top anvil must not be tilted with respect to the bottom angle, so this anvil has 3 screws that, when tightened systematically, can tilt the anvils angle. If the anvils are not parallel, it can be seen with fringes, which are a result of

reflections off of their mismatched surfaces. They are in perfect contact when no fringes are visible. This alignment check is shown in Figure 52, using the Raman spectrometer camera viewing feature.

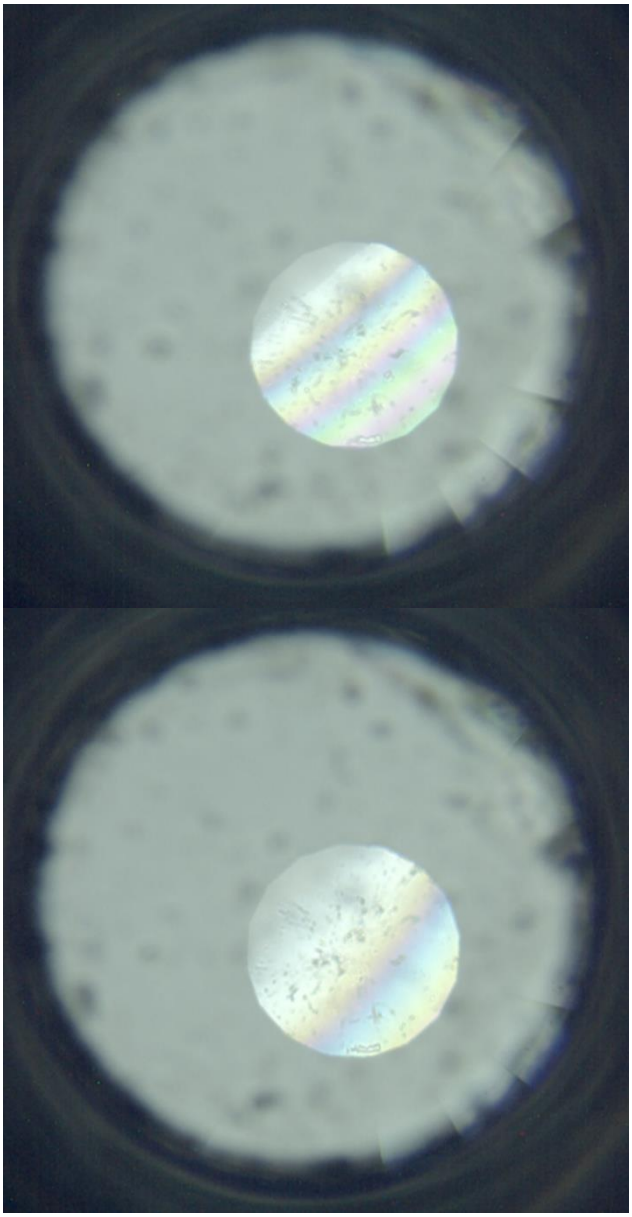

Figure 52: The top image shows a misalignment with respect to tilt between the anvils. The bottom image shows a full alignment accounting for lateral and tilt adjustments.

Alignment of the cell is critical for successful experiments, and thus it must be check and adjusted as needed before each individual experiment. Additionally, when new diamonds are

put into the cell, several excursions to high pressures must be incrementally reached in stages, to allow the diamonds to “break-in”, or be “worn in” like what one does with new shoes. After several high-pressure ramp-ups, the diamonds tend to stay in reasonable alignment, with only minor adjustments necessary between runs.

Pre-indented and drilled gaskets were used for the main experiments. Gaskets, approximately 250 um thick, are indented with a 400 um diameter spherical tip to 1/3 their original thickness (approximately 80 um), and the drilled hole in the center of the gasket is 150 um in diameter. Thus, the sample chamber is an approximate circle of 150 um in diameter with a thickness of 80 um.

For initial experiments, gaskets that were not indented or drilled were used as practice, while also gathering preliminary data to analyze. For those runs, gaskets were carefully indented before the actual experiment, and were then filled with boron carbide powders to bring to high pressures.

Powder samples are carefully loaded into the gasket, and later the gasket hole, with a needle. Occasionally alcohol (ethanol) was used to help powder adhere to the needle, otherwise this method relies on Van der Waals forces to get the powder to adhere to the end of the needle tip for loading.

Ruby is used a pressure calibration during experiments. A small amount of placed into the gasket hole so the pressure imparted to the sample and ruby can be measured during the experiments. The 694 nm R1 ruby line can be observed, and its displacement under pressure can be used to calculate pressure in the cell. This is shown in Figure 53. The equation for pressure calculations, in GPa, is:

Pressure (GPa) = {(*Ruby R1 line shift from 694.24 nm*)*2.9356}-0.4411, from [80] and [81].

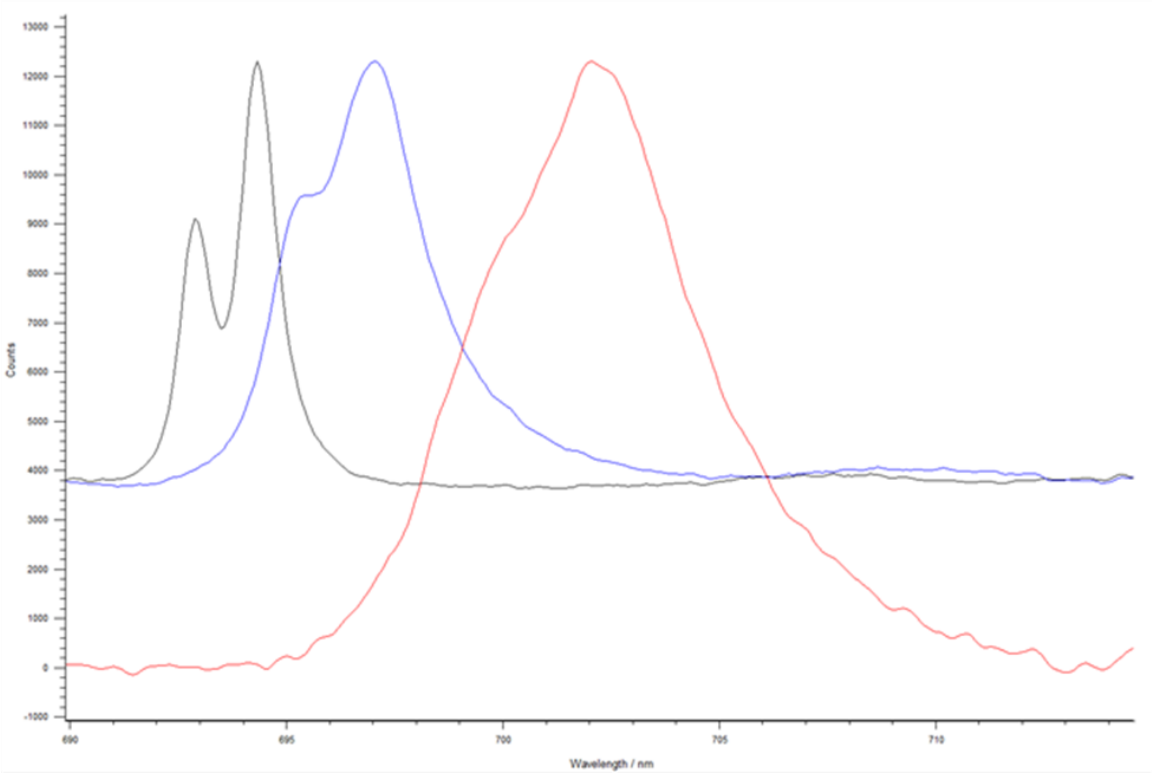

Figure 53: Spectra of ruby at ambient pressure (black) and elevated pressures (blue and red).

Once loaded with powder and ruby chips, the cell is connected to a gas line as a means to transmit pressure to the cell. Inert argon gas is used to apply pressure to the system by way of pressing the piston unit further into the cylinder.

The gas line is directed through a controller, which is connect to the cell. The controller gives an arbitrary number as gas is allowed to flow through it to the DAC setup, will be recorded throughout the experiment. The gas through the controller travels to the membrane, which allows the cell to close on itself. The membrane is limited to move a maximum of 400 um, by means of 4 locking screws, which prevent the membrane from being destroyed by displacing too much.

Before high pressures were reached, initial Raman spectra were taken in the cell to make sure a clear enough signal was obtained of both the sample and the ruby. Signal intensity

of the sample can be very low, because the Raman laser is traveling through the diamond, 3 mm of single crystal carbon, giving a very intense signal at 1330 cm^{-1}. The initial spectra appears as if the only peak present is from the crystalline diamond. However, the boron carbides spectra is contained within the (mostly) flat background noise, and is visually apparent once the appropriate region is magnified. An example of this initial spectra is shown in Figure 54.

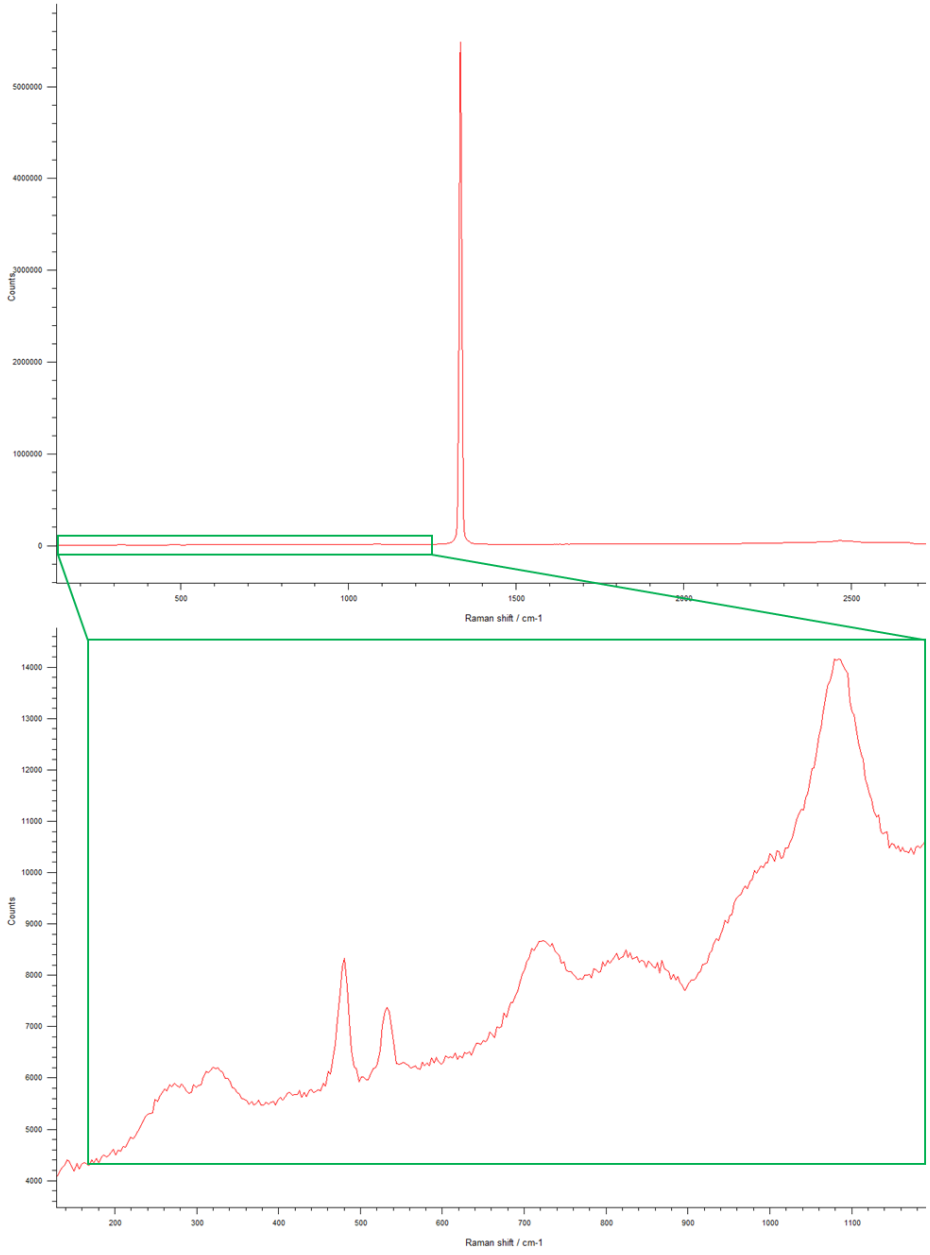

Figure 54: The top image shows a standard Raman spectra obtained through a DAC, and the bottom image shows the spectra zoomed in to properly view and assess the boron carbide spectra.

When running the experiment, gas is applied to the cell in incremental stages, and after a few minutes is given to stabilize pressure in the cell, Raman spectra can be taken.

During these runs, several things need to be noted throughout the experiment to ensure a proper test and to prevent failure of the diamonds. Once pressure in the cell has stabilized and the Raman spectra taken, it is important to note the number on the gas controller and the peak position of the diamond line. The pressure on the diamond can be calculated by the peak shift from 1330 cm^{-1}. A separate Raman spectra is taken, in nanometers as opposed to the standard wavenumbers, for the ruby line to determine its change in position to calculate pressure in the cell.

7.2. Results and Discussion

Early DAC experiments utilized boron carbide and a boron-rich boron carbide, using a gasket without a hole in it. These early compression tests reached maximum pressures that ranged between 25-40 GPa. An example of this is shown in Figure 55, where a boron carbide (left) and boron-rich boron carbide (right) were pressed to approximately 38 GPa before being unloaded. Ascending spectra show the samples being loaded and subsequently unloaded in situ, with post-mortem spectra of amorphized material at the top. The results for standard boron carbide under non-hydrostatic loading conditions are consistent with similar single-crystal DAC findings in the past.[5]

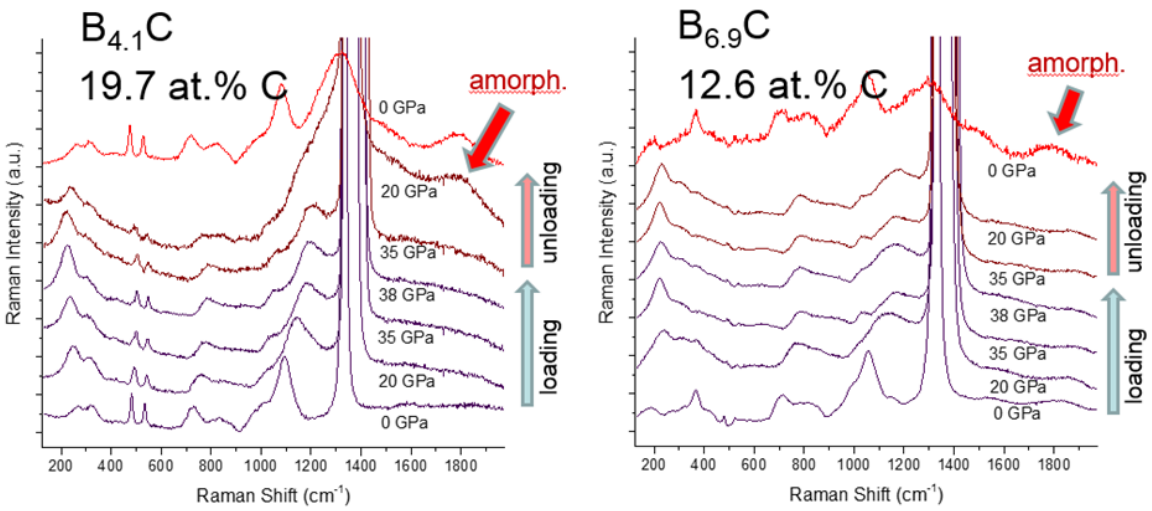

Figure 55: The spectra on the left shows boron carbide being loaded to and from 38 GPa, and the spectra on the right shows the same loading and unloading regime for boron-rich boron carbide. For both spectra, post-mortem amorphized spectra are shown at the top in red.

This result is significant because it is the first time that boron-rich boron carbides have been studied in a DAC. Barring the exact atomic mechanism, amorphization in boron carbide and its effect on the materials performance are well understood at this point. For boron-rich variations, similar findings have yet to be determined or verified. Models can be helpful in that they predict no amorphization in boron-rich materials, but there can be some discrepancies between models and experimentally fabricated materials. Thus, it is important that these experiments validate models and determine exactly how these fabricated materials behave compared to nominal B_4C.

These experiments show that both boron carbide and boron-doped samples exhibit amorphization under the same loading and unloading conditions. All other parameters in the experiments were the same. It is also worthwhile to note that models [8, 67] suggest no amorphization in boron-rich materials, but it is still shown to occur experimentally. Additionally, it occurs under the same conditions, as can also be seen with any instance of indentation in this dissertation, albeit to a lesser extent, as was also shown previously in Objective 2.

Post-mortem maps of the gaskets were generated and are shown below in Figure 56. Maps were the same size and were taken at the center of the pre-indented gasket. Similar results are seen to the indentation maps, where amorphization is induced in all carbon compositions under the same conditions, but here, it is again shown that boron-rich boron carbides appear to amorphize to a lesser degree. Quantification was done using the same method that was used to quantify the indent mapping results from Objective 2.

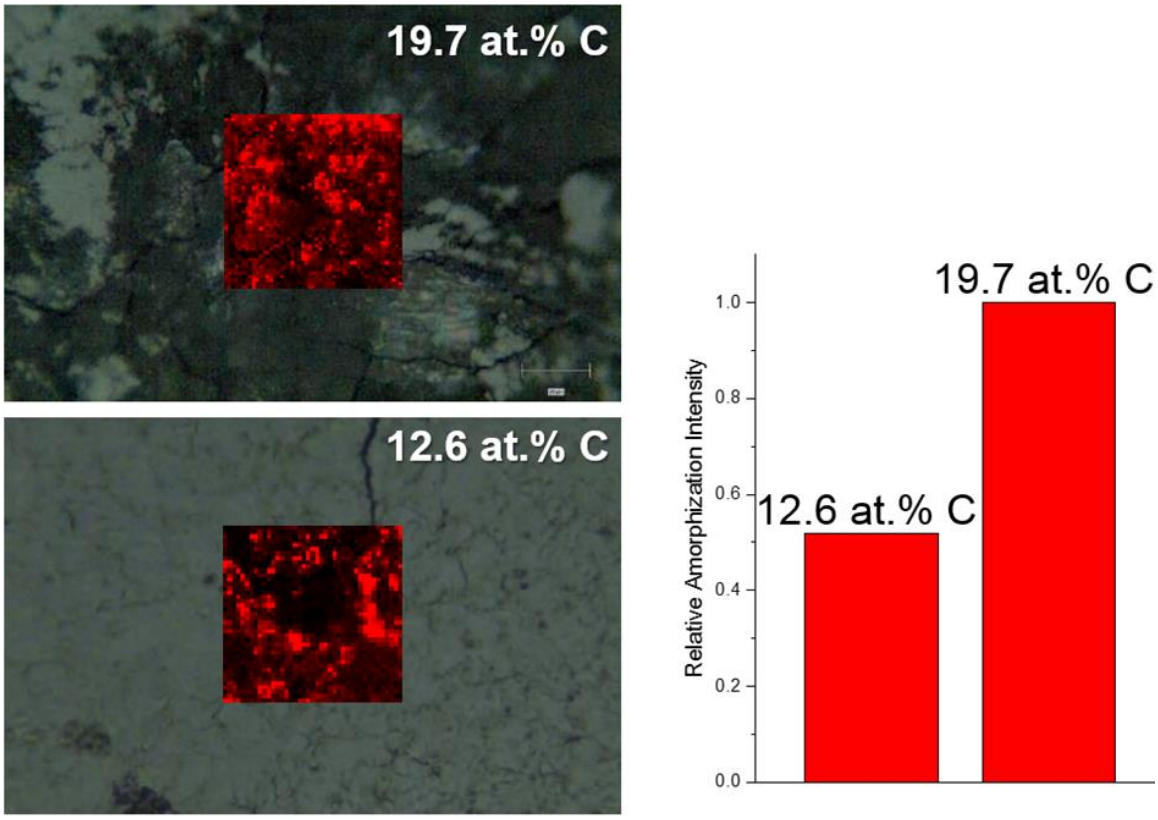

Figure 56: The images on the left show Raman maps of amorphized boron carbides. The plot on the right map quantification results, normalized to nominal boron carbide.

Next, DAC experiments were run using a gasket with a drilled hole in the center. A visual of the gasket hole can be seen through a 50x lens, before (top) and after deformation (bottom) in Figure 57. It can be seen that the gasket hole is typically compressed to about 50 um in diameter, compared to the initial 150 um diameter.

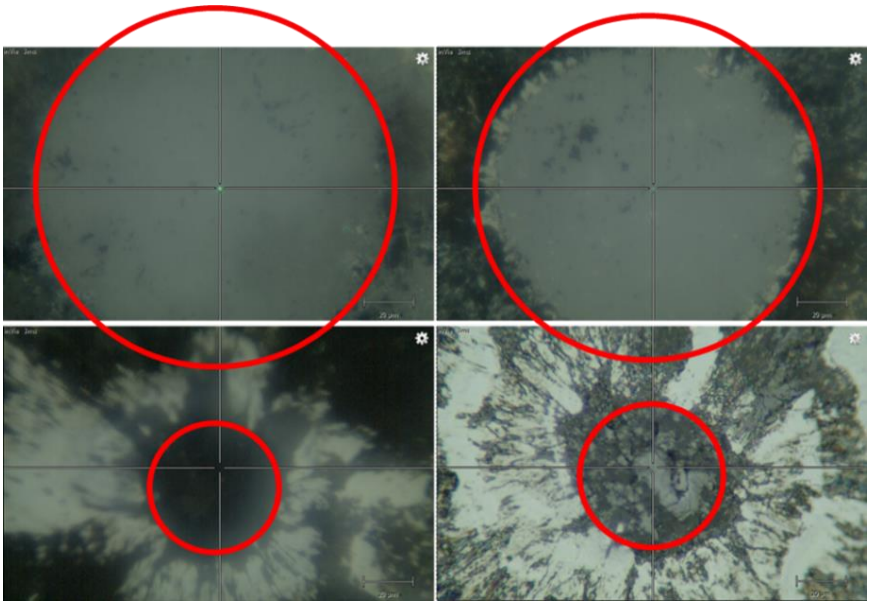

Figure 57: A view of the gasket hole under 50x magnification. Top images show the hole before pressure is applied, while the bottom images show the gaskets after deformation. Red lines are drawn in to help distinguish the holes.

For these runs, a nominal, boron-rich, and intermediate (also slightly boron-rich) sample were investigated, similar to the indentation study in Objective 2. The targeted maximum pressure for this experiment was 25 GPa, with the range of maximum pressures being between 23-27 GPa. Each sample had 4 separate high-pressure experiments executed. Amorphization was seen in all samples during all runs during unloading.

Additionally, 10 post-mortem Raman scans were taken of the samples from near the center of the gasket hole to probe the extent of amorphization the samples underwent. Those scans were quantified similar to the indentation maps from Objective 2 and early compression tests and post-mortem mapping from Objective 4. The results for each sample, plotted below in Figure 58, are then the result of 40 post-mortem Raman spectra from 4 separate DAC experiments loaded to approximately 25 GPa.

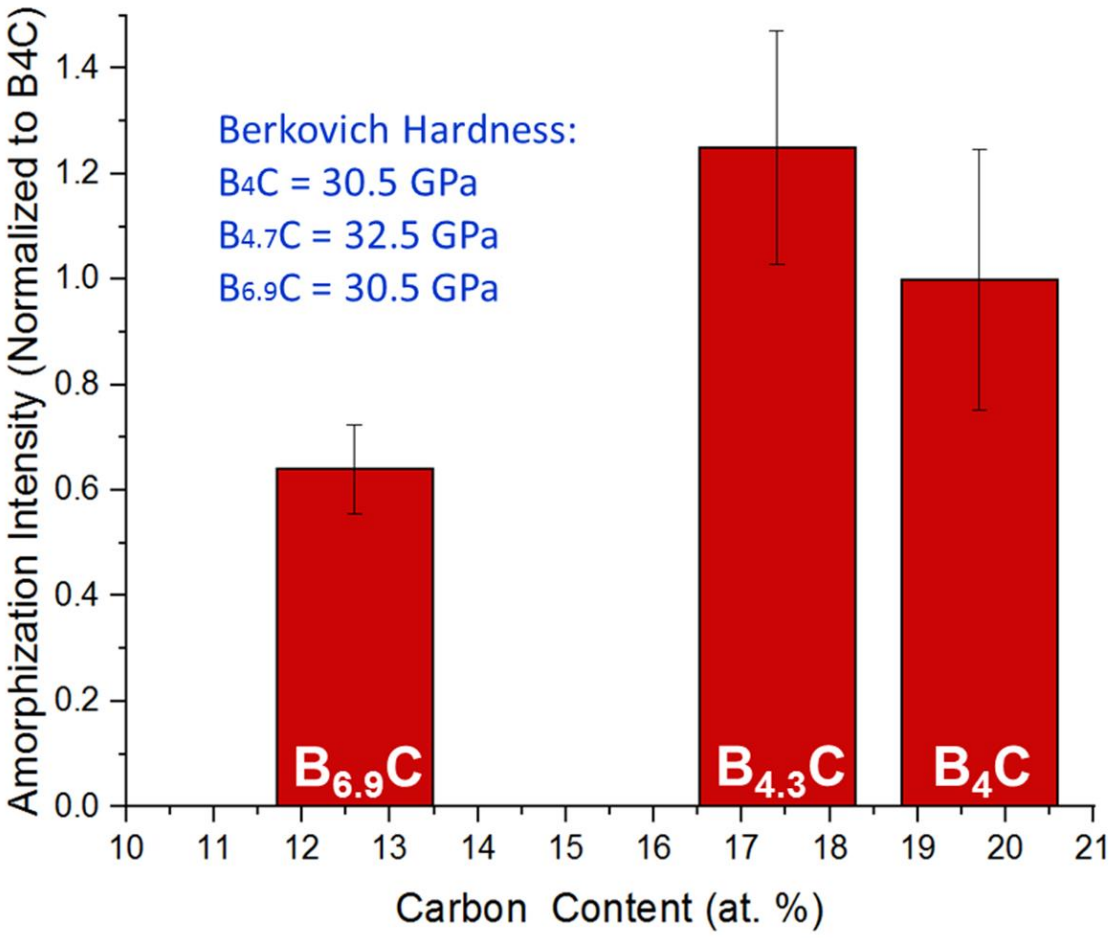

Figure 58: Amorphization intensity quantification for the 3 boron carbide powder samples studied in the DAC, normalized to B_4C.

While the quantification results are useful, and will be discussed shortly, the main reason to use a DAC was to investigate in situ the onset conditions in doped boron carbides. So, amorphization was indeed present in all stoichiometries studied. This has been the case in all doped boron carbides in both this dissertation as well as all literature on the subject matter. Similar to boron carbide, doped specimens present an amorphized Raman spectrum during unloading in a DAC, once a critical loading pressure of 25 GPa is reached.

Silicon-doped boron carbide, created and processed in the Haber group at Rutgers, was also investigated in a similar manner in a DAC to elucidate the onset conditions for

amorphization. Again, once loaded to a critical pressure of 25 GPa, amorphization presents itself at lower pressures during the unloading process.

This would imply that all boron carbide-based doped materials created at Rutgers amorphize by the same mechanism. No amorphization was seen during loading of any samples, nor were the onset pressures different; boron-rich boron carbides did not require a higher critical pressure to induce amorphization upon loading.

Thus, if boron carbide does amorphize by the same mechanism, regardless of the type or extent of doping, it could be argued that the same polytype is still responsible for structural collapse, albeit to a lesser degree, since doping would mitigate the susceptible polytype. This is a good assumption, since boron carbide, and boron-rich variants, can have large amounts of variation in which polytypes are present, and how abundant that polytype is. For silicon-doped samples, because of low doping percentages, on average only 1 in 7 unit cells will have a polytype with a silicon-doped chain structure. This leaves the other 6 unit cells to be B_4C or a boron-rich variation, either of which could also have a chain vacancy. Additionally, if boron carbides propensity for amorphization and material properties are defect-driven, those defects will always be present in some form in any fabricated sample. Using doped materials to mitigate amorphization can still be helpful as a potential pathway to improve the materials dynamic and ballistic performance.

Looking at the quantification results from the loading regimes to 25 GPa, several things appear noteworthy. First is that these results appear to contradict those presented earlier in the indentation mapping from Objective 2. That, however, is not the case. Indentation can induce large pressures to induce amorphization [2, 52, 56, 78], which was what was probed previously. Here, the onset conditions to induce amorphization were reported, which are presumably lower

pressures than indentation. These are the lower pressures to induce and identify amorphization. Past this, if larger maximum pressures are reached during loading, a larger degree of amorphization is seen in post-mortem DAC experiments. This is true in other cases as well.[5] This trend holds until the range of 40-50 GPa, where amorphization intensity reaches is maximum extent, and larger pressures past that do not seem to have a big impact on the degree of amorphization. It is this that can perhaps explain why the $B_{4.7}C$ median sample showed a larger degree of amorphization than standard B_4C. However, it is also important to note that due to a large variation present in these degrees-of-intensity for amorphization, it cannot be conclusively be said that that particular sample exhibits more amorphization than nominal B_4C. Furthermore, the most boron-rich sample studied, $B_{6.7}C$, which is past the critical stoichiometry change of $B_{6.5}C$, does show a large enough reduction in amorphization intensity to claim a reduction is there, since the difference is greater than the variation between the samples themselves.

Spectra during unloading is not well shown. While loading can be well controlled and applied in sequential steps, unloading proved more difficult to show and control. While amorphization was demonstrated in situ during unloading in Figure 55, consistent with what was shown in previous literature [5], it was not always fully apparent until post-mortem analysis. This has to do with how the system applies pressure. The system forces the piston into the cylinder, forcing the sample into a compressed state, whereas during unloading, gas is slowly released, allowing the system and its various parts to relax. This somehow led to the sample being relaxed last, once all gas was removed. No matter how little gas was left still in the pressure-transmitting membrane, the sample would consistently remain under 15-20 GPa pressure, and would remain so, until all gas was removed, at which point the sample would fully relax to an ambient pressure.

Looking in closer detail at the spectra during the loading stages, clear trends into how the materials behave and compress can be discerned from the data. A closer look into the structural evolution under pressure of standard, boron-rich, and silicon-doped boron carbides can be seen in Figures 59, 60, and 61, respectively.

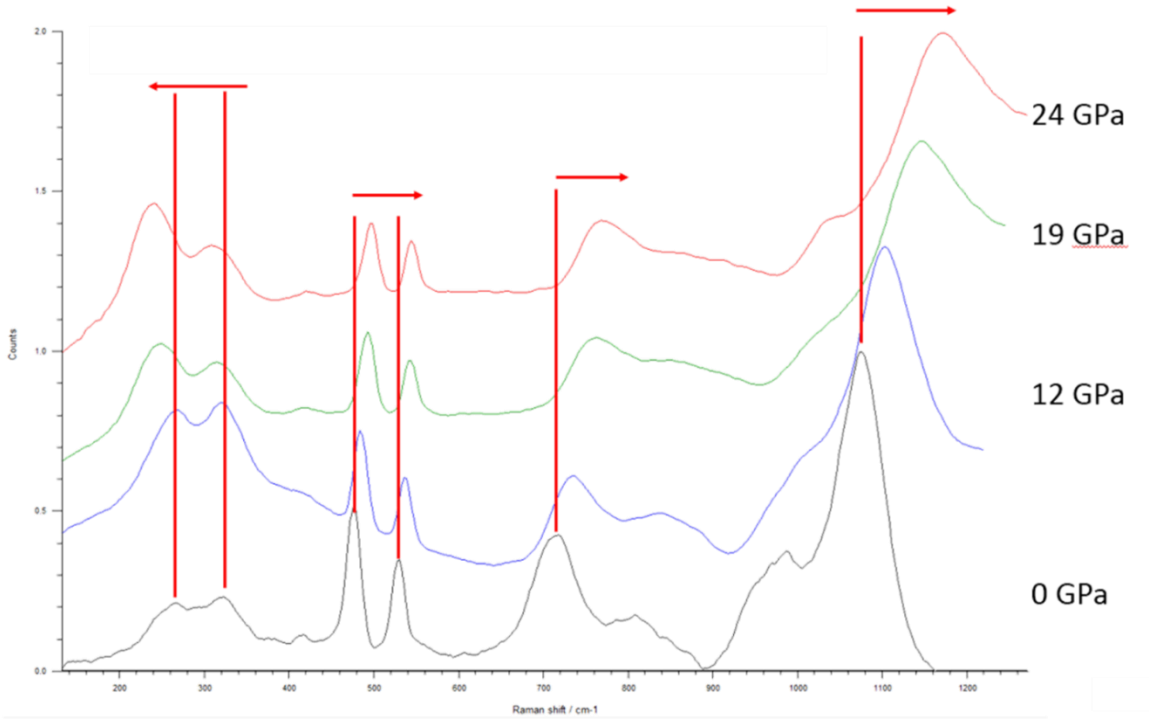

Figure 59: Raman spectra of B_4C. Pressure increases with ascending spectra. Red lines and arrows are guides to show trends as pressure increases.

Studying the peak evolution of boron carbides Raman spectra, it is clear that all peaks are affected by the application of pressure.[5, 34, 61] Most peaks shift to higher frequencies, indicative of compressive forces. Conversely, it is notable that the 270 and 320 cm^{-1} peaks downshift, something that can be representative of tension. Looking more specifically at right-shifting peaks, it is evident that not all peaks shift, and therefore compress, equally. While all models have to make the assumption that boron carbide compresses isotropically, in reality, all experimental data of boron carbide shows the material anisotropically deforming under any compressive forces. This is supported by the data shown here. The IBM peak appears to shift to

a larger degree than other peaks. This is experimental evidence that the icosahedra are more susceptible to deforming under pressure. This finding supports the work of Xie et. al. [57], where it was demonstrated that the icosahedra had weaker bonding than the chain structure. This can be explained by the delocalized bonding nature of the icosahedra, which can lead to a more ductile response to deformations, similar to metals. The difference here is that the surrounding matrix of ceramic material, mainly comprised of covalent bonds elsewhere, such as the chain, get strained by the icosahedras deformation to such an extent that it leads to cavitation and cracking. This can explain boron carbides brittle behavior from plastic deformation, such as with indentation.[2, 52] This data also shows the icosahedras exaggerated compression compared to the chain, supporting previous work by Nelmes [59], who also determined that the icosahedra compressed more than the surrounding matrix.

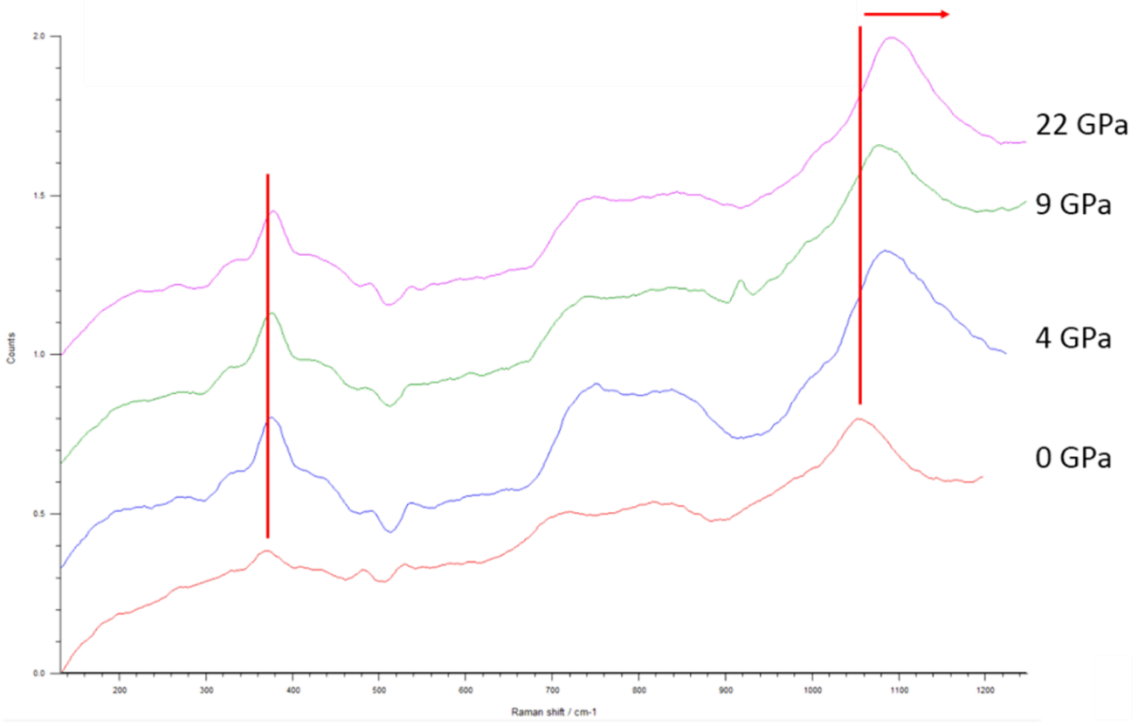

Figure 60: Raman spectra of boron-rich boron carbide. Pressure increases with ascending spectra. Red lines and arrows are guides to show trends as pressure increases.

Looking at the evolution of the $B_{6.9}C$ composition, it is again evident that the icosahedra is much more compressible than the rest of the structure. Meanwhile, the new peak at 370 cm^{-1}, presumably a result of a modified boron-doped chain, is not affected by the application of pressure. While it is noted that a slight right-shift to higher frequencies does occur, it is to a much lesser degree than the shift undergone by the cage structure. Further evidence of a modified chain is observed by the diminishing intensity of the 470 and 530 cm^{-1} peaks. The CBC chains are likely being replaced by boron-rich chains or vacancy chains that are accounting for the peak at 370 cm^{-1}. To reiterate, the icosahedra peak in the boron-rich boron carbide is still most susceptible to compressing and right-shifting under pressure, but it does so to a lesser degree than B_4C. This experimental result could point to the boron addition in the icosahedra strengthening the cage structure and making it less susceptible to collapse.

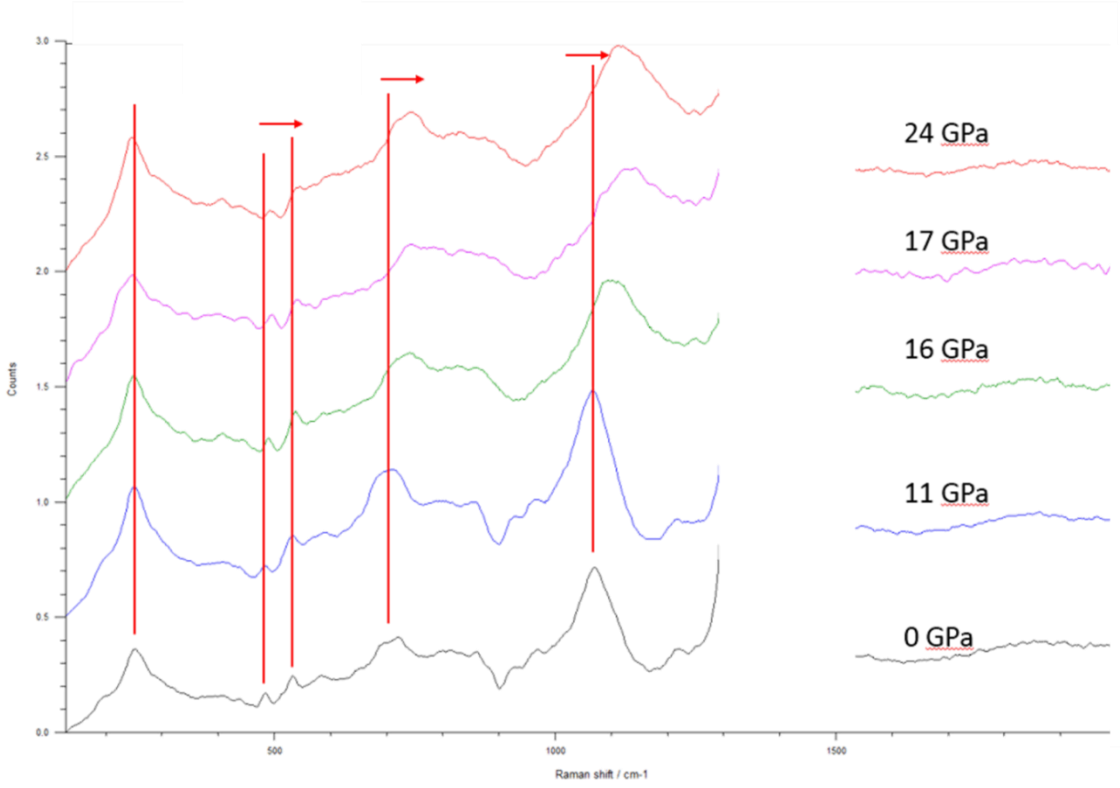

Figure 61: Raman spectra of silicon-doped boron carbide. Pressure increases with ascending spectra. Red lines and arrows are guides to show trends as pressure increases.

The silicon-doped boron carbide spectra behaves similarly to the boron carbide and the boron-rich samples to 25 GPa. The icosahedras strong compressibility is once again shown by the 1060 cm^{-1} peak's larger right-shift to higher frequencies compared to other peaks. Silicon-doped samples also tend to be inherently boron-rich, based on the phase diagram indicating a higher silicon solubility if the B/C ratio is increased to approximately 6.5. If this sample is boron-rich as well, this can explain a similar icosahedral peak shift at 1060 cm^{-1}, where the icosahedra peak shifts more than other peaks present in the spectrum at this stoichiometry, but it shifts to a lesser degree than what is seen in B_4C.

8. Conclusions

Boron-rich boron carbides have been studied across the homogeneity range to validate theoretical suggestions of amorphization mitigation in these materials. Indentation, Raman spectroscopy, and TEM analysis have been used to determine reduced amorphization in boron-rich boron carbide samples. Additionally, the amorphous phase of boron carbides have been investigated in situ in a high temperature apparatus and a high pressure cell, to better understand the stability of the amorphous phase and the onset of amorphization, respectively.

Based on the Raman spectra, all boron-rich samples studied give experimental evidence that initial boron substitution occurs in the icosahedra, transitioning from a ($B_{11}C$) cage to a (B_{12}) icosahedra to stabilize that structure.

Nano-indentation was used to induce amorphization and interrogate hardness in stoichiometrically varied boron carbides. Due to the similarity of the indentation area and the Raman laser spot size, it was difficult to draw any reliable and repeatable conclusions of correlations between amorphization intensity, as measured by Raman, nano-hardness, as measured by the total imprinted area from the Berkovich indenter, and the composition of the sample. Nano-indentation would be helpful later on to observe amorphization in boron-rich materials in TEM specimens.

Micro-indentation was used to observe and quantify amorphization intensity using Raman spectroscopy. This method was more thorough than nano-indentation. The larger areas from the Vickers indents allowed for Raman area maps to be generated, providing significant amounts of data that repeatably and reliably showed amorphization mitigation in boron-rich materials. Compared to nominal boron carbide, boron carbide near the $B_{13}C_2$ configuration showed a 70 % reduction in amorphization intensity. Further, TEM analysis of nano-indents from

the same boron-rich specimen showed a 30% reduction of amorphous bands locally in the indentation subsurface, further asserting conclusions drawn from Raman spectroscopy quantifications. A large reduction in amorphization was also seen for a slightly boron-rich median sample, giving rise to ideas that boron carbides do not need to be very boron-rich to reduce amorphization in boron carbide. This median sample can show the importance of adding a little boron to boron carbide so there are no carbonaceous inclusions in boron carbide, which could still be an instigating factor in amorphization of boron carbide.

In situ heating was conducted to determine the stability of the amorphous phase of varying boron-rich boron carbides. For boron carbide, the amorphous phase is no longer seen at temperatures at or exceeding 550 °C. For boron-rich samples studied, the temperature threshold to anneal away the amorphous phase was reduced by up to 100 °C. This can also support there are less amorphous bands or a smaller amorphized volume of material in boron-rich materials.

Lastly, a diamond anvil cell was used to interrogate the critical pressure threshold to induce amorphization in situ in stoichiometrically varied boron carbides. A silicon-doped boron carbide sample was also investigated. It was found that in all samples, regardless of composition, once loaded a minimum critical pressure of 25 GPa, amorphization was seen during and after the unloading process. Some evidence of amorphization mitigation in doped samples was still seen, but to a varied extent due to the lower pressures used in comparison to indentation. Structural evolution was also studied as pressure was applied to these samples. In all materials, anisotropic compression was observed, such that inverted molecular behavior was seen in these samples. The experimental work done here supports claims that chains are the stable structure in the matrix, and icosahedra are more susceptible to compression and collapse.

References

1. Grady, D.E., *Shock-wave strength properties of boron carbide and silicon carbide*. Conference: EURODYMAT `94: 1st international conference on mechanical and physical behavior of materials under dynamic loading,Oxford (United Kingdom),26-30 Sep 1994; Other Information: PBD: [1994]. 1994: ; Sandia National Labs., Albuquerque, NM (United States). Medium: ED; Size: 8 p.
2. Domnich, V., et al., *Nanoindentation and Raman spectroscopy studies of boron carbide single crystals.* Applied Physics Letters, 2002. **81**(20): p. 3783-3785.
3. Chen, M., J.W. McCauley, and K.J. Hemker, *Shock-Induced Localized Amorphization in Boron Carbide.* Science, 2003. **299**(5612): p. 1563-1566.
4. Domnich, V., et al., *Boron Carbide: Structure, Properties, and Stability under Stress.* Journal of the American Ceramic Society, 2011. **94**(11): p. 3605-3628.
5. Yan, X.Q., et al., *Depressurization amorphization of single-crystal boron carbide.* Phys Rev Lett, 2009. **102**(7): p. 075505.
6. Fanchini, G., J.W. McCauley, and M. Chhowalla, *Behavior of Disordered Boron Carbide under Stress.* Physical Review Letters, 2006. **97**(3): p. 035502.
7. DeCarlos, E.T., W.M. James, and T.W. Wright, *The effects of stoichiometry on the mechanical properties of icosahedral boron carbide under loading.* Journal of Physics: Condensed Matter, 2012. **24**(50): p. 505402.
8. An, Q., W.A. Goddard, 3rd, and T. Cheng, *Atomistic explanation of shear-induced amorphous band formation in boron carbide.* Phys Rev Lett, 2014. **113**(9): p. 095501.
9. An, Q. and W.A. Goddard, *Atomistic Origin of Brittle Failure of Boron Carbide from Large-Scale Reactive Dynamics Simulations: Suggestions toward Improved Ductility.* Physical Review Letters, 2015. **115**(10): p. 105501.
10. Awasthi, A.P. and G. Subhash, *High-pressure deformation and amorphization in boron carbide.* Journal of Applied Physics, 2019. **125**(21): p. 215901.
11. Kuwelkar, K.A., *Chemical and structural characterization of boron carbide powders and ceramics*. 2016.
12. Munhollon, T.L., *Chemical and mechanical analysis of boron-rich boron carbide processed via spark plasma sintering*, in *Ph.D. Thesis*. 2016.
13. Cheng, C., et al., *Structure and mechanical properties of boron-rich boron carbides.* Journal of the European Ceramic Society, 2017. **37**(15): p. 4514-4523.
14. Xie, K.Y., et al., *Microstructural characterization of boron-rich boron carbide.* Acta Materialia, 2017. **136**(Supplement C): p. 202-214.
15. Vargas-Gonzalez, L., R.F. Speyer, and J. Campbell, *Flexural Strength, Fracture Toughness, and Hardness of Silicon Carbide and Boron Carbide Armor Ceramics.* International Journal of Applied Ceramic Technology, 2010. **7**(5): p. 643-651.
16. Thévenot, F., *Boron carbide—A comprehensive review.* Journal of the European Ceramic Society, 1990. **6**(4): p. 205-225.
17. Emin, D., *Unusual properties of icosahedral boron-rich solids.* Journal of Solid State Chemistry, 2006. **179**(9): p. 2791-2798.
18. Tallant, D.R., et al., *Boron carbide structure by Raman spectroscopy.* Physical Review B, 1989. **40**(8): p. 5649-5656.
19. Elliott, R.P., *THE BORON-CARBON SYSTEM. Final Technical Report, May 1, 1960-April 30, 1961*. 1961, Illinois Inst. of Tech., Chicago. Armour Research Foundation.
20. Khan, A.U., V. Domnich, and R.A. Haber, *Boron carbide-based armors: Problems and possible solutions.* American Ceramic Society Bulletin, 2017. **96**(6): p. 30-35.

21. Bouchacourt, M. and F. Thevenot, *The melting of boron carbide and the homogeneity range of the boron carbide phase.* Journal of the Less Common Metals, 1979. **67**(2): p. 327-331.
22. Bouchacourt, M. and F. Thevenot, *Analytical investigations in the B ・ C system.* Journal of the less common metals, 1981. **82**: p. 219-226.
23. Ekbom, L.B. and C. Amundin. *Microstructural evaluation of sintered boron carbides with different compositions*. in *Proc. 11 th International Conf. on Science of Ceramics held at Stenungsund, Sweden, June 14-17, 1981. Edited by R. Carlsson and S. Karlsson. Swedish Ceram. Soc., Gothenburg, Sweden, 1981.* 1981.
24. Beauvy, M., *Stoichiometric limits of carbon-rich boron carbide phases.* Journal of the Less Common Metals, 1983. **90**(2): p. 169-175.
25. Gosset, D. and M. Colin, *Boron carbides of various compositions: An improved method for X-rays characterisation.* Journal of nuclear materials, 1991. **183**(3): p. 161-173.
26. Schwetz, K.A. and P. Karduck. *Investigations in the boron-carbon system with the aid of electron probe microanalysis*. in *AIP Conference Proceedings*. 1991. American Institute of Physics.
27. Kieffer, R., et al., *INVESTIGATIONS ON THE SYSTEM BORON--CARBON*. 1971, Technische Hochschule, Vienna.
28. Holmquist, T.J. and G.R. Johnson, *Characterization and evaluation of boron carbide for plate-impact conditions.* Journal of Applied Physics, 2006. **100**(9): p. 093525.
29. Dekura, H., K. Shirai, and A. Yanase. *Metallicity of boron carbides at high pressure*. in *Journal of Physics: Conference Series*. 2010. IOP Publishing.
30. Kunka, C., A. Awasthi, and G. Subhash, *Crystallographic and spectral equivalence of boron-carbide polymorphs.* Scripta Materialia, 2016. **122**: p. 82-85.
31. Kunka, C., A. Awasthi, and G. Subhash, *Evaluating boron-carbide constituents with simulated Raman spectra.* Scripta Materialia, 2017. **138**(Supplement C): p. 32-34.
32. *Analysis of Texture in Controlled Shear Processed Boron Carbide*, in *Advances in Ceramic Armor II: Ceramic Engineering and Science Proceedings*. p. 189-195.
33. Werheit, H., et al., *On surface Raman scattering and luminescence radiation in boron carbide.* Journal of Physics: Condensed Matter, 2010. **22**(4): p. 045401.
34. Hushur, A., et al., *High-pressure phase transition makes B4. 3C boron carbide a wide-gap semiconductor.* Journal of Physics: Condensed Matter, 2016. **28**(4): p. 045403.
35. Lazzari, R., et al., *Atomic Structure and Vibrational Properties of Icosahedral ${B}_{4}C$ Boron Carbide.* Physical Review Letters, 1999. **83**(16): p. 3230-3233.
36. Vast, N., et al., *Atomic structure and vibrational properties of icosahedral α-boron and B4C boron carbide.* Computational Materials Science, 2000. **17**(2): p. 127-132.
37. Kuhlmann, U. and H. Werheit, *Raman effect of boron carbide (B4. 3C to B10. 37C).* Journal of alloys and compounds, 1994. **205**(1-2): p. 87-91.
38. Shirai, K. and S. Emura, *Lattice Vibrations of Boron Carbide.* Journal of Solid State Chemistry, 1997. **133**(1): p. 93-96.
39. Vast, N., et al., *Lattice dynamics of icosahedral α-boron under pressure.* Physical review letters, 1997. **78**(4): p. 693.
40. Aselage, T., D. Tallant, and D. Emin, *Isotope dependencies of Raman spectra of B 12 As 2, B 12 P 2, B 12 O 2, and B 1 2+ x C 3− x: Bonding of intericosahedral chains.* Physical Review B, 1997. **56**(6): p. 3122.
41. Grady, D., *Dynamic properties of ceramic materials*. 1995, Sandia National Labs., Albuquerque, NM (United States).

42. Grady, D.E. and R.L. Moody, *Shock compression profiles in ceramics*. 1996, ; Sandia National Labs., Albuquerque, NM (United States). p. Medium: ED; Size: 155 p.
43. *Nanoindentation and Raman spectroscopy studies of boron carbide single crystals.* Applied Physics Letters, 2002. **81**(20): p. 3783-3785.
44. Domnich, V., Y. Gogotsi, and M. Trenary, *Identification of Pressure-Induced Phase Transformations Using Nanoindentation.* MRS Proceedings, 2000. **649**: p. Q8.9.
45. Ge, D., et al., *Structural damage in boron carbide under contact loading.* Acta Materialia, 2004. **52**(13): p. 3921-3927.
46. Deb, S.K., et al., *Pressure-induced amorphization and an amorphous–amorphous transition in densified porous silicon.* Nature, 2001. **414**(6863): p. 528-530.
47. Sharma, S.M. and S. Sikka, *Pressure induced amorphization of materials.* Progress in materials science, 1996. **40**(1): p. 1-77.
48. Yan, X., et al., *Raman spectroscopy of pressure-induced amorphous boron carbide.* Applied physics letters, 2006. **88**(13): p. 131905.
49. Fanchini, G., et al., *In Situ Monitoring of Structural Changes in Boron Carbide Under Electric Fields.* Journal of the American Ceramic Society, 2008. **91**(8): p. 2666-2669.
50. Zhao, S., et al., *Directional amorphization of boron carbide subjected to laser shock compression.* Proceedings of the National Academy of Sciences, 2016. **113**(43): p. 12088-12093.
51. Gosset, D., et al., *Evidence of amorphisation of B4C boron carbide under slow, heavy ion irradiation.* Nuclear Instruments and Methods in Physics Research Section B: Beam Interactions with Materials and Atoms, 2015. **365**: p. 300-304.
52. Subhash, G., et al., *Characterization of the 3-D amorphized zone beneath a Vickers indentation in boron carbide using Raman spectroscopy.* Acta Materialia, 2013. **61**(10): p. 3888-3896.
53. Tabor, D., *The physical meaning of indentation and scratch hardness.* British Journal of Applied Physics, 1956. **7**(5): p. 159-166.
54. Ghosh, D., et al., *Influence of stress state and strain rate on structural amorphization in boron carbide.* Journal of Applied Physics, 2012. **111**(6): p. 063523.
55. Parsard, G. and G. Subhash, *Raman spectroscopy mapping of amorphized zones beneath static and dynamic Vickers indentations on boron carbide.* Journal of the European Ceramic Society, 2017. **37**(5): p. 1945-1953.
56. Reddy, K.M., et al., *Atomic structure of amorphous shear bands in boron carbide.* Nature communications, 2013. **4**(1): p. 1-5.
57. Xie, K.Y., et al., *Breaking the icosahedra in boron carbide.* Proc Natl Acad Sci U S A, 2016. **113**(43): p. 12012-12016.
58. Annenkov, M., et al., *Structure of boron carbide after applying shear deformations under a pressure to 55 GPa.* Physics of the Solid State, 2017. **59**: p. 929-933.
59. Nelmes, R., et al., *Observation of inverted-molecular compression in boron carbide.* Physical review letters, 1995. **74**(12): p. 2268.
60. Fujii, T., et al., *X-ray diffraction study of B4C under high pressure.* Journal of Physics: Conference Series, 2010. **215**: p. 012011.
61. Dera, P., et al., *New insights into the enigma of boron carbide inverse molecular behavior.* Journal of Solid State Chemistry, 2014. **215**: p. 85-93.
62. *Root Causes of the Performance of Boron Carbide Under Stress*, in *Advances in Ceramic Armor II: Ceramic Engineering and Science Proceedings*. p. 179-188.
63. Raucoules, R., et al., *Mechanical properties of icosahedral boron carbide explained from first principles.* Physical Review B, 2011. **84**(1): p. 014112.

64. Betranhandy, E., N. Vast, and J. Sjakste, *Ab initio study of defective chains in icosahedral boron carbide B4C.* Solid state sciences, 2012. **14**(11-12): p. 1683-1687.
65. Subhash, G., et al., *In search of amorphization-resistant boron carbide.* Scripta Materialia, 2016. **123**(Supplement C): p. 158-162.
66. Lee, H. and R.F. Speyer, *Hardness and Fracture Toughness of Pressureless-Sintered Boron Carbide (B4C).* Journal of the American Ceramic Society, 2002. **85**(5): p. 1291-1293.
67. An, Q. and W.A. Goddard, *Nanotwins soften boron-rich boron carbide (B13C2).* Applied Physics Letters, 2017. **110**(11): p. 111902.
68. An, Q. and W.A. Goddard, *Microalloying Boron Carbide with Silicon to Achieve Dramatically Improved Ductility.* The Journal of Physical Chemistry Letters, 2014. **5**(23): p. 4169-4174.
69. Tang, B., Q. An, and W.A. Goddard, *Improved Ductility of Boron Carbide by Microalloying with Boron Suboxide.* The Journal of Physical Chemistry C, 2015. **119**(43): p. 24649-24656.
70. Werheit, H., et al., *Mode Grüneisen parameters of boron carbide.* Solid State Sciences, 2017. **72**: p. 80-93.
71. Yakel, H.L., *The crystal structure of a boron-rich boron carbide.* Acta Crystallographica Section B: Structural Crystallography and Crystal Chemistry, 1975. **31**(7): p. 1797-1806.
72. Aselage, T.L. and R.G. Tissot, *Lattice Constants of Boron Carbides.* Journal of the American Ceramic Society, 1992. **75**(8): p. 2207-2212.
73. Niihara, K., A. Nakahira, and T. Hirai, *The effect of stoichiometry on mechanical properties of boron carbide.* Journal of the American Ceramic Society, 1984. **67**(1): p. C-13-C-14.
74. Mohanty, R. and K. Balasubramanian. *Boron rich boron carbide: an emerging high performance material*. in *Key Engineering Materials*. 2009. Trans Tech Publ.
75. Morosin, B., et al., *Neutron powder diffraction refinement of boron carbides nature of intericosahedral chains.* Journal of alloys and compounds, 1995. **226**(1-2): p. 121-125.
76. Roszeitis, S., et al., *Reactive sintering process and thermoelectric properties of boron rich boron carbides.* Journal of the European Ceramic Society, 2014. **34**(2): p. 327-336.
77. Kwei, G.H. and B. Morosin, *Structures of the boron-rich boron carbides from neutron powder diffraction: Implications for the nature of the inter-icosahedral chains.* The Journal of Physical Chemistry, 1996. **100**(19): p. 8031-8039.
78. Yang, Q., et al., *Fabrication and characterization of arc melted Si/B co-doped boron carbide.* Journal of the European Ceramic Society, 2019. **39**(16): p. 5156-5166.
79. Chandrashekhar, M., et al., *Laser Induced Graphitization of Boron Carbide in Air*. 2019, Google Patents.
80. Piermarini, G.J., et al., *Calibration of the pressure dependence of the R 1 ruby fluorescence line to 195 kbar.* Journal of Applied Physics, 1975. **46**(6): p. 2774-2780.
81. Chijioke, A.D., et al., *The ruby pressure standard to 150 GPa.* Journal of Applied Physics, 2005. **98**(11): p. 114905.